National Library of Canada
Bibliothèque nationale du Canada

Canadian Theses Service
Service des thèses canadiennes

Ottawa, Canada
K1A 0N4

NOTICE

The quality of this microform is heavily dependent upon the quality of the original thesis submitted for microfilming. Every effort has been made to ensure the highest quality of reproduction possible.

If pages are missing, contact the university which granted the degree.

Some pages may have indistinct print especially if the original pages were typed with a poor typewriter ribbon or if the university sent us an inferior photocopy.

Reproduction in full or in part of this microform is governed by the Canadian Copyright Act, R.S.C. 1970, c. C-30, and subsequent amendments.

AVIS

La qualité de cette microforme dépend grandement de la qualité de la thèse soumise au microfilmage. Nous avons tout fait pour assurer une qualité supérieure de reproduction.

S'il manque des pages, veuillez communiquer avec l'université qui a conféré le grade.

La qualité d'impression de certaines pages peut laisser à désirer, surtout si les pages originales ont été dactylographiées à l'aide d'un ruban usé ou si l'université nous a fait parvenir une photocopie de qualité inférieure.

La reproduction, même partielle, de cette microforme est soumise à la Loi canadienne sur le droit d'auteur, SRC 1970, c. C-30, et ses amendements subséquents.

NL-339 (r. 88/04) c

Canada

UNIVERSITY OF ALBERTA

EVALUATION OF IMMOBILIZED 8-HYDROXYQUINOLINE ON XAD-2 TO DETERMINE FREE MAGNESIUM

AND

ADSORPTION OF SOLUTE AT THE LIQUID-LIQUID INTERFACE

BY

GOCOOL PERSAUD

A THESIS

SUBMITTED TO THE FACULTY OF GRADUATE STUDIES AND RESEARCH

IN PARTIAL FULFILLMENT OF THE REQUIREMENTS FOR THE DEGREE

OF DOCTOR OF PHILOSOPHY

DEPARTMENT OF CHEMISTRY

EDMONTON, ALBERTA

SPRING, 1990

National Library of Canada
Bibliothèque nationale du Canada

Canadian Theses Service
Service des thèses canadiennes

Ottawa, Canada
K1A 0N4

NOTICE

The quality of this microform is heavily dependent upon the quality of the original thesis submitted for microfilming. Every effort has been made to ensure the highest quality of reproduction possible.

If pages are missing, contact the university which granted the degree.

Some pages may have indistinct print especially if the original pages were typed with a poor typewriter ribbon or if the university sent us an inferior photocopy.

Reproduction in full or in part of this microform is governed by the Canadian Copyright Act, R.S.C. 1970, c. C-30, and subsequent amendments.

AVIS

La qualité de cette microforme dépend grandement de la qualité de la thèse soumise au microfilmage. Nous avons tout fait pour assurer une qualité supérieure de reproduction.

S'il manque des pages, veuillez communiquer avec l'université qui a conféré le grade.

La qualité d'impression de certaines pages peut laisser à désirer, surtout si les pages originales ont été dactylographiées à l'aide d'un ruban usé ou si l'université nous a fait parvenir une photocopie de qualité inférieure.

La reproduction, même partielle, de cette microforme est soumise à la Loi canadienne sur le droit d'auteur, SRC 1970, c. C-30, et ses amendements subséquents.

ISBN 0-315-60159-0

NL-339 (r. 88/04) c

Canada

UNIVERSITY OF ALBERTA

RELEASE FORM

Name of Author: GOCOOL PERSAUD

Title of Thesis: EVALUATION OF IMMOBILIZED 8-HYDROXYQUINOLINE ON XAD-2 TO DETERMINE FREE MAGNESIUM AND ADSORPTION OF SOLUTE AT THE LIQUID-LIQUID INTERFACE

Degree: Ph.D.

Year this degree granted: 1990

Permission is hereby granted to the UNIVERSITY OF ALBERTA to reproduce single copies of this thesis and to lend or sell such copies for private, scholarly or scientific research purposes only.

The author reserves other publication rights, and neither the thesis nor extensive extracts from it may be printed or otherwise reproduced without the author's written permission.

Gocool Persaud

(Student Signature)

(Student permanent address)

36D, Bath Settlement,

West Coast Berbice,

Guyana, South America.

Date: Dec 18/89

THE UNIVERSITY OF ALBERTA

FACULTY OF GRADUATE STUDIES AND RESEARCH

THE UNDERSIGNED CERTIFY THAT THEY HAVE READ, AND RECOMMEND TO THE FACULTY OF GRADUATE STUDIES AND RESEARCH FOR ACCEPTANCE, A THESIS ENTITLED EVALUATION OF IMMOBILIZED 8-HYDROXYQUINOLINE ON XAD-2 TO DETERMINE FREE MAGNESIUM **AND** ADSORPTION OF SOLUTE AT THE LIQUID-LIQUID INTERFACE

SUBMITTED BY GOCOOL PERSAUD

IN PARTIAL FULFILLMENT OF THE REQUIREMENTS FOR THE DEGREE OF DOCTOR OF PHILOSOPHY

F.F. Cantwell (Supervisor)

G. Hörlick

J.A. Plambeck

K.R. Kopecky

S. Hrudey

R.D. Guy (External examiner)

Date:

For my parents

Abstract

Part I of this thesis involves the evaluation of 8-hydroxyquinoline immobilized on a macroporous resin (XAD-oxine) for the determination of free magnesium using a previously described semi-automated column equilibration-atomic absorption spectrophotometry technique. Essentially the technique involves equilibration of a magnesium containing solution with the resin, and then eluting the sorbed magnesium directly into the atomic absorption spectrometer.

Two column equilibration procedures were characterized. The with washing procedure has 4 steps in a measurement cycle i.e. column equilibration, water wash, elution and another water wash. The other, without washing, procedure has two steps i.e. column equilibration and elution. The effect of pH, ionic strength, and other cations on the sorption behavior of Mg^{+2} on XAD-oxine, in the absence of other magnesium complexes, is the same for both procedures. Sorption studies of Mg^{+2} in the presence of neutral magnesium oxalate and cationic magnesium EDTA complexes showed that the with washing procedure perturbs the equilibrium and cannot be used. On the other hand, the without washing procedure is specific for Mg^{+2} in the presence of these neutral and cationic complexes. However, the neutral magnesium picolinate complex which contains a large hydrophobic moiety is sorbed on the hydrophobic surface XAD-oxine surface. Also the cationic magnesium picolinate complex is sorbed on the XAD-oxine. It is concluded that ligands immobilized on a hydrophobic support will have only limited utility for determining concentrations of free metal ions because of their tendency to sorb some metal-ligand complexes.

In Part II of this thesis, the behavior of solute adsorbed at the liquid-liquid interface during solvent extraction with porous membrane phase separators was investigated. It is shown experimentally for the interfacially adsorbed component, methylene blue perchlorate, that the distribution isotherm between chloroform and water is the same in stirred and unstirred mixtures. This suggests that the interfacially

adsorbed solute remains at the interface and does not enter the bulk liquid phases during membrane induced coalescence and phase separation. Theoretical calculations also show that adsorbed solute does not enter the bulk liquid at the surface of the membrane during phase separation.

Acknowledgement

I would like to express my sincerest appreciation to Dr. Federick F. Cantwell for his supervision, guidance and enthusiasm during the course of this research program and for his helpful suggestions in the presentation of this manuscript.

My special thanks also go to everyone who, in one way or the other, contributed to the success of this work.

Financial support from the University of Alberta is gratefully acknowledged.

Table of contents

Part I: EVALUATION OF IMMOBILIZED 8-HYDROXYQUINOLINE ON XAD-2 TO DETERMINE FREE MAGNESIUM

CHAPTER	PAGE
1 Introduction	1
1.1 Importance of magnesium	2
1.2 Experimental Methods to determine $[Mg^{+2}]$	3
1.2.1 Spectrophotometric methods	3
1.2.2 Magnesium ion selective methods	4
1.2.3 Ion exchange methods	4
1.2.4 Other methods for determination of $[Mg^{+2}]$	5
1.3 Research proposal for Part I	5
2 Preparation and Characterization of immobilized 8-Hydroxyquinoline immobilized on XAD-2	7
2.1 Introduction	7
2.2 Experimental	8
2.2.1 Apparatus	8
2.2.2 Chemicals and Reagents	8
2.2.3 Preparation of 5-chloromethyl-8-hydroxyquinoline hydrochloride	12
2.2.4 Immobilization of methyl-8-hydroxyquinoline on XAD-2	13
2.2.5 Adsorption of 5-chloromethyl-8-hydroxyquinoline on XAD-2	13
2.2.6 Determination of the capacity of the resin	14
2.2.7 Microanalysis	14

2.2.8 Titration of the XAD-oxine resin 15

2.3 Results and Discussion 15

2.3.1 Stability 15

2.3.2 Capacity 17

2.3.3 Titration of the resin 18

3 Sorption behavior of Mg^{+2} on XAD-oxine in the column equilibration experiments 21

3.1 Introduction 21

3.2 Experimental 24

3.2.1 Chemicals and Reagents 24

3.2.2 Apparatus 25

3.2.2.1 Apparatus used for experiments with washing after column equilibration 25

3.2.2.2 Apparatus used for experiments without washing after column equilibration 28

3.2.3 Column equilibration procedure 31

3.2.3.1 Procedure for experiments with washing after column equilibration 31

3.2.3.2 Procedure for experiments without washing after column equilibration 32

3.2.4 Column construction 34

3.2.5 Preparation of test solutions 36

3.3 Results and Discussion 36

3.3.1 Choice of variables for the AAS-flow system 36

3.3.2 Column equilibration 40

3.3.3 Column washing conditions 45

3.3.4 Column elution conditions 48
3.3.5 Column conditioning 51
3.3.6 Mg^{+2} isotherm 51
3.3.7 Effect of solution pH 55
3.3.8 Ionic strength 59
3.3.9 Effect other sorbed cations 66
3.3.10 Overloaded column conditions with washing 68
3.4 Conclusion 71

4 Speciation of Mg^{+2} with XAD-oxine 75
4.1 Introduction 75
4.2 Experimental 76
4.2.1 Chemicals and Reagents 76
4.2.2 Apparatus 76
4.2.3 Column equilibration procedure 76
4.2.4 Preparation of test solutions 77
4.2.5 Determination of $\alpha_{Mg^{+2}}$ in ligand containing solutions 78
4.2.6 Calculation of $\alpha_{Mg^{+2}Calc}$ from theory 78
4.3 Results and Discussion 83
4.3.1 Selectivity in the presence of EDTA 83
4.3.2 Selectivity in the presence of oxalate 95
4.3.3 Selectivity in the presence of picolinic acid 97
4.3.3.1 Sorption on XAD-2 as a function of C_{HP} i.e. [picolinic acid] ... 102
4.3.3.2 Sorption on XAD-2 as a function of solution pH 106
4.3.3.3 Sorption on XAD-oxine as a function of solution pH 106
4.3.3.4 Sorption on XAD-oxine as a function of C_{Mg} 110
4.3.3.5 Mechanism of sorption of MgP^{+} on XAD-oxine 119

4.4 Conclusion 122

5 Conclusions of part I and suggestions for future work 125

Part II: ADSORPTION OF SOLUTE AT THE LIQUID-LIQUID INTERFACE

6 Behavior of solute adsorbed at the liquid-liquid interface during solvent extraction with porous membrane phase separators 127

6.1. Introduction 127

6.2. Experimental 128

6.2.1. Apparatus 128

6.2.2. Chemicals and Reagents 130

6.2.3. Measurement of the distribution isotherm 132

6.2.4. Measurement of V_{max} 133

6.3. Results 133

6.3.1. Hydrodynamics 133

6.3.2. Adsorption of $MB.ClO_4$ 136

6.3.3. Distribution isotherm 138

6.4. Discussion 146

6.4.1. Coalescence 146

6.4.2. Residence time 150

6.4.3. Model of the interface 154

6.4.4. Diffusion layer thickness 156

6.4.5. Desorption/Diffusion 156

6.5. Conclusion 160

REFERENCES 163

Appendix 172

LIST OF FIGURES

FIGURE		PAGE
2.1	Fraction of copper eluted from 0.5 g of XAD-oxine as a function of volume of 0.1 M HNO_3	19
2.2	Titration of XAD-oxine with NaOH	20
3.1	Technique of column equilibration (a) apparatus and (b) breakthrough curve	23
3.2	Apparatus for column equilibration with washing	26
3.3	Apparatus for column equilibration without washing	29
3.4	The column	35
3.5	The signal height when a solution containing 8.23×10^{-6} M magnesium was pumped at various rates into the Model 290B Perkin-Elmer AAS	38
3.6	The signal height when a solution containing 1.23×10^{-5} M magnesium was pumped at various rates into the Model 4000 Perkin-Elmer AAS	39
3.7	The relative P.A. (■), P.H. (▲) and Area/height ratio (+) when 10 µL of 2.47×10^{-4} M Mg^{+2} was injected into the HNO_3 stream entering the Model 290B AAS at various pumping rates	41
3.8	The signal response of the Model 290B Perkin-Elmer AAS during loading, washing and elution steps	42
3.9	Loading curve with washing	44
3.10	Loading curve without washing	46
3.11	Washing conditions	47
3.12	Double peaks after the column was loaded for 20 min then eluted with 0.001 M HNO_3 without washing	50
3.13	Isotherm (i.e. P.A. vs $[Mg^{+2}]$) with washing	53
3.14	Isotherm (i.e. P.A. vs $[Mg^{+2}]$) without washing	54
3.15	Isotherm with washing at various pH	56

3.16 The effect of solution pH on the distribution ratio 58

3.17 The effect of solution pH on the distribution ratio using the without washing procedure 60

3.18 With washing isotherms using NaCl ( ) and $NaNO_3$ (x) for ionic strength adjustment 61

3.19 With washing isotherms using only 0.25 M NaCl ( ) and 0.05 M KCl + 0.20 M NaCl (x) for ionic strength adjustment 63

3.20 The effect of ionic strength on the distribution ratio using the with washing procedure 64

3.21 The effect of ionic strength on the distribution ratio using the without washing procedure 65

3.22 Loading curve for a copper containing solution using the with washing procedure 67

3.23 Effect of varying concentration of Ca^{+2} on Mg^{+2} sorption using the with washing procedure 69

3.24 Effect of varying concentration of Ca^{+2} on Mg^{+2} sorption using the without washing procedure 70

3.25 Effect of 2.0×10^{-3} M (x), 5.0×10^{-3} M (+) and 1.0×10^{-2} M (■) added Ca^{+2} on Mg^{+2} isotherm using the with washing procedure 72

3.26 Plot of P.A. vs $[Ca^{+2}]$ for the points when $[Mg^{+2}] = 1.65 \times 10^{-3}$ M 73

4.1 Loading curve using the with washing procedure EDTA 86

4.2 Washing conditions with EDTA 91

4.3 Species distribution of Mg^{+2}, MgP^{+} and MgP_2 at various pH and $C_{picolinic\ acid}$ (0.001 M, 0.01 M and 0.05 M) 101

4.4 The amount of Mg-picolinate complexes sorbed at a pH of 6.00 on XAD-2 vs the calculated $[MgP_2]$ in solution 104

4.5 The amount of Mg-picolinate complexes sorbed at a pH of 7.50 on XAD-2 vs the calculated [MgP_2] in solution 105

4.6 The excess amount of Mg-picolinate complex sorbed (i.e. P.A. excess) as a function of solution pH on columns packed with XAD-2 (curve A) and XAD-oxine (curve B) 107

4.7 Overall Mg-picolinate isotherm without washing at a pH of 6.00 112

4.8 Overall Mg-picolinate isotherm without washing at a pH of 7.50 113

4.9 Mg^{+2} isotherm without washing at a pH of 6.00 114

4.10 Mg^{+2} isotherm without washing at a pH of 7.50 115

4.11 MgP^{+} isotherm without washing after subtraction of the P.A. contribution due to Mg^{+2} and MgP_2 at a pH of 6.00 117

4.12 MgP^{+} isotherm without washing after subtraction of the P.A. contribution due to Mg^{+2} and MgP_2 at a pH of 7.50 118

4.13 Plot of $\frac{P.A._{Excess}}{\alpha_{MgP_2}}$ vs $\frac{\alpha_{MgP^{+}}+\alpha_{Ox}}{\alpha_{MgP_2}}$ 123

6.1 Diagram of the apparatus to study adsorption at liquid-liquid interfaces 129

6.2 Exploded view of the end of the "filter probe" 131

6.3 Side view of "filter probe" membrane phase separator showing in dashed lines the Pitot tube 134

6.4 A sketch of typical chart recording that shows the change in absorbance values on changing from stirring to non-stirring 140

6.5 Distribution isotherm for methylene blue perchlorate between chloroform and aqueous phases..... 141

6.6 Coalescence of a droplet of dispersed phase with a flat layer of the same phase showing the fate of interfacially adsorbed solute 148

6.7 Flow of a two-phase liquid near the surface of a porous membrane 152

LIST OF TABLES

TABLE PAGE

2.1 Instrumental conditions used with the model 290B Atomic Absorption Spectrophotometer 9

3.1 Instrumental conditions used for the Model 4000 Perkin-Elmer atomic absorption spectrophotometer in the without washing flow system 30

4.1 Values of formation constants used in this chapter to calculate the fraction of individual species in metal-ligand solutions 80

4.2 Effect of varying [EDTA] on the fraction of free metal using the with washing procedure 84

4.3 Effect of EDTA at various pH on the fraction of free metal using the with washing procedure 87

4.4 The sorption of Mg-EDTA solutions on columns packed with 1 cm of XAD-2 and XAD-oxine. Also, the effect of varying [EDTA] on the fraction of free metal after correcting for sorption on a blank XAD-2 column, using the with washing procedure 89

4.5 Effect of EDTA on the fraction of free metal immediately on using the without washing procedure 92

4.6 Effect of EDTA on the fraction of free metal using the without washing procedure 93

4.7 Effect of varying [Oxalic acid] on the fraction of various species using the with washing procedure 96

4.8 Effect of varying [Oxalic acid] on the fraction of free metal using the without washing procedure 98

4.9 Table shows the amount of magnesium sorption (i.e. P.A.) with solutions of varying picolinic acid concentration done on XAD-oxine and XAD-2 using

the without washing procedure 99

4.10 Effect of varying [picolinic acid] on XAD-2 using the without washing procedure. Table also shows the calculated concentration of the various species 103

4.11 Effect of varying solution pH on XAD-oxine using the without washing procedure 109

4.12 Effect of varying C_{Mg} on XAD-oxine and XAD-2 using the without washing procedure 111

6.1 Absorbances of the chloroform phase (A_O) and aqueous phase (A_A) for 60 mL of each phase containing various amounts of methylene blue perchlorate with no stirring (NS) and vigorous stirring (S) 142

6.2 Slope and intercept values from linear least squares regression analysis of plots of A_O vs A_A under stirring (S) and non-stirring (NS) conditions 143

6.3 The surface excess for the various concentrations of both phases used in Table 6.1 145

6.4 Percentages of the total amount of solute initially adsorbed at the interface which have desorbed and which have diffused to or beyond a given distance in a given time 161

6.8 Whitman two film model of the interface 155

6.9 Solute concentration vs distance from the liquid-liquid interface at t = 0.1 s. Curve A includes the effect of desorption from the interface. Curve B shows the hypothetical behavior if interfacial adsorption were present 159

LIST OF SYMBOLS

(CHAPTERS 1- 5 ONLY)

Mg^{+2}, Cu^{+2}, Ca^{+2}, K^{+} - free metal ion, ionic form of the metal, hydrated metal ion

% column loading ~ % of oxine sites on XAD-oxine used for sorption

C_i	total concentration of all species of a particular compound or metal
CPG-oxine	8-hydroxyquinoline immobilized on controlled pore glass
XAD-oxine	8-hydroxyquinoline immobilized to XAD-2 resin
$R\text{-}Ox^{-}$	XAD-oxine in the anionic form
R-OxH	XAD-oxine in the neutral form
$R\text{-}OxH_2^{+}$	XAD-oxine in the cationic form
P.A.	general symbol for peak area
$P.A._{.tot}$	P.A. due to sorption plus P.A. due to interstitial fluid (Note: P.A. of the appropriate blank subtracted)
$P.A._{.void}$	P.A. contribution due to the void volume (interstitial fluid) in the without washing procedure
$P.A._{.sorb}$	$P.A._{.tot}$ - $P.A._{.void}$
$P.A._{.excess}$	P.A. due to sorption of MgP_2 and MgP^{+} i.e. $P.A._{.tot}$ - $P.A._{.Mg^{+2}}$
Total P.A.	sum of $P.A._{.Mg^{+2}}$ + $P.A._{.MgP^{+}}$ + $P.A._{.MgP_2}$
[i]	concentration of the indicated species in solution
$[i]_R$	concentration of the indicated species in the resin phase
AAS	atomic absorption spectrophotometer
ISE	ion selective electrode
UV-VIS	ultraviolet-visible
k	moles per unit P.A. per unit wt. of resin
K_i	formation constant; stability constant of the indicated species
K_1 and K_2	first and second dissociation constants of 8-hydroxyquinoline

M	molarity
X	mol per unit P.A.
V_m	void volume
±	standard deviation of the number in front
i.d.	internal diameter
nm	nanometers
mA	milliamperes
min	minutes
s	seconds
l	column length
d	packing density of resin per mm of column
v	sorptive capacity of XAD-oxine
z_i	charge of the ion
Y	EDTA ligand
Ox	oxalate ligand
P	picolinate ligand
α_i	fraction of the species indicated by the subscript
$\alpha_{Mg^{+2},Expt}$	experimentally determined fraction of Mg^{+2}
$\alpha_{Mg^{+2},Calc}$	fraction of Mg^{+2} calculated from theory
β_i	first formation constant
γ_i	activity coefficient of the indicated species
λ_o	distribution ratio; ratio of the concentration of a particular species in the resin phase to that in solution phase
λ_{max}	wavelength at maximum absorbance
λ_i	distribution ratio of indicated species (MgP_2 or MgP^+)
μ	ionic strength

(CHAPTER 6 ONLY)

V_{max}	free stream linear velocity
V_X	linear velocity at some distance X cm from the surface
$V_{X,Int}$	velocity of the interface at some distance X cm from the surface
$\bar{c}$	dimensionless constant
ρ	density of the liquid
l	distance along the membrane
η	viscosity
N_{Re}	Reynolds number
D	distribution ratio between the organic and aqueous phase
K_{Diss}	dissociation constant
$K_{I,O}$	distribution ratio between the interface and organic phase
$K_{I,A}$	distribution ratio between the interface and aqueous phase
i_S	the S subscript represent stirring conditions
i_{NS}	the NS subscript represent non-stirring
n_T	total number of moles in both phases
X_{BL}	thickness of the boundary layer
δX	diffusion layer thickness
t	total time for diffusion
$B_{o(X,t)}$	concentration of solute at a distance x and time t
D'	diffusion coefficient

CHAPTER 1

INTRODUCTION TO Mg^{+2} SPECIATION

In many natural systems e.g. surface waters and biological fluids, a metal exist in many different forms or species. The various forms of the metal can be categorized as (1):

(a) simple dissolved compounds of molecular weight of up to 200 e.g. free metal ions, inorganic complexes, small organic molecules

(b) larger dissolved compounds of molecular weight between 200 to 1×10^4 e.g. complexes of fulvic and fatty acids

(c) colloidal material of molecular weight between 10^4 to 10^6 e.g. complexes of humic acids and proteins, as well as inorganic colloids

(d) suspended organic and inorganic particles.

It is the determination of one or more chemical species of a metal that is termed speciation. The individual species of a metal can be kinetically inert or labile. The importance and analytical aspects of metal speciation has been the subject of many reviews and books (2-10). Speciation studies are important for many reasons. The transport, fate, behavior and biological effects (bioavailability, toxicity) of a trace metal in the environment is dependent on its physiological form. For example, the growth of algae is dependent on the concentration of free metal ion (11,12). The bioavailability and subsequent transfer in the food chain is dependent on the chemical form of the metal (13). Similarly, chemical speciation is just as important in clinical studies (14).

The analytical techniques developed for chemical speciation have been discussed in many of the above reviews (2-10). In summary, there are two approaches to chemical speciation viz. calculation and experimental methods. The calculation method

involves the simultaneous solution of all the metal-ligand equilibria using the experimentally determined total metal and ligand concentrations, and published values of the relevant equilibria constants, for example, the $[Mg^{+2}]$ in rat tissues has been determined by this method (15). The experimental approach is based on a direct measurement of the particular chemical species of the metal. Examples of chemical measurement techniques are: ion selective electrodes, voltammetric methods (e.g. differential pulse polarography, anodic stripping voltammetry), separation techniques (e.g. dialysis, ultrafiltration, ion exchange, size exclusion chromatography, solvent extraction) and spectrometric methods (e.g. UV-VIS spectrometry).

In this thesis, the term "speciation" refers to the determination of the concentration of the kinetically labile free metal ion (hydrated cation) for a particular metal.

1.1 Importance of magnesium

The biological significance of magnesium and its importance for the existence of life has been the subject of many books (16-20). It is involved in every key process of life e.g. photosynthesis and development of an oxygen rich atmosphere (21) and synthesis involving adenosine triphosphate (21) which in turn is required for glucose utilization, fat, protein, nucleic acid, coenzyme synthesis, muscle contraction, methyl group transfer and other reactions (17). The health of all forms of life is furthermore influenced by the magnesium in the environment because the amount of exchangeable magnesium in the soil affects agricultural productivity (17). Although chelated magnesium is necessary in the biological system, it is the free magnesium ion (i.e. Mg^{+2} or ionic magnesium or hydrated magnesium ion) in physiological concentrations that coordinates all the essential processes for the maintenance of life (17). Clearly, the development of analytical methods to determine $[Mg^{+2}]$ in environmental and biological samples is justified.

1.2 Experimental Methods to determine [Mg^{+2}]

Although calcium and magnesium have similar properties, analytical methods for determining Mg^{+2} are not as widespread as are methods for free calcium (Ca^{+2}). There is no universal method to determine Mg^{+2}, as compared to Ca^{+2} where there is a commercially available ion selective method. Attempts to develop analytical methods to determine [Mg^{+2}] started as early as 1960 (22), but so far there has been limited success. Examples of methods to determine Mg^{+2} and their limitations are discussed below:

1.2.1 Spectrophotometric methods

The method of Scarpa (23) was successful for the determination of Mg^{+2} in biological samples with a narrow pH range of 7.1 to 7.2. It is based on the selective association between Mg^{+2} and Eriochrome Blue SE and dual wavelength spectroscopy to measure the change in absorbance due to complex formation. The metallochromic indicator possessed some ideal properties for measuring [Mg^{+2}] including: (a) low affinity for Mg^{+2} so that the ambient equilibrium is not significantly perturbed; (b) large difference in molar absorptivity between the uncomplexed and complexed forms of the indicator, and; (c) high specificity for Mg^{+2} at the selected wavelength (the use of dual wavelength spectroscopy eliminates most interferences due to other metal complexes which have much broader absorption bands than the magnesium complex). Mn^{+2} showed similar absorption changes as Mg^{+2}, but because [Mn^{+2}] is small in biological samples, it did not affect the technique. Another major limitation of Eriochrome Blue SE is its strong pH dependence - the workable pH range is extremely narrow. Casillas *el. al.* (24) estimated an average change in absorbance of 0.010 per 0.1 pH unit with this method. Furthermore, some binding of the Eriochrome Blue SE onto biological systems was observed.

Other indicators were used for the spectrophotometric determination of Mg^{+2}, but they were either non-selective or the equilibrium was significantly perturbed. Eriochrome Black was proposed, but it was just as pH sensitive as Eriochrome Blue SE (22). Calmagite was used to measure $[Mg^{+2}]$ (25), but since masking agents were used to prevent interferences of other metals, this method cannot be considered as a method for the determination of kinetically labile Mg^{+2}.

1.2.2 **Magnesium Ion Selective Electrodes**

Despite the large volume of literature on ion selective electrodes (ISE) with high selectivity for Na^+, K^+ and Ca^{+2}, there is no known ISE that shows a high selectivity for Mg^{+2} (26,27). Rouilly *et. al.* (27) summarized the literature on magnesium ISE's. In most of the reported cases, the selectivity of the ISE to Ca^{+2} and Mg^{+2} were the same, and thus, these ISE's can only be applied in analysis where the $[Ca^{+2}]$ is low. In other cases, the ISE shows poor selectivity with respect to alkali metals, particularly K^+ (28) or H^+ (27).

To eliminate the effect of interferences on the magnesium ISE, Otto and Thomas (29) proposed a chemometric approach to determine Mg^{+2} in biological fluids. This approach requires the simultaneous ISE analysis of Na^+, K^+, Ca^{+2} and Mg^{+2} using standards containing mixtures of these cations and then data reduction by partial least squares.

1.2.3 **Ion Exchange Method**

The ion exchange method to determine $[Mg^{+2}]$ is based on equilibration of the resin with the test solution, removal of the sorbed Mg^{+2} with a suitable eluent and then total analysis of the eluted Mg^{+2} (30,31). The amount of sorbed Mg^{+2} (which is the same as the amount of Mg^{+2} eluted) is directly proportional to the $[Mg^{+2}]$ in solution under certain conditions. However, the major limitation of ion exchange resins for free

metal determination is the sorption of cationic complexes of the metal on the resin (32). On elution, both Mg^{+2} and the cationic complexes are measured.

1.2.4 Other methods for the determination of $[Mg^{+2}]$

The measurement of $[Mg^{+2}]$ in plasma by ultrafiltration has been used (33). The drawback of this method is that the filters have been reported to sorb complex species (34). An HPLC-AAS system has been reported for speciation of Mg^{+2} (35). Because of dilution of the sample in the HPLC mobile phase, and thus decomposition of the complexes, this method can only be considered as the analysis of the inert forms of the Mg^{+2}. Rousselet *et al.* (36) in their review on methods to determine magnesium, mentioned enzymatic methods, as well as their non-selectivity.

1.3 Research objectives for Part I

Because of the necessity of measuring $[Mg^{+2}]$ and the limitations in reported analytical methods to determine free magnesium, Part I of this thesis deals with the feasibility of an alternative analytical method. The method chosen was the column equilibration technique, which was previously used to determine free nickel (37), free copper (32) and free calcium (38,39) in the presence of their complexes. In the column equilibration method, as previously used, there were some difficulties. When a sulfonated ion exchange resin was used as the sorbent for the determination of Cu^{+2}, the experimentally measured $[Cu^{+2}]$ was slightly higher than the theoretically calculated $[Cu^{+2}]$. The non-selectivity of the sulfonated resin, due to sorption of cationic and neutral complexes, was believed to be the reason for the higher experimentally measured $[Cu^{+2}]$ (32).

Similarly it was observed that the experimentally measured $[Ca^{+2}]$ was slightly higher than the theoretically calculated $[Ca^{+2}]$, when sulfonated ion exchange resins were used (39). Work is presently underway to explain these observations (40). In

contrast, use of the chelating ligand 8-hydroxyquinoline (oxine) bound on controlled pore glass (CPG-oxine) did not show a higher experimentally measured [Ca^{+2}] (38). Therefore, immobilized 8-hydroxyquinoline was chosen as the sorbent for Mg^{+2} measurements. Because oxine immobilized on silica type surfaces (e.g. CPG, silica gel) has been reported to be unstable in alkaline solutions (41-44), the oxine ligand was immobilized on a polystyrene matrix in this present work. Besides the high stability reported reported for 8-hydroxyquinoline immobilized on XAD-2, higher capacities and more easily controlled variations in capacity were reported for XAD-2 type supports as compared to glass support (45).

Chapter 2 deals with the immobilization of 8-hydroxyquinoline on XAD-2 to form the sorbent XAD-oxine and characterization of this sorbent. In Chapter 3, various instrumental parameters of the column equilibration technique will be optimized for two versions of the technique (i.e. with washing and without washing), and then the effect of pH, ionic strength and other cations on Mg^{+2} sorption will be characterized. Also the limitations of XAD-oxine for the determination of [Mg^{+2}] will be investigated. In Chapter 4, the specificity of XAD-oxine to determine [Mg^{+2}] in the presence of various organic ligands will be investigated. Furthermore, Chapter 4 is concerned with a detailed investigation of the non-specificity of XAD-oxine to Mg^{+2} sorption, in the presence of other ligands, in order to understand the sorption process as well as to aid in subsequent selection of suitable sorbents for free metal determination.

CHAPTER 2

PREPARATION AND CHARACTERIZATION OF 8-HYDROXYQUINOLINE IMMOBILIZED ON XAD-2

2.1 Introduction

Functionalization of polystyrene resins has been the subject of a number of reviews (46,47). More specifically, the immobilization of chelating ligands on a variety of supports has been recently reviewed by Myasoedova and Savvin (48,49). In their review titled "New chelating sorbents and their use in analytical chemistry," the combinations of various chelating groups with each individual support were tabulated (49). Supports included cross linked polymers, polycondensation type resins and cellulose type supports. Also included in the tables are well referenced applications of their use in analytical chemistry. A more extensive review by these authors included: general characteristics of chelating sorbents, methods of synthesis, physicochemical properties, analytical properties and applications of individual chelating sorbents (48). Sahni and Reedijk (50) also extensively reviewed the coordination chemistry of chelating resins. This review covers 32 types of immobilized chelating ligands and covers all aspects of the subject including: history, functionalization of organic polymers, commercial availability, analytical properties and characterization (50).

Approaches to immobilize 8-hydroxyquinoline on resins vary widely. The earliest approach to immobilize 8-hydroxyquinoline is based on condensation of 8-hydroxyquinoline, formaldehyde and resorcinol (51-56). Alternative approaches to immobilize 8-hydroxyquinoline are based on functionalization of the polystyrene then chemically bonding the 8-hydroxyquinoline to the functional group on the resin. The general approaches are: (a) nitration of the resin, reduction to the amine group and then immobilization of the 8-hydroxyquinoline via an azo linkage (57,42,58); (b) nitration of the resin, reduction to the amine, introduction of a spacer arm by reacting with p-

nitrobenzoyl chloride, reduction of the nitro group on the spacer arm to the amine and finally coupling with the 8-hydroxyquinoline via an azo linkage (57), and; (c) immobilization of 8-hydroxyquinoline via a methylene linkage by a Friedel-Crafts alkylation (57,45,59).

Resins based on condensation are reported to be less stable and to exhibit slow rates of exchange (58). By contrast, the polystyrene based resins show superior properties with regards to stability and equilibration rates (52,53) When the 8-hydroxyquinoline is immobilized via an azo linkage, residual groups such as amine groups remain because each of these steps is about 60% efficient (53). Since amine groups form complexes with many cations in homogeneous solution, it is likely that these groups will behave similarly on the resin surface. In order to minimize the presence of these "impurity" groups, the immobilization of 8-hydroxyquinoline on macroporous XAD-2 resin via a methylene linkage was chosen.

2.2 Experimental

2.2.1 Apparatus

A model 290B atomic absorption spectrometer (Perkin-Elmer) was used to determine the copper concentration. The instrumental conditions are listed in Table 2.1.

Measurements of pH were made with a Fisher Accumet Model 320 Expanded Scale Research pH meter using a combination electrode (Cat. No. 13-639-90, Fisher Scientific Co.) calibrated with Fisher Certified buffers to ± 0.01 pH units.

A Haake circulating thermostat model R20 was used to circulate water at 25 ± 0.5 °C through the water jacket surrounding the titration cell.

2.2.2 Chemicals and Reagents

Distilled deionized water was prepared by passing the laboratory distilled water through a mixed bed ion exchange resin column (Amberlite MB-1, Analytical reagent,

Table 2.1: Instrumental conditions used with the Model 290B Atomic Absorption Spectrophotometer

Parameter	Setting
Wavelength	324.8 nm (Cu)
Lamp current	4 mA (Cu)
Spectral slit width	0.7 nm
Flame	oxidizing (lean,blue)
Acetylene setting	13.10 at 9 psi
Air setting	12.7 at 50 psi
Meter damping	setting #3
Recorder	Fisher Recordall series 5000
Voltage range	10 mV
Chart speed	2.5 cm/min

Mallinckrodt Inc., Paris, Kentucky). This water was used for all experiments including rinsing of glassware.

1.8 M anhydrous aluminium chloride (Anachemia) in nitrobenzene (Baker analyzed reagent). This solution was prepared from freshly opened bottles and used immediately.

Formaldehyde (36-38%) was reagent grade (MaArthur Chemical Co.) and used as supplied.

8-hydroxyquinoline (8-hydroxyquinol, m.p. 74-76 °C) was used as supplied by Aldrich Co. Its structure is:

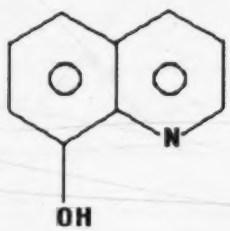

Sodium hydroxide (BDH analytical grade). Sodium carbonate was precipitated by allowing a 50% w/w NaOH solution to stand overnight. Standard NaOH was prepared by diluting the supernatant with freshly distilled boiled water (CO_2 free) followed by standardization against potassium hydrogen phthalate (Anachemia) that was dried overnight at 80 °C.

Acetate Buffer (0.1 M) was prepared by combining appropriate volumes of 0.1 M sodium acetate with 0.1 M acetic acid to give a final pH = 5.00.

Methanol, chloroform, and diethyl ether were all reagent grade and used as supplied.

Technical grade hydrogen chloride gas was obtained from Linde Div., Union Carbide Corp.

Other chemicals such as hydrochloric acid, nitric acid, acetic acid, sodium carbonate, sodium perchlorate monohydrate, anhydrous sodium sulfate, copper sulfate

pentahydrate, potassium hydrogen phthalate and sodium acetate trihydrate were all analytical grade and used as supplied.

Copper standards for AAS : An accurately known weight of copper powder (1 g) (Baker and Allied Chemical Corp.) was dissolved in about 10 mL of 50% nitric acid and the resulting solution was quantitatively transferred to a volumetric flask and diluted to 1 L with 1% HNO_3 (1008 ppm copper). Working standards were prepared by serial dilution of this stock solution with water, and their concentrations were confirmed by comparison with working standards prepared by dilution of a 1000 ppm copper certified AAS reference standard (Fisher Scientific Co.).

Amberlite XAD-2 resin was supplied by Rohm and Haas Co.,Philadelphia. Grinding of the XAD-2 resin has been previously described (60). The resin (40 g) was sieved and the fraction between 100-200 standard wire mesh (150-75 μM) was collected. Fines were removed by repeatedly (x3) slurrying the resin with methanol, allowing 20 min for sedimentation and then decanting the methanol. The resin was successively washed with water, 1.2 M HCl, water, 1 M NaOH, water and then methanol. Finally, the resulting resin was dried overnight in a vacuum oven at 50 °C.

Both XAD-2 and the XAD-oxine resin surfaces are hydrophobic and thus aqueous solutions cannot easily get into the pores. Therefore, throughout in this study, the resin was first wetted with a small amount of methanol which was then displaced with the appropriate aqueous solution.

2.2.3 Preparation of 5-chloromethyl-8-hydroxyquinoline hydrochloride

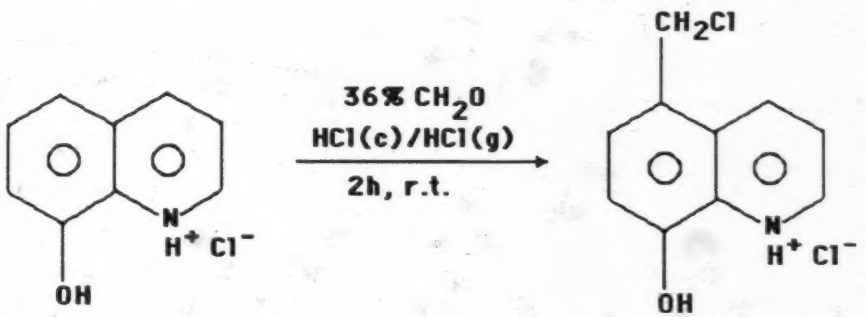

Oxine Hydrochloride

5-ClMe-oxine Hydrochloride

The chloromethylated derivative of 8-hydroxyquinoline was prepared as described in the literature (61,62). A mixture of 20.1 g of 8-hydroxyquinoline, 60 mL of conc. hydrochloric acid and 60 mL of 36-38% formaldehyde was stirred while HCl gas (CAUTION: use a safety trap) was passed into the solution over a period of 2 h. The mixture was kept overnight at room temperature. The yellow crystals which had formed were filtered, washed with diethyl ether and dried at 50 ^{o}C in vacuum to give a yield of 25.6 g (80%). Total analysis of this product was: 52.0% C, 6.13% N, 3.94% H and 29.4% Cl which was consistent to the calculated values of 52.2% C, 6.09% N, 3.91% H and 30.9% Cl. The NMR spectrum of the neutralized 5-chloromethyl-8-hydroxyquinoline (5-ClMe-oxine) in chloroform (section 2.2.5) was the same as that reported in the literature (63).

2.2.4 Immobilization of methyl-8-hydroxyquinoline on XAD-2

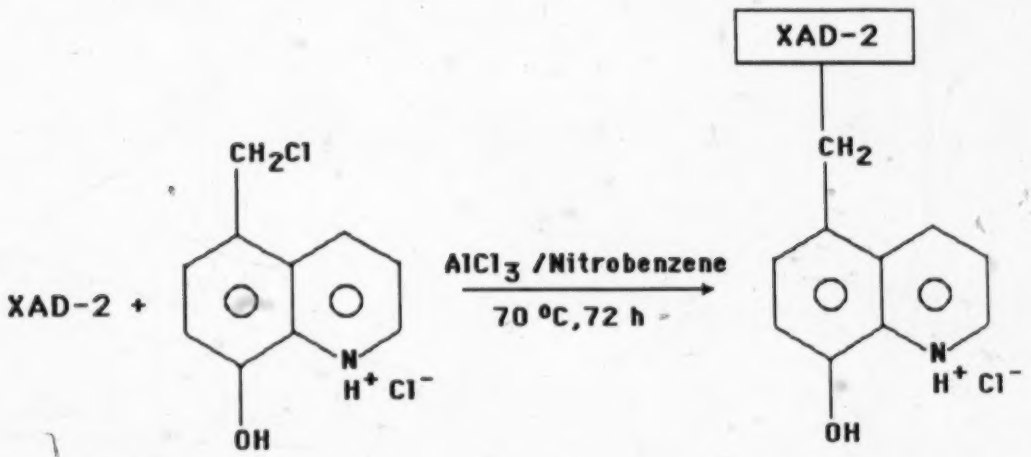

XAD-oxine

The procedure by Warshawsky *et al.* (45,59) was used. A mixture of 4.0 g XAD-2, 12 mL of freshly prepared anhydrous $AlCl_3$ in nitrobenzene (1.8 M) and 1.84 g 5-ClMe-oxine hydrochloride was stirred for 72 h at 70 °C. The mixture was then poured into 100 mL of methanol, filtered, and washed successively with 100 mL of methanol, 200 ml of 1:1 hot methanol/conc. hydrochloric acid, 100 mL of methanol,100 mL of chloroform, and finally with 100 mL of diethyl ether. The brownish free flowing resin which will be referred as XAD-oxine was dried in vacuum at 70 °C overnight.

2.2.5 Adsorption of 5-chloromethyl-8-hydroxyquinoline on XAD-2

The 5-ClMe-oxine was adsorbed on the resin by the procedure of Warshawsky and Kalir (59). An aqueous solution of 5-ClMe-oxine HCl (2.6 g in 120 mL) was

neutralized with excess sodium bicarbonate (4 g). The resulting precipitate was extracted with 3 - 100 mL portions of chloroform, the combined extracts were then dried with anhydrous Na_2SO_4 and the volume reduced to 40 mL under vacuum. The XAD-2 resin (4.0 g) was added and allowed to remain for 5 h. The chloroform was removed under vacuum, and the remaining derivative on the flask walls was transferred to the resin by repeatedly (x3) adding 5 mL of $CHCl_3$ and removing it under vacuum. The final product was a cream colored lump which was easily broken up with a spatula.

2.2.6 **Determination of the capacity of the resin**

The XAD-oxine resin (0.5 g) was wetted with water by first wetting with methanol then changing the solvent to water. Resin particles that were not wetted with water floated on the surface and were removed during decantation. The water-wetted XAD-oxine was equilibrated for 36 h with 50 mL of a solution containing 0.1 M $CuSO_4$ and 0.1 M acetate buffer (pH 5.00). The mixture was transferred to a tared sintered glass funnel (10-20 μM), the copper solution filtered off, and the resin washed with water until copper in the filtrate could not be detected by AAS. The sorbed Cu^{+2} was eluted (gravity flow) with 0.1 M HNO_3 and 50 mL fractions were collected in volumetric flasks. The total copper per 50 mL fraction was determined by AAS. The resin in the sintered funnel was dried to constant weight under vacuum.

2.2.7. **Microanalysis**

Samples of XAD-oxine were converted to the cationic hydrochloride form by allowing 200 mL of 1 M HCl to flow by gravity through 0.2 g of resin in a sintered glass funnel (10-20 μm). Excess HCl was removed in a vacuum oven at room temperature. Microanalysis for C, H and N were performed using standard methods by the Microanalytical Laboratory of the University of Alberta Chemistry Department.

2.2.8 Titration of the XAD-oxine resin

The titration cell consisted of a plastic beaker fitted with a Teflon cover having 3 holes for the following to pass through: a standard combination pH electrode (Fisher Scientific Co.), the tip of a 2 mL micrometer buret (Roger Gilmont, Great Neck, N.Y.) and a Pasteur pipet tip through which N_2 flowed. A weighed quantity of the cation form of the XAD-oxine, which was described in section 2.2.7, was placed in the empty titration cell. The resin was wetted with 2 mL of methanol, and 198 mL of the appropriate aqueous solution (0.1 M $NaClO_4$ or 0.1 M NaCl or no electrolyte) was added. The mixture was allowed to equilibrate overnight under N_2 which was first made CO_2 free by passing through a drying tube containing Ascarite (Arthur H. Thomas Co., Philadelphia), and was then water saturated with a bubbler. The titration cell was thermostated by placing it in a glass jacketed beaker and circulating water from the water bath maintained at 25 °C. The apparatus was then placed on top of a magnetic stirrer (Fisher Scientific Co.) to stir the suspension. The pH was monitored continuously by connecting a chart recorder (Fisher Recordall 5000) to the pH meter. Increments of standardized 0.1 M NaOH were delivered from the microburet and the pH was monitored until constant between the addition of each increment. Blanks consist of the HCl washed XAD-2 resin in the corresponding aqueous solution.

2.3 Results and Discussion:

2.3.1 Stability

Immobilization of 8-hydroxyquinoline on XAD-2 was chosen because of the reported stability of the XAD-oxine with respect to extremes of pH (64,51). In contrast for 8-hydroxyquinoline immobilized on silica substrates (silica gel or glass beads), hydrolysis occurs at alkaline conditions (57,42) and for condensation resins of the type resorcinal-formaldehyde-8-hydroxyquinoline, stability in acid solutions is reported to be low (65).

To determine the stability of the XAD-oxine, 0.1 g samples were soaked for 3 days in 5 mL of 1 M HCl, 1 M NaOH, or water. For the resin in NaOH, the resin color was slightly darker than in water, but the solutions above the resin samples in NaOH and water both remained colorless. Darkening of the XAD-oxine in basic solution is probably due to the formation of anionic oxine. On the other hand, for the resin in HCl, the solution above the resin had a yellowish tinge.

Furthermore, XAD-oxine samples that were allowed to soak overnight in 2 M HNO_3 leached a yellow color. The UV-VIS spectrum of the yellow leachate obtained by overnight soaking in 2 M HNO_3 and subsequent dilution with methanol was similar to that of 5-ClMe-oxine in methanol (λ_{max} = 370 nm). The leached color becomes more intense (darker) with increasing HNO_3 concentration (0.1-2.0 M). In contrast, pure XAD-2 soaked in HNO_3 does not give any measurable absorbance at over wavelengths of 300 nm. Also 5-ClMe-oxine adsorbed on XAD-2 (section 2.2.5) was easily washed off with methanol (λ_{max} = 320 nm) and no yellow leachings were obtained it was when subsequently soaked in 2 M HNO_3.

Attempts to exhaustively extract the yellow color from the XAD-oxine with a variety of solvents (methanol, chloroform, toluene) by Soxhlet extraction failed. The yellow leachings were found to appear in the organic solvents only after the XAD-oxine was soaked in strong acid. This suggests that the oxine is chemically bound to the XAD-2 surface, and long periods of contact with strong acid cleaves the bond. Thus, in subsequent experiments the resin was allowed to contact the acid eluent for the minimum required time. These conditions did not appear to remove significant amounts of bound oxine from the resin. After months of daily use, resin columns did not show a decrease in its ability to sorb Mg^{+2}.

2.3.2 **Capacity:**

The sorptive capacity of the XAD-oxine resin for metal ions reflects the metal-chelate interaction and is the most important parameter in experimentally characterizing the chelating groups. Equilibration of the resin in excess Cu^{+2} at pH 5.00 is the standard procedure for measuring sorptive capacity (66,51,65). The experimentally measured sorptive capacity can be compared to the theoretical capacity which expresses the amount of complexing groups per unit wt of resin, and can differ from the theoretical capacity.

Assuming Cu^{+2} forms a 1:1 complex with the immobilized oxine (66,51), the experimentally measured sorptive capacity of XAD-oxine was 264 ± 2 μmol/g of dry resin. This compares to a theoretical capacity of 440 ± 20 μmol/g of resin on the basis of nitrogen content obtained by microanalysis. The XAD-oxine sample used for microanalysis never contacted nitric acid. The lower sorptive capacity could possibility be due to the occurrence of some 1:2 complexation or to having some of the complexing groups inaccessible to Cu^{+2} owing to steric hindrance (51,48,67). This observation is consistent with subsequent observations that will be discussed in sections 3.3.6 and 4.3.3.4.

After about 100 h in contact with HNO_3 solutions the sorptive capacity had been decreased to 110 ± 6 μmol/g of dry resin. Microanalysis of the XAD-oxine, that was used for stability studies, gave theoretical capacities of 600 ± 50 μmol/g. This discrepancy suggests that nitrogen other than that in oxine may be present on the resin. On the assumption that it is coming from sorbed nitrate ions, the resin was washed in an attempt to remove these ions. Washing the resin with 1:1 HCl/MeOH (250 mL) and 2 M HCl (500 mL) did not significantly decrease the nitrogen content. Presumably, more extensive acid washing will be required to desorb the nitrate. Thus, no meaningful results would be obtained by extended acid washing because the oxine will be desorbed.

A curve showing the desorption of Cu^{+2} from XAD-oxine with 0.1 M HNO_3 is presented in Fig 2.1, where it can be seen that 300 mL of eluent/0.5 g of resin removed 95% of the total Cu^{+2} and roughly 500 mL/0.5 g of resin is required for 99% removal of the copper. This corresponds to a minimum requirement of 1 L eluent/g of resin (or 1 mL/mg).

2.3.3 Titration of resin

Data from potentiometric titrations are usually used to characterize the acidic and basic properties of immobilized chelating agents (48,66,68-73). In the simplest models, dissociation constants of the functional groups are calculated from the Henderson-Hasselbalch equation (48). More commonly, description of the protonation equilibria of chelating resins are based on models used for ion-exchange resins, e.g. the polyelectrolyte gel model (74-76). A more appropriate model for chelating resins considers the equilibrium existing between the components of the resin and solution phases (71-73).

A typical titration curve for XAD-oxine against standardized NaOH is shown in Fig 2.2. Besides an ill defined end point, an additional problem of very long times of 1-3 h was required to get a reasonably constant pH reading after the addition of an increment of NaOH. Drifting of the pH reading was observed even 10 h after the last increment addition. Attempts to increase the kinetics of the titration by grinding the XAD-oxine to pass through No. 325 standard mesh (< 45 μm) proved unsuccessful. A sharper end point was obtained when the smaller size XAD-oxine was titrated, but there was no improvement in the time required to achieve equilibrium after the addition of each increment of NaOH. These observations of slow titration kinetics were previously reported for immobilized oxine bound to silica gel (69) which suggests that the titration was because of slow chemical kinetics. Because of the slow kinetics, the acid - base properties of XAD-oxine were not investigated any further.

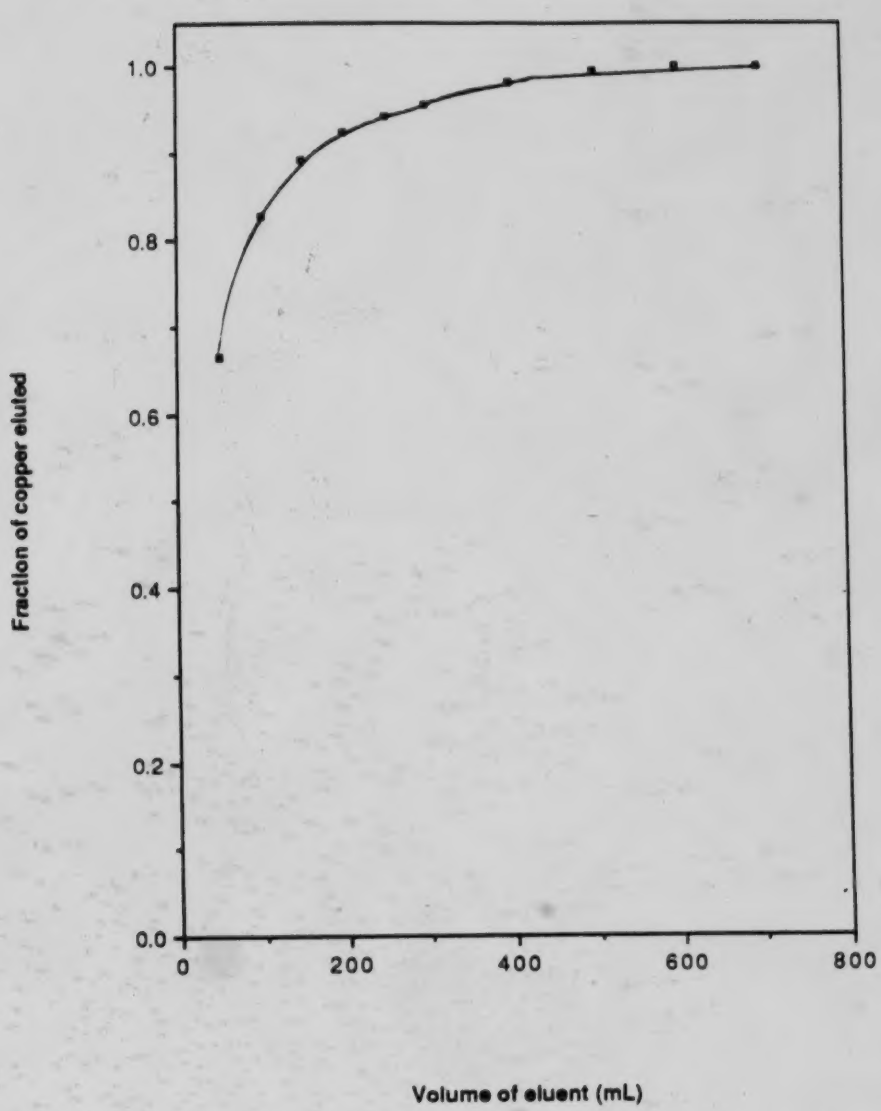

Fig 2.1: Fraction of copper eluted with 0.1 M HNO_3 from 0.5 g XAD-oxine

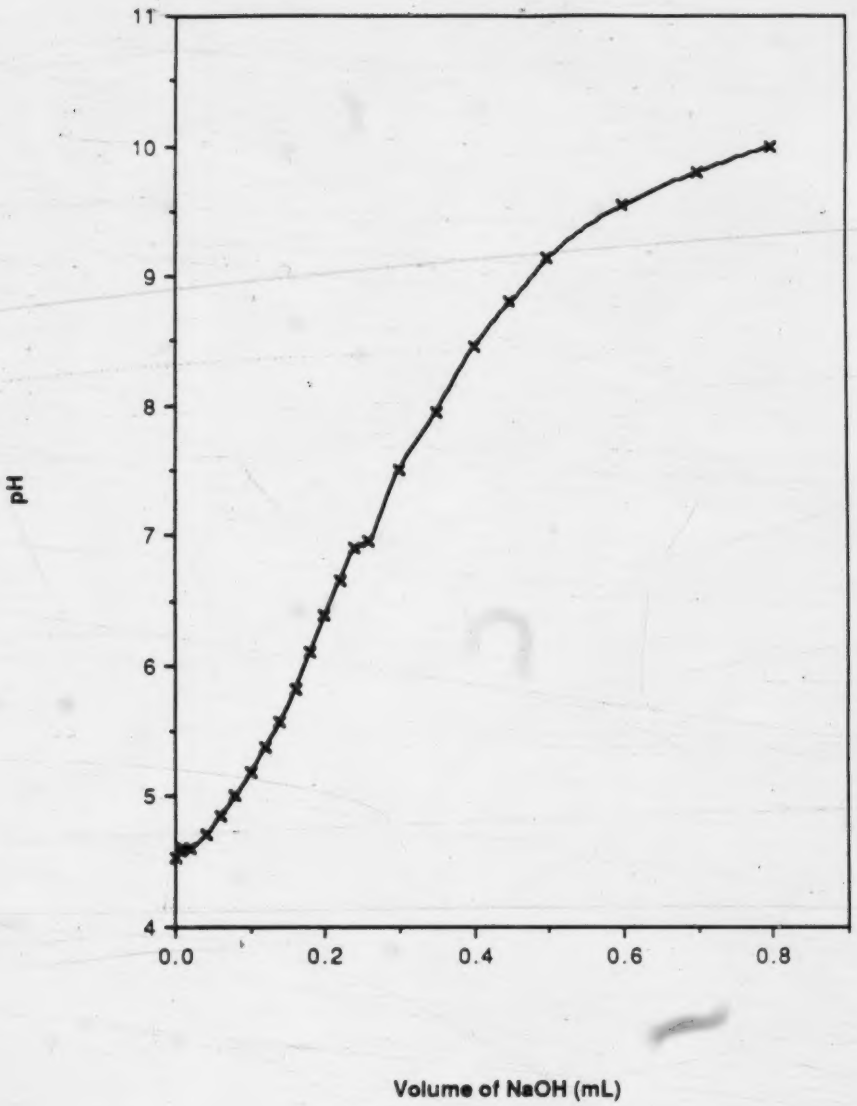

Fig 2.2: Titration of 0.4669 g XAD-oxine with 0.139 M NaOH

CHAPTER 3

SORPTION BEHAVIOR OF Mg^{+2} ON XAD-2 IN THE COLUMN EQUILIBRATION EXPERIMENTS

3.1 Introduction

The flow through column equilibration method using XAD-oxine was chosen to measure [Mg^{+2}]. The principle of the method has been presented in greater detail for sulfonated resin (32,37,38,68,77,78). By analogy, the same principle is applicable for XAD-oxine. Consider the simplified case of a solution containing magnesium and ligand ions forming two complexes i.e.

$$Mg^{+2} \overset{L^-}{\rightleftharpoons} MgL^{+} \overset{L^-}{\rightleftharpoons} MgL_2 \quad \text{..... 3.1}$$

The XAD-oxine ionizes with the the following equilibria

$$R\text{-}Ox^{-} \overset{H^+}{\rightleftharpoons} R\text{-}OxH \overset{H^+}{\rightleftharpoons} R\text{-}OxH_2^{+} \quad \text{..... 3.2}$$

The column equilibration technique is based on equilibration between the magnesium-ligand solution and the XAD-oxine. In other words, the ionized oxine on the XAD-oxine (R-Ox^-) forms a metal chelate complex with Mg^{+2} i.e.

$$R\text{-}Ox^{-} \overset{Mg^{+2}}{\rightleftharpoons} R\text{-}OxMg^{+} \quad \text{..... 3.3}$$

The equilibration technique requires all species in both phases be at equilibrium i.e. equations 3.1, 3.2 and 3.3 are in simultaneous equilibrium. In this technique, trace

loading of the column is desirable i.e. only a small fraction of the oxine sites (< 1%) is used for sorption of Mg^{+2}. In other words, at trace loading:

$$[R\text{-}OxH_2^+] + [R\text{-}OxH] + [R\text{-}Ox^-] >> [R\text{-}OxMg^+] \quad \text{..... 3.4}$$

Trace loading is achieved by fixing the pH and ionic strength so that the conditional formation constant is low, and the distribution ratio λ_o, is constant. λ_o for Mg^{+2} is defined as:

$$\lambda_o = \frac{[Mg^{+2}]_R}{[Mg^{+2}]} \quad \text{..... 3.5}$$

where $[Mg^{+2}]_R$ is the concentration of magnesium in the resin phase.

After column equilibration, the sorbed cation is removed with a suitable eluent, with or without a prior water wash, and the amount of sorbed Mg^{+2} is determined in the eluent. For cases where there is a water wash prior to elution, the amount of Mg^{+2} in the eluent is directly proportional to the $[Mg^{+2}]_R$, hence the $[Mg^{+2}]$ in the test solution under constant instrumental conditions. In the other case without a water wash prior to elution, the amount of magnesium in the interstitial fluid is determined and then subtracted from the total amount of magnesium in the eluent. The difference is the amount of sorbed Mg^{+2} which is proportional to $[Mg^{+2}]$ in the test solution.

The principle of the column equilibration technique is illustrated in Fig 3.1.a. Essentially, the test solution is passed through a column (containing a known weight of resin) until equilibration is achieved. In other words, the metal ion concentration in the influent (C_i) is the same as the concentration in the effluent (C_e). If the ratio of C_i to C_e is plotted against the volume of eluent, a curve similar to Fig 3.1.b will be obtained.

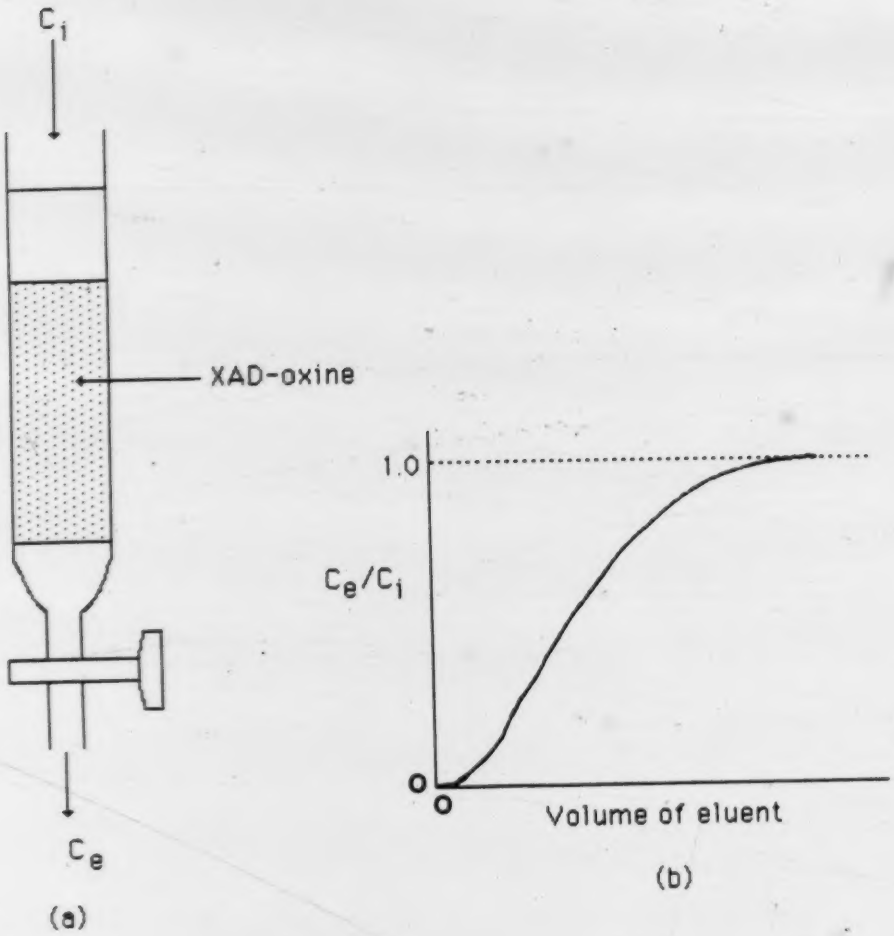

Fig 3.1: Technique of column equilibration (a) apparatus and (b) breakthrough curve.

When the ratio of C_i to C_e is 1.0, the column is in equilibrium with the test solution, and complete "column breakthrough" has been achieved.

In this study, the previously described miniaturized, semiautomated flow system (37) will be used for column equilibration determination of $[Mg^{+2}]$ with XAD-oxine. The design and procedural details of this with washing version of the column equilibration experiment will be given later on in this chapter, but it is essentially involves 4 steps for every measurement viz. (a) the resin in the column is brought to equilibrium with a test solution (i.e. load step); (b) the interstitial test solution is removed with a water wash; (c) the sorbed Mg^{+2} is eluted directly into an AAS, and; (d) the column is washed with water before another a load step.

In the second version of the column equilibration technique (i.e. without washing) a slightly altered miniaturized, semiautomated flow system without water washing steps will also be used for column equilibration determination of $[Mg^{+2}]$ with XAD-oxine. This without washing system has two steps: a load step (equilibration) and an elution step.

Chapter 3 is concerned with optimization of the experimental parameters of these two column equilibration experiments (i.e. with and without washing) in order to measure $[Mg^{+2}]$. The approach used will be to study each individual parameter while the other experimental parameters are held constant. After choosing the optimum parameter for each experimental variable, all experiments were repeated using the chosen optimum parameter. In studies reported in this chapter no ligand was present in the magnesium containing solutions. Also investigated in Chapter 3 are the solution variables that influence the free metal determination.

3.2 Experimental

3.2.1 Chemicals and Reagents

Magnesium standards: A 1000 ppm stock solution was prepared by cautiously dissolving an accurately known weight of magnesium (Fisher Scientific Co.) in 6 M HNO_3,

and diluting with 1% HNO_3 to an accurately known volume. The concentration of this stock solution was checked against magnesium standards prepared from serial dilution of 1000 ppm Fisher Certified AAS Reference standards.

0.1 M Buffer stock solution: PIPES, piperazine-N,N'-bis[2-ethanesulfonic acid] (Sigma Chemical Co.) was dissolved with the aid of 50% w/w NaOH. Prior to dilution to the final volume, the pH was adjusted to 6.00 by the addition of 1 M HCl or NaOH.

1 M Sodium Chloride (BDH Analytical Reagent) was used for ionic strength adjustments. For column equilibrium experiments without washing, traces of Mg^{+2} were removed by passing this 1 M NaCl solution through a 16 cm x 2.5 cm bed of Dowex Chelating resin (Sigma Chemical Corp.)

1 M Disodium Ethylenediammine - tetraacetic acid,EDTA(Fisher Certified Reagent) was dissolved with the aid of 50% NaOH. Prior to dilution to final volume, the pH was adjusted by the addition of NaOH to the pH at which studies were done.

XAD-oxine and XAD-2 were prepared as described in sections 2.2.4 and 2.2.2 respectively.

Distilled deionized water, NaOH, Cu AAS standards and nitric acid were the same as described in section 2.2.2.

3.2.2 Apparatus

3.2.2.1 Apparatus used for experiments with washing after column equilibration

The instrumental setup was similar to that previously used with CPG-oxine (38) except valves V_1,V_2,V_3, and V_4 were all 4-way slider valves (Laboratory Data Control, Milton Roy Co.) as shown in Fig 3.2. The variable speed peristaltic pump (Minipuls 2, Gilson, Villers-le-Bel, France) was fitted with three 0.09 in. i.d. clear Tygon pump tubes (Cole - Palmer Instrument Co.,Ill.). One tube pumped the test solution to the two coupled valves V_2 and V_3. The other two tubes pumped water and eluent to valve V_1 which,

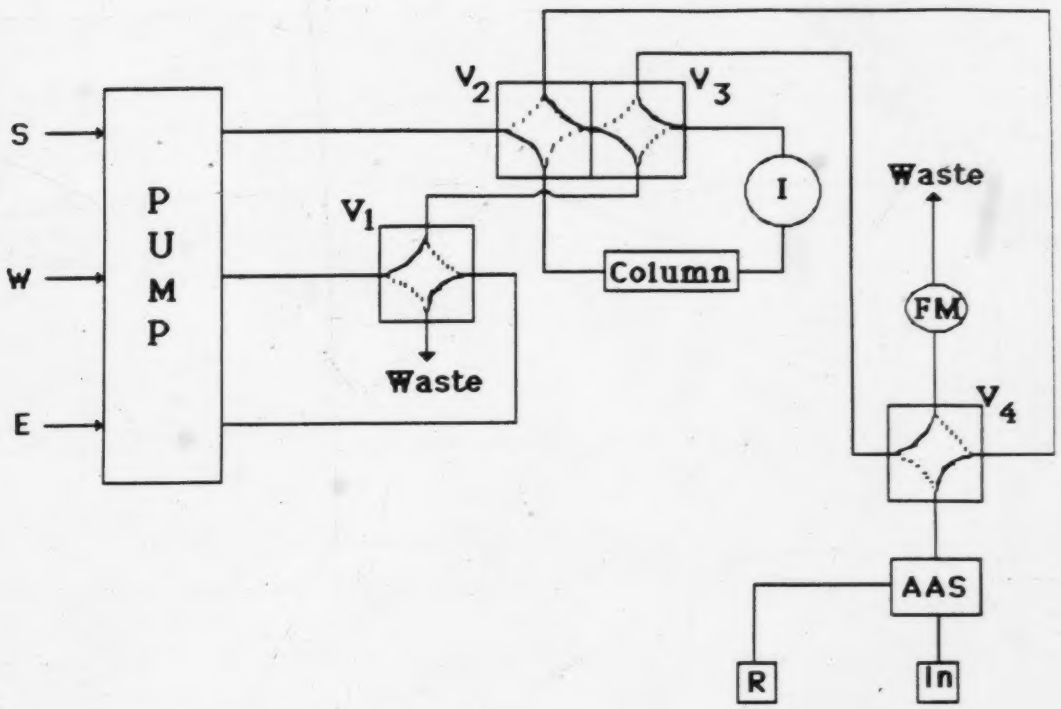

Fig 3.2: Apparatus for column equilibration with washing. S - sample line; W - water line; E - eluent line; V_1, V_2, V_3, V_4 - 4-way slider valves; FM - flow meter; AAS - Model 290B; R - chart recorder; I - 10 µL injection valve and In - Integrator. Full lines represent fluid flow during loading and dotted lines represent washing/elution fluid flow.

depending on its position, allowed water or eluent to flow into the two coupled valves. The [illegible]led valves V_2 and V_3 were mechanically coupled so that they were switched simultaneously. They were used to direct either sample solution or the water-eluent line through the column. The outlet flow from the coupled valves was fed into valve V_4. Normally,except during flow rate measurements, V_4 diverts the sample line to the waste and the water-eluent line to the nebulizer of the model 290B PE AAS. Valve I, was a 10 µL slider injection valve, located between valve V_3 and the column. It was used to inject known volumes of Mg^{+2} standard solution into the eluent stream upstream of the column for calibration purposes. The flow meter FM, (home made from a 25 mL buret) was placed on one outlet of V_4. Flow rates were measured with FM and a stopwatch, while fluid flows through the column. Usually, a pump setting of 550 to 600 maintains a flow rate of 4.5 to 5.0 mL/min for all 3 lines. All connecting tubing was 0.5 mm i.d. Teflon (Laboratory Data Control).

The column was connected between valves V_2 and V_3 with 20 cm pieces of 0.5 mm i.d. tubing to allow immersion into a water bath in a jacketed beaker. A model R20 Haake circulating thermostatted water bath was used to circulate water at 25 ± 0.5 ^{o}C through the water jacketed beaker.

Magnesium concentration was monitored with a Model 290B Perkin-Elmer flame atomic absorption spectrophotometer (AAS) fitted with either a Mg-Ca or Mg hollow cathode lamp. A strip chart recorder (Fisher Recordall 5000) was used to trace the analog signal. The magnesium concentration was determined using the 285.2 nm line using lamp currents of 4 mA for Mg and 6 mA for Ca-Mg. The other AAS and recorder settings are listed in Table 2.1. Peak areas, expressed as counts, were measured with a Model 3390A Reporting Integrator (Hewlett - Packard Co.) with the following settings: Zero = 0; Attenuation = 4; Chart speed = 1.0 cm/min; Data sampling (PK WT) = 0.04; Noise rejection (THRSH) = 4, and; Peak rejection (AR REJ) = 0.

Measurements of pH were performed in the same manner as described in section 2.2.1.

3.2.2.2. Apparatus used for experiments without washing after column equilibration

A schematic diagram of the flow system designed without a water wash step is shown in Fig 3.3. Essentially, it is similar to Fig 3.2, except the water line and valve V_1 were removed, V_4 was replaced by a 3 way valve and a Model 4000 Perkin-Elmer AAS was used. V_2 and V_3 are the same mechanically coupled valves. However, they are shown separately in Fig 3.3. to illustrate void volume contributions of the tubes connecting ports of V_2 and V_3.

With the exclusion of the wash step, the signal detected will be the sum of both the Mg^{+2} sorbed by the resin and that in the interstitial fluid (i.e. void volume). For this reason, reduction of the void volume was a major consideration in the design of this system. Since the interstitial fluid in lines A and B was included in the void volume when the valves were switched to elution mode, their volumes were reduced to a minimum by using 9 cm x 0.3 mm i.d. Teflon tube. One end of the column was directly connected to the port of the coupled valves to eliminate the necessity of using an extra connecting tube. Because of the considerable reduction of tubing length between the column and the coupled valves, the column was not thermostated in a water bath.

Magnesium concentration was monitored with a Model 4000 Perkin-Elmer AAS equipped with a Perkin - Elmer Burner control unit and a Model PRS 10 printer sequencer (Perkin - Elmer) to provide a printout of the desired signal. Integration of the eluted peak was done with the internal integrator of the Model 4000 AAS. Also, a stripchart recorder (Fisher Recordall 5000) was used to follow the analog signal. The flow system - AAS parameters are listed in Table 3.1.

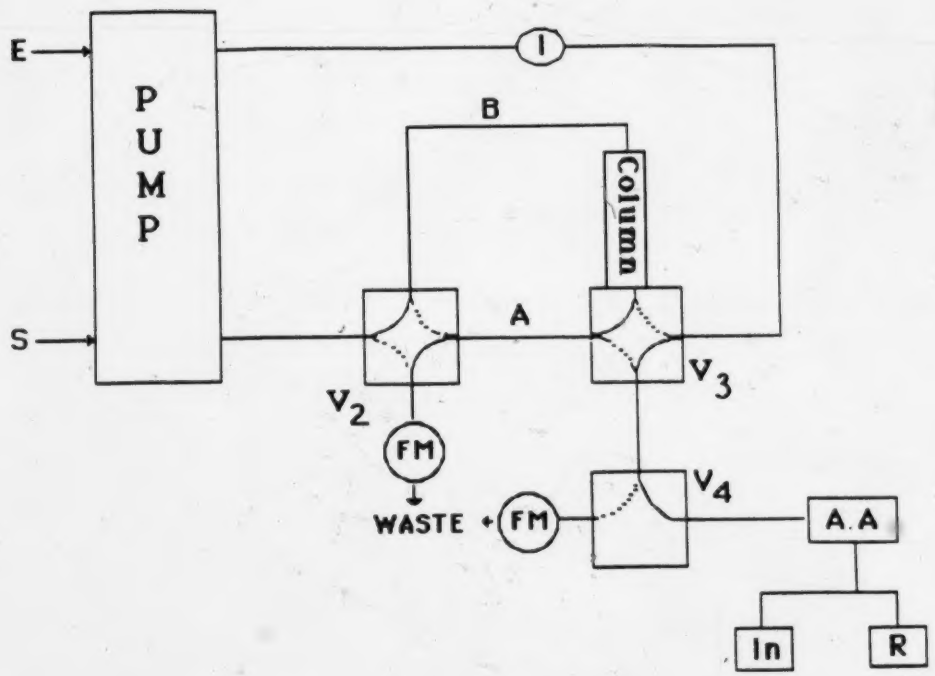

Fig 3.3: Apparatus for column equilibration without washing. S - sample line; E - eluent line; V_2, V_3 - 4-way slider valves; V_4 - 3-way slider valve; FM - flow meter; AAS - Model 4000; R - chart recorder; I - 10 µL injection valve; In - Integrator; A and B - 9 cm x 0.3 mm i.d. Teflon tube. Full lines represent fluid flow during loading and dotted lines represent elution fluid flow.

Table 3.1: Instrumental conditions used for the Model 4000 Perkin-Elmer atomic absorption spectrophotometer in the without washing flow system.

Parameter	Setting
Wavelength	285.2 nm (Mg); 324.8 nm (Cu)
Spectral slit width	0.7 nm
Lamp current	6 mA (Mg); 10 mA (Cu)
Flame	Oxidizing (lean,blue)
Mode	Absorbance
Signal	Peak Area
Integration time	30 s
Acetylene pressure	12 psig
Air pressure	30 psig
Pump setting	550 (4.5-5.0 ml/min)
Nebulizer	Flow spoiler
Recorder	Fisher Recordall 5000
Recorder voltage range	10 mV
Chart speed	2.5 cm/min

3.2.3 Column equilibration procedure

3.2.3.1 Procedure for experiments with washing after column equilibration

The solid lines in Fig 3.2 show the simultaneous flow of sample, water and eluent during the loading step. The magnesium-containing solution flows through the column via valves V_2 and V_3 then to V_4. Eluent flows to the waste through V_1, and water flows to V_4 via V_1, V_2 and V_3. To prevent fouling and deposition of salts on the nebulizer, V_4 was set so that water goes into the AAS and the magnesium containing solution goes to the waste. The time required to achieve complete column breakthrough (i.e. equilibration) was determined from equilibration studies in section 3.3.2 below.

After column equilibration was achieved, the interstital magnesium solution was removed by switching the coupled valves V_2 and V_3. The flow system was designed so that the column was washed in the reverse direction. Also V_4 was switched so that the wash water goes into the nebulizer. The time required for washing was determined from washing studies described in section 3.3.3 below.

After washing, valve V_1 was switched so that the eluent takes the place of water. Immediately after switching V_1, the integrator was turned on. The eluted peak takes about 10 s to reach the flame on switching V_1. This was found to be enough time for the integrator to set the baseline. Also, with the integrator conditions given in section 3.2.2.1, it automatically decides the tail of the peak. Integrator readings were given as counts. Optimum elution time will be discussed in section 3.3.4 below. After the peak was eluted and baseline established, V_1 was switched to give another water wash before the start of another sample loading step. Pump flow rates through the column was periodically checked with the flow meter FM, and a stopwatch.

Throughout all column equilibration procedures, the 10 µL injection valve I, was used to inject known concentration of Mg^{+2} standards into the eluent stream when all the valves were in the elution mode. The most convenient time for this injection was

immediately after elution of the sorbed Mg^{+2} from the column. This standard injection step was done to check for instrumental drift and changes in flow rate. As well, it serves to calibrate the AAS-flow system and thus allows comparison of all peak areas throughout this study.

Throughout this thesis, this procedure will be referred as with washing. Unless otherwise stated, the following conditions will be used for the with washing procedure : pump flow rates = (4.5-5.0) ± 0.1 mL/min; load = 5 min; water wash = 2 min; elution with 0.1 M HNO_3 = 2 min; water wash = 2 min; [PIPES] = 0.01 M; ionic strength = 0.1 M, and the AAS was a Model 290B.

3.2.3.2 Procedure for experiments without washing after column equilibration

The solid lines in Fig 3.3 show the flow of eluent and test solution during column equilibration (loading). The test solution flows through the column via the coupled valves V_2 and V_3 to waste. Eluent flows to the AAS via V_3 of the coupled valves and V_4. Loading times under various conditions will be discussed in section 3.3.2.

After column equilibration, the sorbed Mg^{+2} was eluted without prior removal of the interstital fluid, by switching the coupled valves. The dotted lines on V_2 and V_3 show the flow of eluent and test solution during elution. Test solution goes to waste via V_2, while eluent flows through the column, in the reverse direction, to the AAS via V_4. Normally V_4 was set so that eluent enters the AAS, but during flow rate measurements of the eluent through the column, V_4 was set to flow through FM. At about 1 min prior to elution of the magnesium, the integrator was triggered and then zeroed. Immediately, upon switching the coupled valves the AAS integrator was triggered, and data was collected for 30 s. This time was enough to allow the eluted peak to reach the AAS (5-10 s) and allow the peak to reach baseline (width at baseline ~ 15 s). The Model 4000 AAS gives integrator readings as (Absorbance x s). The measured P.A. ($P.A._{tot}$) was the sum of the P.A. due to sorption by

the resin plus the P.A. contribution due to the interstitial fluid (void volume, P.A. $_{void}$). After the eluted magnesium peak was integrated, 10 µL of a known concentration of Mg^{+2} was injected (using I) into the HNO_3 stream. The choice of eluent and elution time was determined as discussed in section 3.3.4. On completion of elution, the coupled valves were switched back for another load step.

The P.A. contribution due to test solution in the void volume was determined as follows: Using the 10 µL injection valve I, 4.02 x 10^{-4} M Mg^{+2} solution was injected into the eluent stream with all the valves set to the elution mode. From the measured P.A., the mol/unit P.A., X was calculated with equation 3.6

$$X = \frac{(\text{Vol injected})\,[Mg]_{inj}}{\text{P.A.}} \qquad \text{.....3.6}$$

Next the void volume V_m was determined by measuring the eluted peak area after known concentrations of Mg^{+2}, dissolved in the eluent ($C_{Mg,std}$), were loaded for 5 min. Because the magnesium was prepared in the eluent (dil HNO_3), the resin will not sorb Mg^{+2} and the measured P.A. will be only due to the magnesium in the void volume. V_m was calculated using equation 3.7

$$V_m = \frac{X(\text{P.A.})}{C_{Mg,std}} \qquad \text{.....3.7}$$

The P.A. contribution (P.A.$_{void}$) due to the void volume was calculated as follows:

$$\text{P.A.}_{viod} = \frac{C_{Mg} V_m}{X} \qquad \text{.....3.8}$$

Finally the P.A. contribution due to Mg^{+2} sorbed on the resin during an equilibration experiment (P.A.$_{sorb}$) was calculated using equation 3.9

$$P.A._{sorb} = P.A._{tot} - P.A._{void} \quad \text{.....3.9}$$

where C_{Mg} is the concentration of magnesium in the test solution.

Throughout this thesis, this procedure will be referred as without washing. Unless otherwise stated, the following conditions will be used for the without washing procedure : pump flow rates = (4.5-5.00) ± 0.1 mL/min; [PIPES] = 0.001 M; load = 20 min; elution with 1 M HNO_3 = 2 min, and the AAS was the Model 4000 PE.

3.2.4 **Column construction**

Figure 3.4 shows the details of column construction. The two end fittings (B) and washers, A (Cheminert, Laboratory Data Control, Rivera Beach, Fl.) were fitted on a 50 mm x 1.5 mm Teflon column tube (E) and the 2 ends of the tube were flared. A cylindrical glass frit, C (2 mm long x 1.5 mm diameter) was inserted about 20 mm from one of the flared ends. Glass frits were made by drilling cores from a sintered glass plate (pore size 50 μm), followed by rolling/grinding on a piece of sand paper to a diameter that will tightly fit inside the 1.5 mm Teflon tube. A 1 cm length resin bed was packed by drawing up a methanolic slurry of the desired resin (XAD-2 or XAD-oxine) from the end farthest from the frit. This was followed by inserting another tight fitting frit to loosely sandwich the resin particles. Finally, the dead volume was reduced by inserting short pieces of 0.5 mm Teflon retaining tube (F) on either side of the glass frits.

Measurements of the resin weight per unit length of column tubing was made as follows: a 15 cm x 1.5 mm Tubing was flared at one end, and a glass frit was placed 1 cm from the flared end. A known length of resin bed (~ 10 cm) was slurry packed as above, then the resin was quantitatively transferred into a tared beaker by flowing methanol in the reverse direction. After evaporation of methanol, the resin was dried to constant weight.

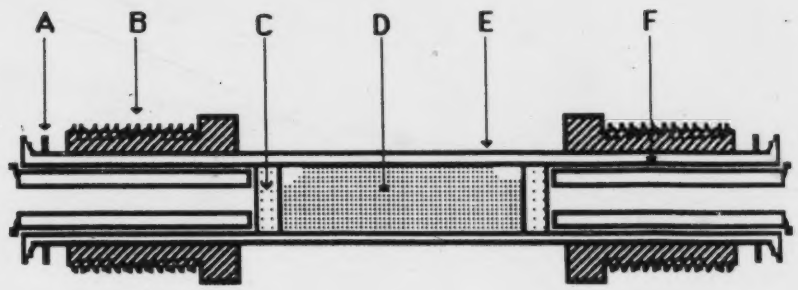

Fig 3.4: The column. A - 1.5 mm washer; B - end fitting; C - glass frit; D - resin bed; E - column tube, and; F - retaining tube.

3.2.5 Preparation of test solutions

The pH and ionic strength were accurately controlled in all test solutions. The pH was controlled with PIPES buffer which does not complex Mg^{+2} (79). In controlling the ionic strength, corrections were made for ionic strength contributions due to the buffer. Final adjustment to the desired ionic strength was made with NaCl.

For example, for a test solution having $C_{Mg} = 1.32 \times 10^{-5}$ M, $\mu = 0.100$ M, at a fixed pH, the following procedure was used: 10 mL of PIPES buffer solution (pH = 6.00, 0.100 M), 8.9 mL NaCl stock solution (1 M, pH ~ 6.0), 4.00 mL of Mg^{+2} stock solution (3.29×10^{-4} M) and about 20 mL water were added to a small beaker. The pH of the mixture was accurately adjusted to the desired pH between 5.00 to 7.00 with dilute NaOH or HCl. The mixture was quantitatively transferred into a 100 mL volumetric flask and then made up to mark. The pH of the final solution was rechecked and if necessary readjusted.

3.3 Results and discussion

3.3.1 Choice of variables for the AAS - flow system

In interfacing a flow system at an AAS, the limitations of the flow system and the AAS response to the flow system were taken into consideration. The major limitation of the flow system was that a maximum of 5.0 mL/min pumping flow rate could only be achieved after extended use, due to the column frits in the flow system. With newly made columns, the flow system can handle flow rates as high as 7 mL/min, but after a few hours of usage, the frits accumulate particles, become clogged, and can only sustain a pumping rate of about 5 mL/min for long periods. On the other hand, at the chosen pumping rate, it is desirable that the AAS response should be independent of the pump flow rate. In other words, the pumping flow rate should be at a plateau for a plot of AAS response against pumping flow rate.

In order to determine a suitable pumping flow rate, the peristaltic tube was connected directly to the Model 290B AAS nebulizer with a 50 cm piece of 0.5 mm i.d. Teflon tube. A solution containing only 8.23×10^{-6} M Mg^{+2} was pumped into the model 290B AAS and the relative absorbance measured. The AAS has its own "natural" aspiration rate which is dependent on the position of the nebulizer tip and the sample tube dimensions. Using a 50 cm x 0.5 mm i.d. sample capillary tube, the "natural" aspiration rate of water was 7.5 mL/min when all the AAS parameters were optimized. Using this nebulizer tip position, measurement of the AAS sensitivity at various pumping flow rates shows the AAS sensitivity was constant at rates > 4.0 mL/min (Fig 3.5). This is consistent with the observation of Triet *et al.* (37). Positioning the nebulizer tip to get different aspiration rates gives the same constant sensitivity at pumping rates > 4.0 mL/min and is consistent with previous observations (80). On the basis of these observations, a natural aspiration rate of 7.5 ml/min and a pumping flow rate of (4.5-5.0) ± 0.1 mL/min was chosen for magnesium measurements using the Model 290B AAS, which was used for all measurements using the with washing procedure.

With the Model 4000 AAS, the "natural" aspiration rate of water when all the AAS parameters were optimized, was 9 mL/min using a 50 cm x 0.5 mm i.d. sample tubing. At this optimized nebulizer tip position, the AAS sensitivity was constant between pumping flow rates of 4-6 mL/min (Fig 3.6) and starts to decease at pump rates > 7.0 mL/min. This decrease at high pump rates was previously observed (80). Thus, a pumping rate of (4.5-5.0) ± 0.2 mL/min was used for the PE 4000, which was used for all studies using the without washing procedure.

Peak areas rather than peak heights were chosen for quantification of magnesium, because of the lower % rel. std. dev. obtained for 12 replicate injections containing the same quantity of Mg^{+2}. Using the 10 µL injection valve I, known volumes of Mg^{+2} standards (1.23×10^{-4} M) were injected into the eluent stream when all the valves were positioned so that the eluent passes through the column to the 290B AAS. The rel. std. dev.

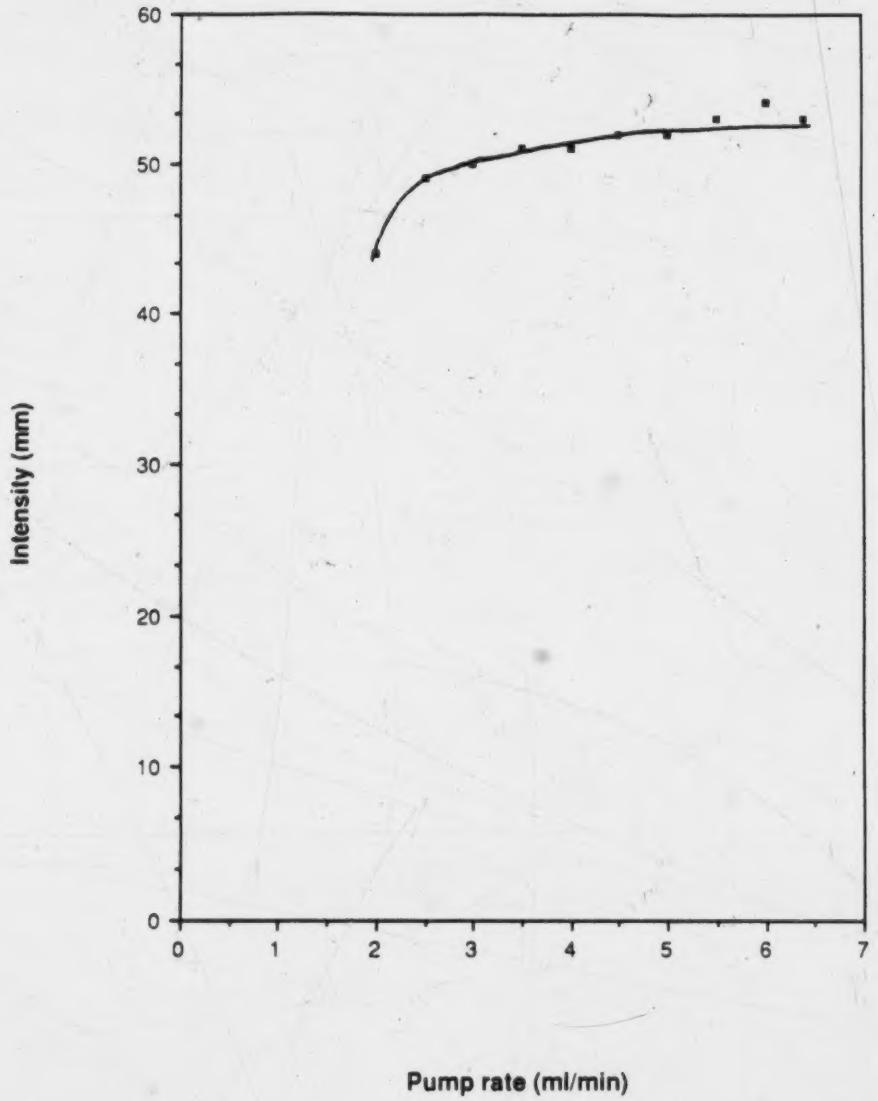

Fig 3.5: The signal height when a solution containing 8.23×10^{-6} M magnesium was pumped at various rates into the Model 290B Perkin-Elmer AAS.

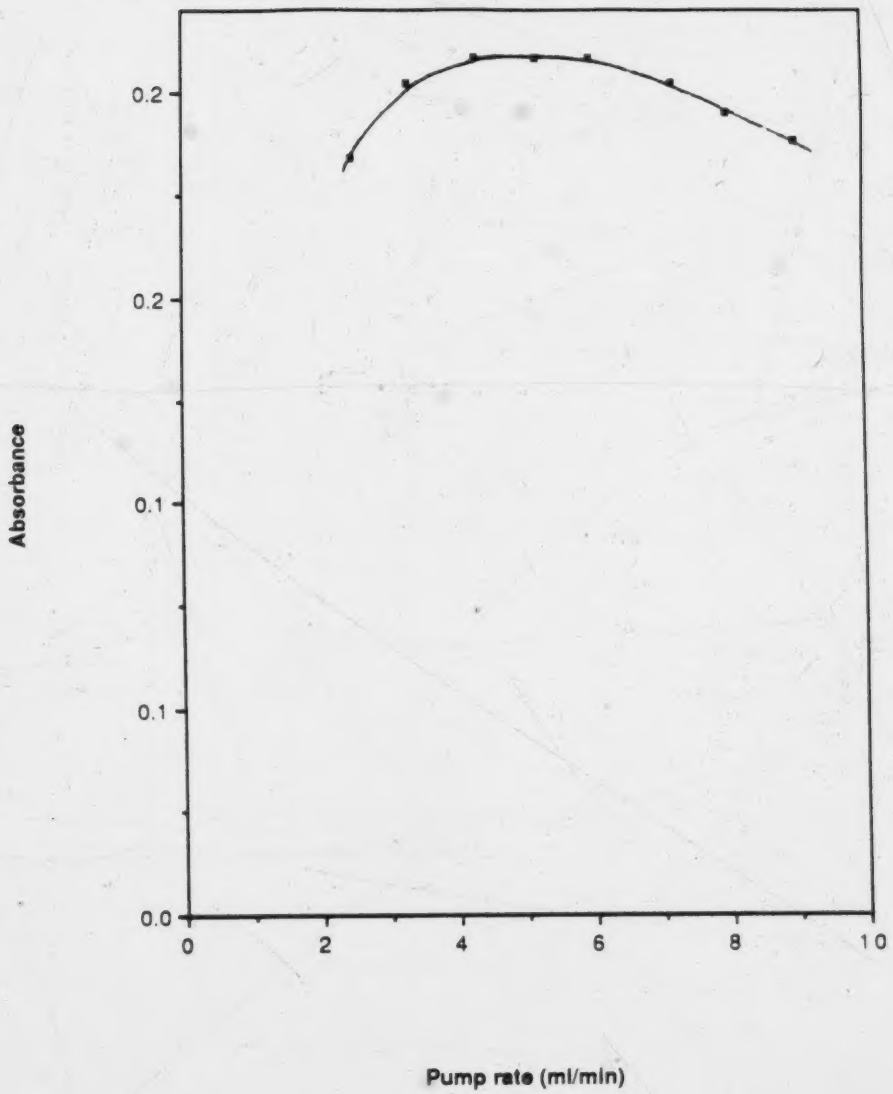

Fig 3.6: The signal height when a solution containing 1.23×10^{-5} M magnesium was pumped at various rates into the Model 4000 Perkin-Elmer AAS.

for the integrated peak areas was 4.5% as compared to 8.5% for the same peaks when their heights were measured on the chart recorder output. In addition, the use of peak areas eliminates the need to exactly match the width of the injected standard peaks with that of the eluted Mg^{+2} peaks in order to calculate the number of moles of eluted magnesium entering the nebulizer.

Peak areas however, were extremely sensitive to flow rate changes. Figure 3.7 shows the relative changes of peak height and peak area on the Model 290B AAS for the same concentration of Mg^{+2} standards injected into the eluent via valve I, when the eluent flow rate was varied. Peak areas and heights were obtained as above. The HP 3390A Integrator also gives the area/height ratio, which is shown in Fig 3.7. Because of the considerable effect of flow rate on P.A., pumping flow rates were periodically measured during every experiment, and if necessary, adjusted to remain within ± 0.1 mL of the nominal value. Also the frits on the column, after prolonged use (> 3.0 months), tend to become clogged and no longer permit flow rates > 4.5 mL/min. When this happens, columns were completely replaced.

In all column equilibration experiments, the P.A. and P.H. of the eluted peaks were always kept in the linear region of the AAS - flow system. The whole system linearity was checked by injecting varying concentrations of Mg^{+2} with the 10 µL injection valve into the HNO_3 stream. For both the Model 290B and Model 4000 AAS, the plot fo P.A. against number of moles injected was linear through the origin. Similarly, if peak heights on the recorder output were measured, the results were the same.

3.3.2 Column equilibration

Successful use of column equilibration requires complete breakthrough i.e. the resin bed is in complete equilibrium with the solution in contact with it. In other words, the composition of the effluent is identical with that of the influent, and the resin does not sorb anything more. Fig 3.8 shows the AAS signal obtained during a load, wash, elute and

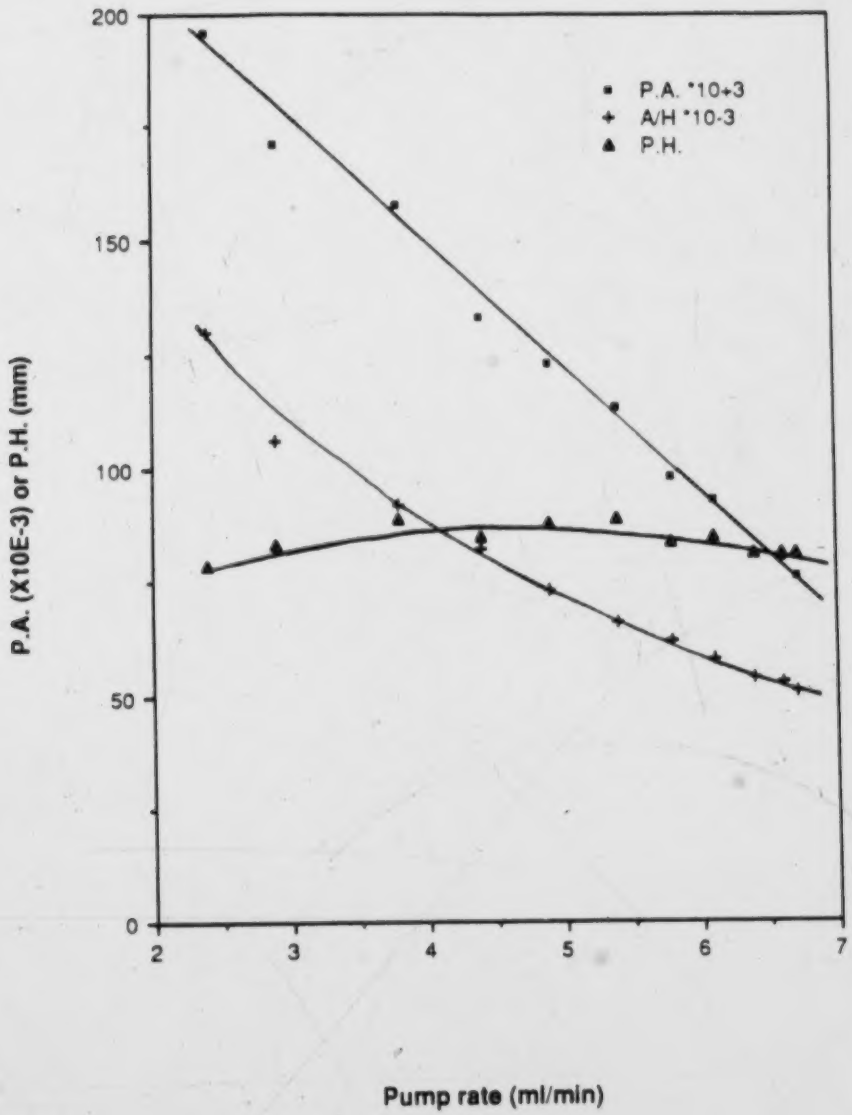

Fig 3.7: The relative P.A. (■), P.H. (▲) and Area/height ratio (+) when 10 µl of 2.47 x 10^{-4} M Mg^{+2} was injected into the HNO_3 stream entering the Model 290B AAS at various pumping rates.

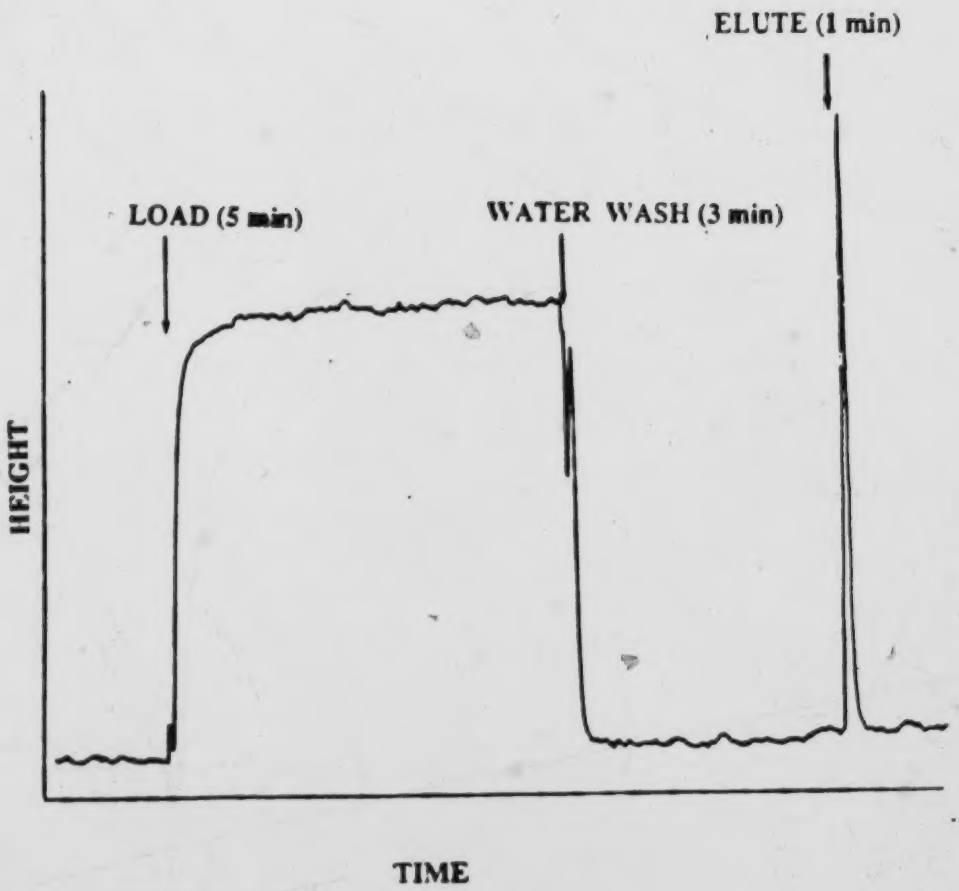

Fig 3.8: The signal response of the Model 290B Perkin-Elmer AAS during loading, washing and elution. Conditions: C_{Mg} = 1.23 x 10^{-5} M, PIPES = 0.01 M, μ = 0.10 M and pH = 6.00.

wash cycle. To obtain such a curve, valve V_4 in Fig 3.2 was switched so that the solution exiting the column enters the AAS during all four steps in its cycle. Breakthrough curves such as that shown in Fig 3.8, which show the absorbance during loading are the simplest way to determine when equilibrium is reached. Complete equilibrium will be achieved when the AA signal reaches a plateau, and will be the minimum time required for loading. Breakthrough curves could in principle, be obtained for every time a sample or standard solution is loaded. However, the nebuilizer becomes easily fouled due to deposition of the inert electrolyte so that in normal runs, V_4 was switched so that the test solution goes to waste.

A more lengthy but more accurate procedure to demonstrate column breakthrough is to measure loading curves. These were obtained by studying the peak areas obtained upon elution after various loading times, when all other experimental variables were kept constant. Figure 3.9 shows the eluted P.A. at various loading times, for a solution containing 1.24×10^{-5} M Mg^{+2} of fixed a pH of 6.00 and ionic strength of 0.1 M, using the with washing procedure. From Fig 3.9, the eluted P.A. reaches a plateau after about 5 min, and remains constant up to at least 60 min. Thus, a 5 min load time was the minimum time required for the column to reach equilibrium at the conditions used to obtain the loading curve, and was thus chosen for all studies using the with washing procedure. No further loading studies using the with washing procedure was carried out because they were extensively studied previously (37,68). These loading studies using the with washing procedure, showed that the equilibration time was independent of C_{Ca}, pH and particle size but was dependent on column size and buffer concentration (39,68).

In the column equilibration experiment performed without washing the eluent was passed through the column immediately after the test solution, without an intermediate water wash. The eluent solution comes in contact with the test solution in the column. As discussed in section 3.3.4 below, the buffer concentration used with washing (i.e. 0.01 M PIPES) was found to give a precipitate, most probably the acid insoluble diprotonated

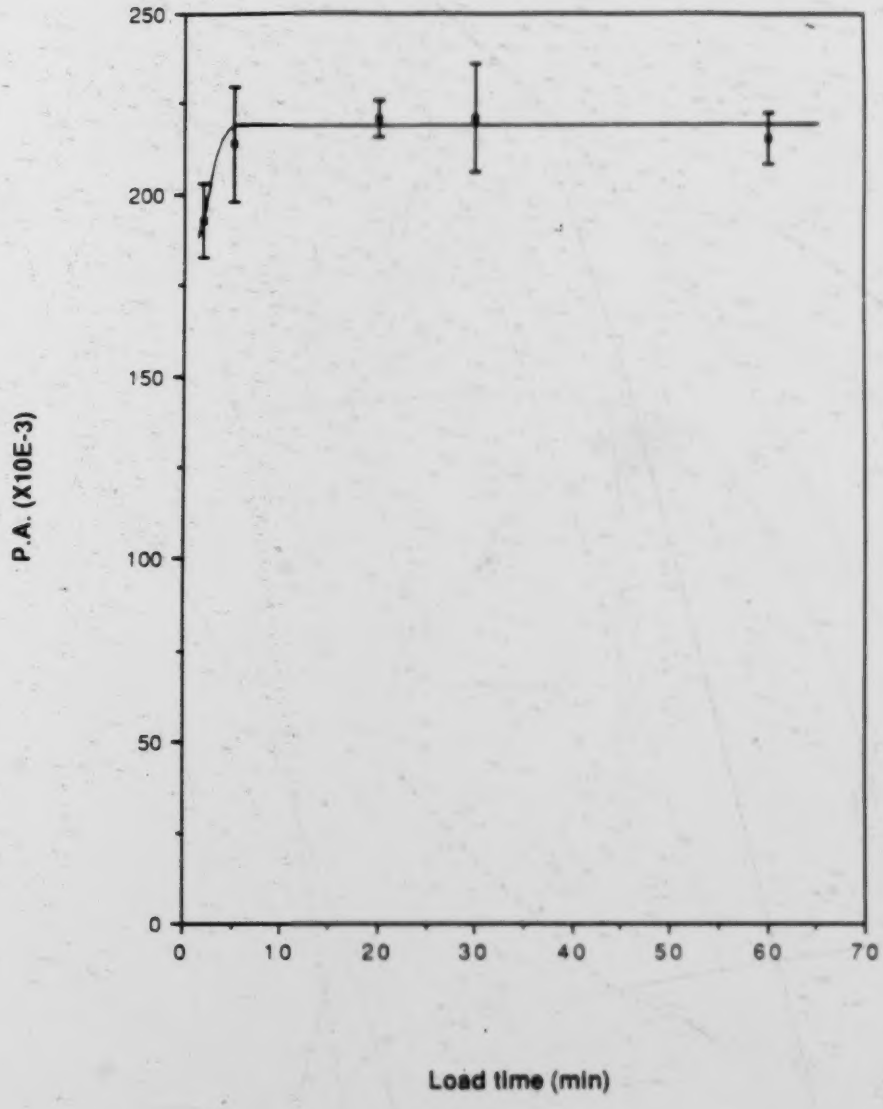

Fig 3.9: Loading curve with washing. Eluted peak areas were obtained when the column was loaded for varying periods, washed for 2 min, eluted for 1 min and finally washed for 2 min. Conditions: C_{Mg} = 1.23 x 10^{-5} M, PIPES = 0.01 M, μ = 0.10 M and pH = 6.00.

PIPES, when contacted with the eluent. A lower buffer concentration of 0.001 M did not give a precipitate with the eluent and thus was chosen for all subsequent studies without washing.

As discussed above, in connection with experiments done with washing on CPG-oxine column, the time required for column equilibration was dependent on the buffer concentration. With the new and lower buffer concentration of 0.001 M, a minimum load time of 15 min was required for complete breakthrough as seen from the loading curve in Fig 3.10. Thus a 20 min equilibration time was used for all experiments without washing. Similar loading curves were obtained using 0.001 M buffer when the following were varied: total Mg^{+2} concentration, ionic strength, pH, eluent strength, and length of time that the eluent was pumped through the column. It was demonstrated, over the entire ranges of those parameters employed in this present work, that a 20 min loading time was sufficient to reach equilibrium. For example, equilibrium was achieved in less than 20 min for the range from 0.005 M to 0.99 M NaCl.

3.3.3 Column washing conditions

Previous speciation studies by the column equilibration method have included a water washing step between the load and elution steps (32,37-39,77,78). Usually a brief water wash (~ 1 min) was found to be enough to completely remove the interstitial test solution, thus eliminating the necessity to determine the total amount of metal in the interstitial test solution. Furthermore in previous studies, the wash step did not remove any sorbed metal, irrespective of the length of washing time.

Based on these previous studies, a brief wash cycle was included after column equilibration of the test solution with XAD-oxine. Using a test solution containing 1.23×10^{-5} M Mg^{+2}, a pH of 6.00 and ionic strength of 0.1 M, the column was loaded to equilibrium for 5 min, then washed for varying times and the relative amount of sorbed Mg^{+2} determined after elution. As predicted, Fig 3.11 shows that the interstitial fluid was

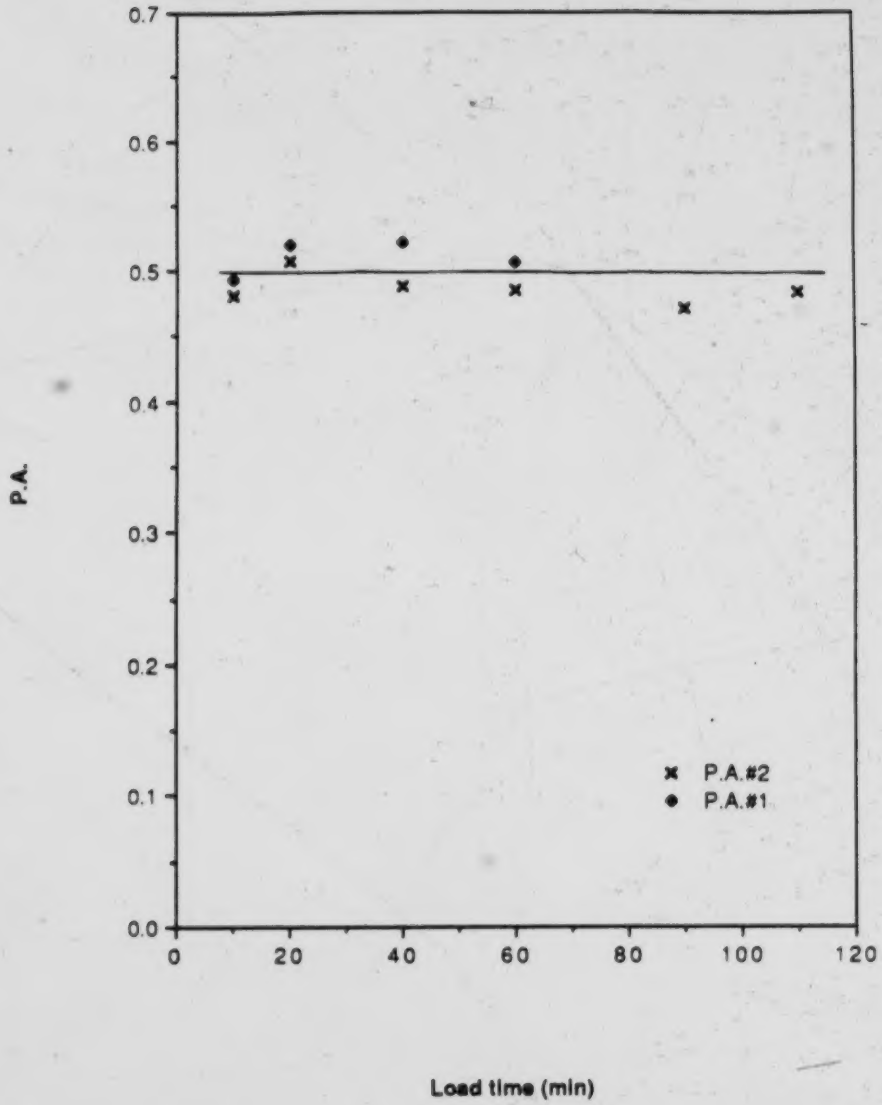

Fig 3.10: Loading curve without washing. Eluted peak areas were obtained when the column was loaded for varying periods and eluted for 2 min with 1 M HNO_3 Conditions: C_{Mg} = 5.76 x 10^{-6} M, PIPES = 0.001 M, μ = 0.10 M and pH = 6.00.

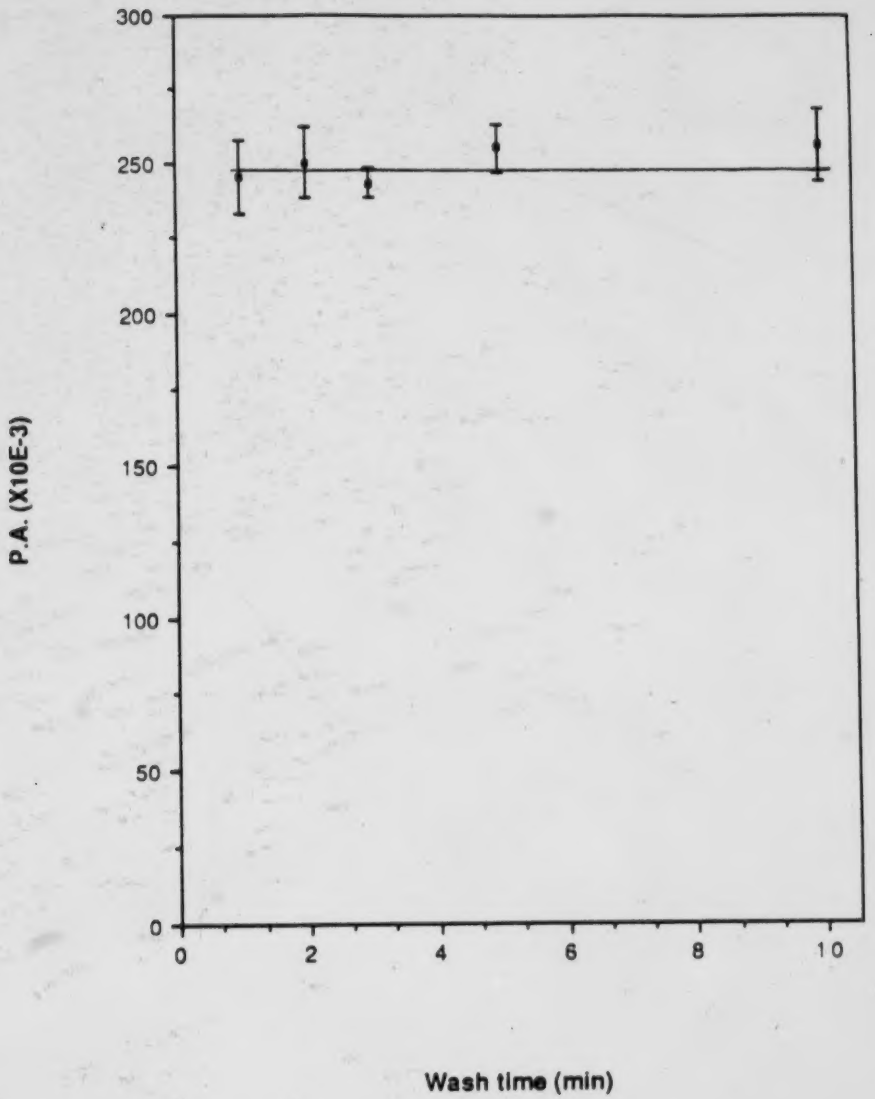

Fig 3.11: Washing conditions. Eluted peak areas were obtained when the column was loaded for 5 min, water washed for varying periods, eluted for 1 min and finally washed for 2 min. Conditions: C_{Mg} = 1.23 x 10^{-5} M, PIPES = 0.01 M, μ = 0.10 M and pH = 6.00.

completely removed within 1 min, and washing up to 10 min did not decrease the signal due to Mg^{+2} desorption. Thus, for all cycles with washing after column equilibration, a wash time of 2 min was chosen. Also, a 2 min wash cycle after the elution step was included to remove the interstitial eluent (HNO_3).

3.3.4 Column elution conditions

In choosing a suitable eluent, the factors considered were: sharpness of the eluted peak and complete removal of all sorbed species. Incomplete removal of sorbed species will show up as a "memory" effect and will affect replicate cycles. Since previous column equilibration experiments with washing successfully used 0.1 M HNO_3 eluent for Ca - oxine (38), it was chosen as the eluent. As shown in Fig 3.8, elution of the equilibrated column with 0.1 M HNO_3 gave a sharp peak (baseline width ~ 15 s). Furthermore, the use of 0.1 M HNO_3 eluent did not show any memory effect because all replicate data points with washing experiments show a scatter around the mean. Because prolonged contact with dilute HNO_3 was observed to leach a yellow color from XAD-2 (section 2.3.1), unnecessarily long contact time between the resin and eluent was avoided. With these precautions, the use of 0.1 M HNO_3 for 1 min did not show any decrease in Mg^{+2} sorption by the XAD-oxine with extended use.

Elution conditions for column equilibration without washing were systematically studied because of possible precipitation when the eluent and the test solution contact each other. Because PIPES precipitates when 0.1 M HNO_3 and the test solution (0.01 M) were mixed in a test tube, a search for an alternative eluent was made. EDTA which was successfully used previously to elute Cu^{+2} (37), failed to elute sorbed Mg^{+2} from XAD-oxine. Use of 0.001 M EDTA between pH 4-8 did not desorb Mg^{+2} from the resin, although the pH 4.00 solution did give an extremely broad peak. When a high EDTA concentration (0.01 M) was used at pH 3.00 and 4.00, peak areas of similar size to those obtained with 0.1 M HNO_3 eluent were obtained. This suggests that the protons and not the EDTA were

desorbing the Mg^{+2}. Thus there was no advantage to using EDTA, considering the other complications such as: peak tailing, nebulizer fouling because eluent continuously enters the AAS during loading, and high background signal from traces of magnesium in the EDTA.

The failure of EDTA as an eluent necessitated an extensive study of HNO_3 as an eluent. Since a precipitate was obtained when 0.1 M HNO_3 eluent was added to test solutions containing 0.01 M PIPES buffer, the effect of varying concentrations of PIPES and HNO_3 on precipitation was checked, by dropwise addition of dilute HNO_3 to 1 mL of PIPES solution in a test tube. For PIPES concentrations of 0.01 M, a white precipitate was obtained when dilute HNO_3 of any concentration was added. When the PIPES concentration was reduced to 0.001 M, no precipitate was observed when eluent concentrations of up to 2 M HNO_3 were added. On this basis, HNO_3 was chosen as the eluent, but the buffer concentration was reduced to 0.001 M in all test solutions.

As mentioned before, a sharp eluted peak and complete removal of all sorbed species were the most important considerations. The choice of eluent concentration was determined by loading the column with a solution containing 5.76×10^{-6} M Mg^{+2} and the lower 0.001 M buffer concentration, then eluting the Mg^{+2} with varying HNO_3 concentrations. For eluent strength below 0.001 M, double peaks as shown in Fig 3.12 were obtained. The first peak was due to Mg^{+2} in the void volume and the second to Mg^{+2} desorption. Peaks obtained with 0.01 M, 0.1 M and 1.0 M HNO_3 appear as single peak of exactly the same peak area, but the height of these peaks increases with eluent concentration. In other words, the eluent containing 1.0 M HNO_3 gave the sharpest peak. Loading curves such as those described in section 3.3.2, but using eluent containing 0.01 M, 0.1 M and 1.0 M HNO_3 showed exactly the same result i.e. a 20 min load time was the minimum time for the column to reach equilibrium and replicate cycles were unaffected by a "memory" effect. Furthermore, when the AAS lamp was changed to detect copper, the use of 1 M eluent showed complete removal of trace quantities of copper in the test solutions. Also, a study of varying elution times for columns that contained the same

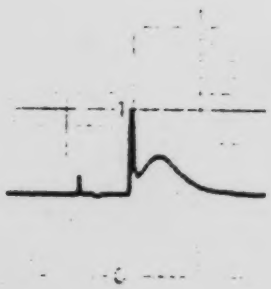

Fig 3.12: Double peaks after the column was loaded for 20 min then eluted with 0.001 M HNO_3 without washing. Conditions: C_{Mg} = 5.76 x 10^{-6} M, PIPES = 0.001 M, μ = 0.10 M and pH = 6.00.

amount of Mg^{+2} loading shows that 1 M HNO_3 completely eluted sorbed Mg^{+2} within 1 min. Thus, the final elution conditions chosen for without washing were 1 M HNO_3 for 2 min.

3.3.5 Column conditioning

During loading studies, it was noticed that the peak areas for the first few runs differ from those obtained in later runs. Thus, in all studies, the first few data points were discarded until replicates yielded the same peak areas. The reason why the column needs conditioning cannot be explained and will require an extensive study. However, one possibility that can be ruled out was instrumental and flow rate changes because peak areas for standards injected directly into the eluent stream via valve I, did not show that drift.

3.3.6 Mg^{+2} Isotherm

The distribution ratio λ_o, by definition was given by eq 3.5. Under constant instrumental conditions, the measured P.A. is directly proportional to $[Mg^{+2}]_R$ as given by eq 3.10

$$[Mg^{+2}]_R = k\ (P.A.) \quad \text{.....3.10}$$

where k is the moles per unit peak area per unit weight of resin in the column. Using eq 3.5 and 3.10, λ_o can be defined by eq 3.12

$$\lambda_o = \frac{k\ (P.A.)}{[Mg^{+2}]} \quad \text{..... 3.11}$$

Successful use of the column equilibration technique requires that all free metal determinations be done at trace loading conditions i.e. the distribution coefficient λ_o is constant and independent of $[Mg^{+2}]$. In other words, a plot of $[Mg^{+2}]_R$ or eluted P.A.

against [Mg^{+2}] in solution is linear. Usually, at trace conditions, the number of sites used for sorption (i.e. % column loading) is <1%.

Mg^{+2} isotherms were routinely measured as part of every study of experimental variables. Two typical isotherms are shown in Figs 3.13 and 3.14 for with washing and without washing respectively. The P.A. sorb in Fig 3.14 was corrected for the P.A. contributions due to Mg^{+2} in the void volume. Calculation of the P.A. sorb was described in section 3.2.3.2. Both Figs 3.13 and 3.14 were corrected for P.A. contributions of the blank.

Indicated in Figs 3.13 and 3.14 were the P.A. contribution of the blank solution, which was a solution of fixed pH containing only NaCl and PIPES. Analysis of stock solutions of NaCl and PIPES showed that the NaCl solution was the major contributor of blank Mg^{+2}. For solutions used for without washing experiments, the measured P.A. of the blank was the contribution due to Mg^{+2} sorption plus that in the interstitial solution. Thus, in order to reduce the blank P.A., it was necessary to remove traces of Mg^{+2} in the NaCl stock solution, by flowing it through a column containing Chelex-100 resin.

A major characteristic of both isotherms was that the curves are non-linear even though the eluted magnesium signals were well within the instrument linearity and the maximum sites occupied by the Mg^{+2} was less than 1% of the total. Estimation of the maximum % of sites occupied by sorption of Mg^{+2} on the XAD-oxine (% column loading) was done in the following way: Consider, for example, Fig 3.13. The sensitivity of the Model 290B AAS was estimated by determining the P.A. when 10 μL of 1.23×10^{-4} M Mg^{+2} was injected into the eluent stream. For 1.23×10^{-9} moles (10 μL x 1.23×10^{-4} M), the measured P.A. was $(63.9 \pm 4.9) \times 10^3$ counts. From Fig 3.13, the upper limit of the isotherm is 400,000 counts, which will correspond to 7.7×10^{-9} moles of eluted Mg^{+2}, at the same instrumental sensitivity. Using eq 3.12, the sorptive capacity of the column used for the isotherm in Fig 3.13 was 7.44×10^{-7} moles.

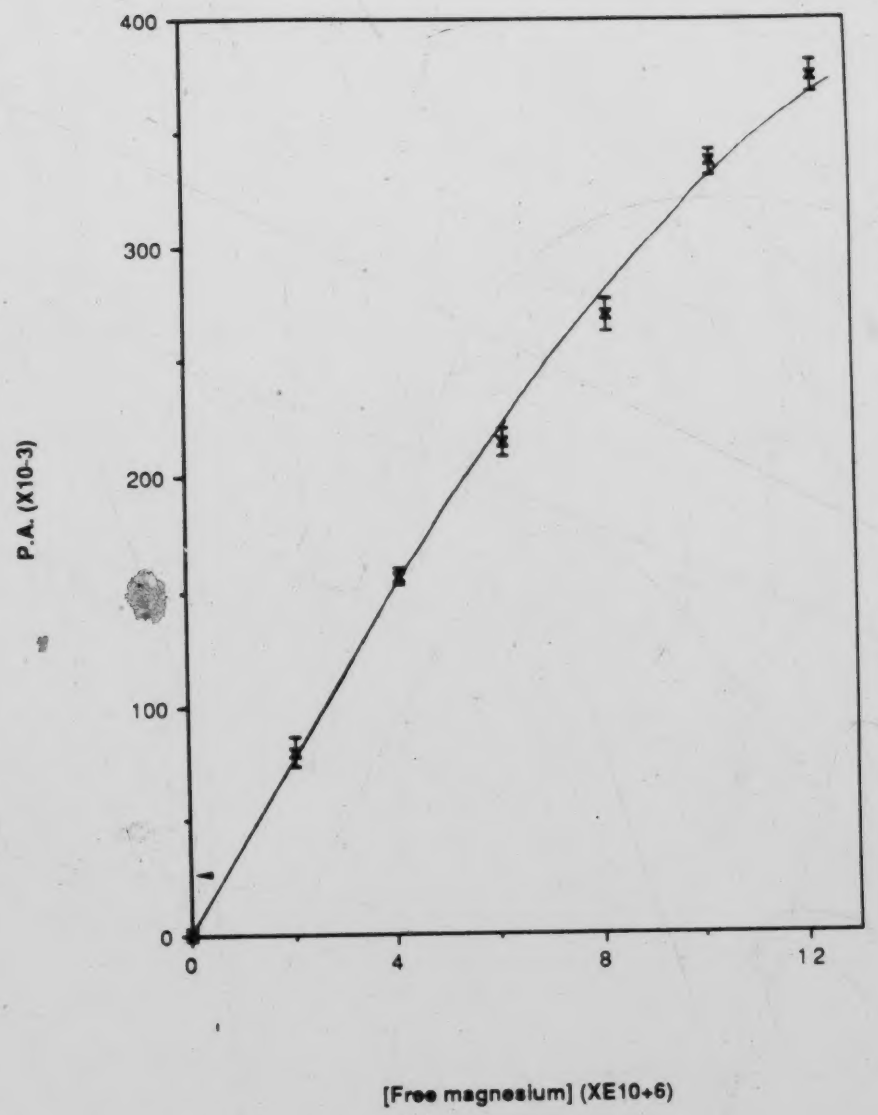

Fig 3.13: Isotherm (i.e. P.A. vs $[Mg^{+2}]$) with washing. Conditions: PIPES = 0.01 M, μ = 0.10 M, pH = 6.50, load = 5 min, wash = 2 min, elute = 1 min with 0.1 M HNO_3 and wash = 2 min.

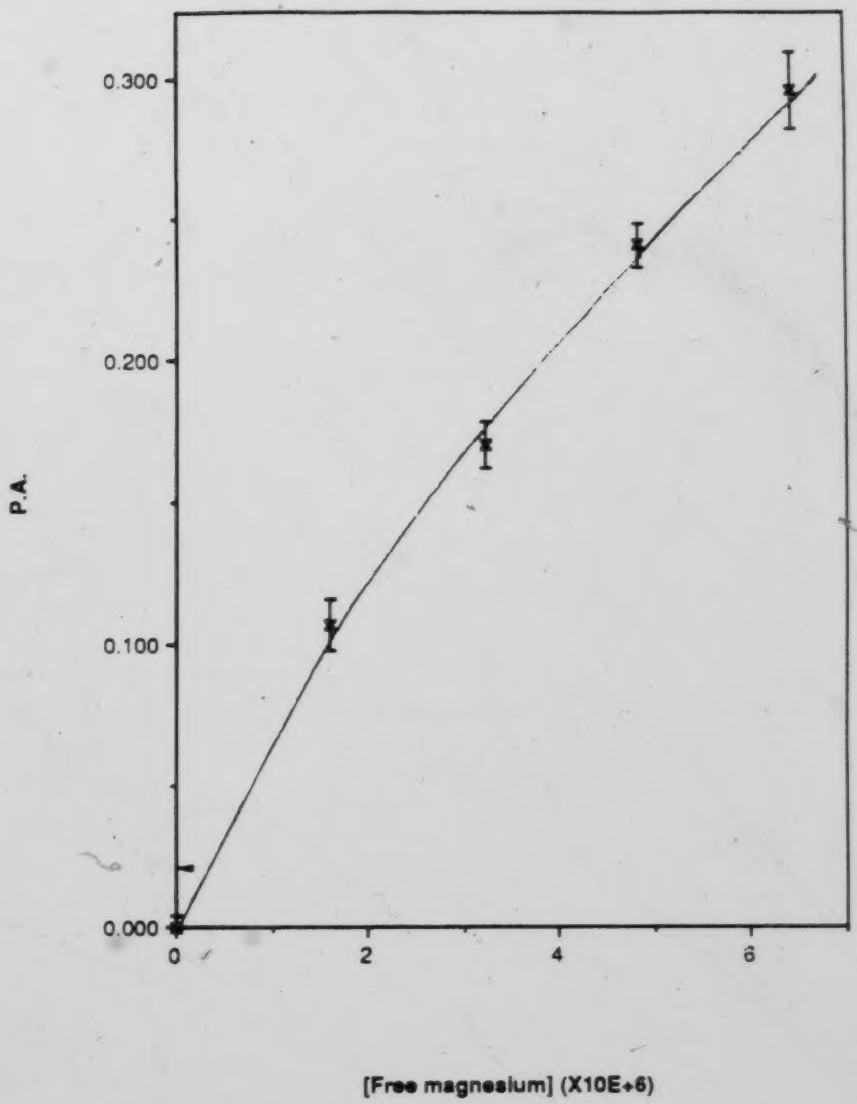

Fig 3.14: Isotherm (i.e. P.A. vs $[Mg^{+2}]$) without washing. Conditions: PIPES = 0.001 M, μ = 0.25 M, pH = 6.00, load = 20 min and elute = 2 min with 1 M HNO_3. **Note**: in this plot, the P.A. was corrected for the P.A. due to the void volume (as well as the blank).

Column capacity = l . d . v 3.12

where l was the column length (13 mm), d was the packing density of the resin in a 1.5 mm i.d. tube (0.52 mg/mm) and v was the sorptive capacity of the XAD-oxine (0.110 µmol/mg). From equation 3.13, the % column loading was 1.0 of the total sites at the highest point of Fig 3.13 isotherm i.e.

$$\% \text{ column loading} = \frac{\text{moles eluted from column}}{\text{column capacity}} \times 100 \quad \text{.....3.13}$$

One possible explanation for the non linear Mg^{+2} isotherm can be given in terms of Mg^{+2} : oxine ratio. In capacity studies (section 2.3.2.), the sorptive capacity and the total capacity differed. These differences suggest mixed ratios of Mg^{+2} : oxine i.e. a mixture of 1:1 and 1:2 formation for the isotherms. More evidence of mixed ratios will be presented in section 4.3.3.4, where linear isotherms were obtained when conditions were created so that mainly 1:1 ratios forms.

Since Mg^{+2} isotherms were non-linear, the application of XAD-oxine for speciation requires that working curves of the appropriate $[Mg^{+2}]$ range be prepared. The $[Mg^{+2}]$ in unknown samples will thus require reading off the $[Mg^{+2}]$ from the measured P.A. after column equilibration, rather than calculating it from a constant λ_o value.

3.3.7 **Effect of solution pH**

Isotherms with washing measured at various pH are shown in Fig 3.15. If these isotherms were linear, then at a constant pH, λ_o should be independent of $[Mg^{+2}]$ in solution. In that case, a plot of λ_o vs pH, obtained by taking the points on vertical slices through Fig 3.15, would give the same curve regardless of the $[Mg^{+2}]$ at which the vertical slice was made. However, because the isotherm in Fig 3.15 is non-linear, and λ_o

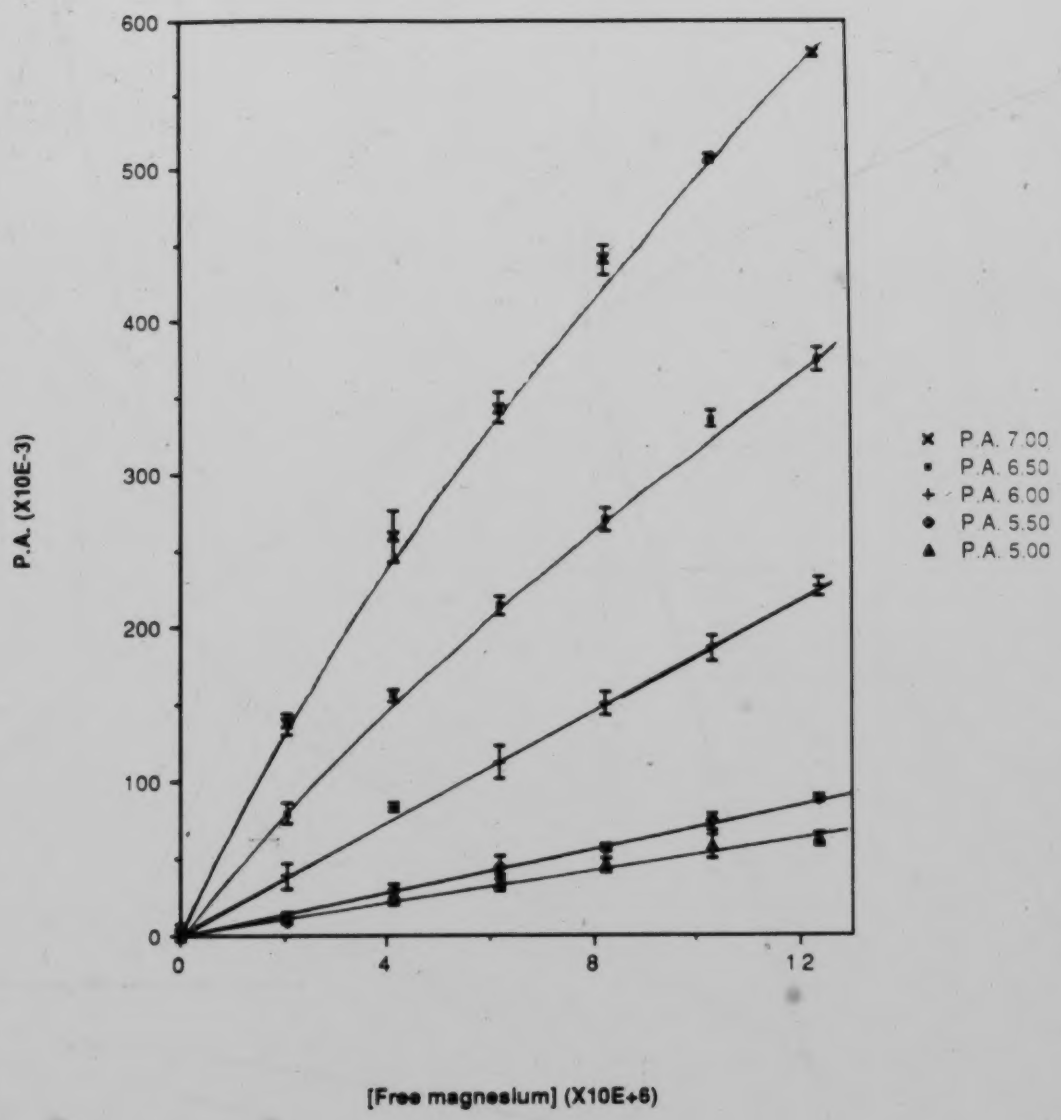

Fig 3.15: Isotherm with washing at various pH ~ (x) pH 7.00, (■) pH 6.50, (+) pH 6.00, (◇) pH 5.50 and (▲) pH 5.00. Conditions: PIPES = 0.01 M, μ = 0.10 M, pH = specified by the symbol, load = 5 min, wash = 2 min, elute = 1 min with 0.1 M HNO_3 and wash = 2 min.

depends on $[Mg^{+2}]$, plots of λ_o vs pH yield different curves when slices are made at different $[Mg^{+2}]$. Such plots are shown in Fig 3.16 (the calculation of λ_o from the measured P.A. was discussed in section 3.3.6).

Figure 3.16 shows that λ_o increases in an ever increasing way with increasing pH. This behavior is quantitatively consistent with reported sorption of other divalent ions by immobilized oxine (51,81-84). To understand the trend shown in Fig 3.16, one can consider the behavior of XAD-oxine to be analogous to 8-hydroxyquinoline in homogeneous solution. In homogeneous solution, an increase in pH increases the fraction of complex forming species α_{L^-} which is given by eq 3.14

$$\alpha_{L^-} = \frac{K_1 K_2}{H^2 + K_1 H + K_1 K_2} \qquad \text{.....3.14}$$

where H is the hydrogen ion concentration, K_1 and K_2 are the first and second proton dissociation constants of 8-hydroxyquinoline. Thus, for XAD-oxine, an increase in pH will increase the fraction of Mg^{+2} sorbing sites (i.e. α_{L^-}) and will be related by an equation similar to eq 3.14.

For 8-hydroxyquinoline immobilized on CPG, a modified ionizable surface group model was successfully applied to quantitatively relate the solution pH to the amount sorbed (38). This model used proton dissociation constants of 8-hydroxyquinoline immobilized on CPG obtained from a previous study (84). For XAD-oxine, attempts to quantitatively use the ionizable surface group model to relate the solution pH to the distribution ratio proved unsuccessful for two reasons: (a) non-linear isotherms which were discussed in section 3.3.6 above and (b) unknown surface charge. A known value of the surface charge is required to calculate the pH immediately adjacent to the surface, which in turn is required to determine the degree of ionization of the bound oxine. Although one can use the protonation constants in homogeneous solution to estimate the surface

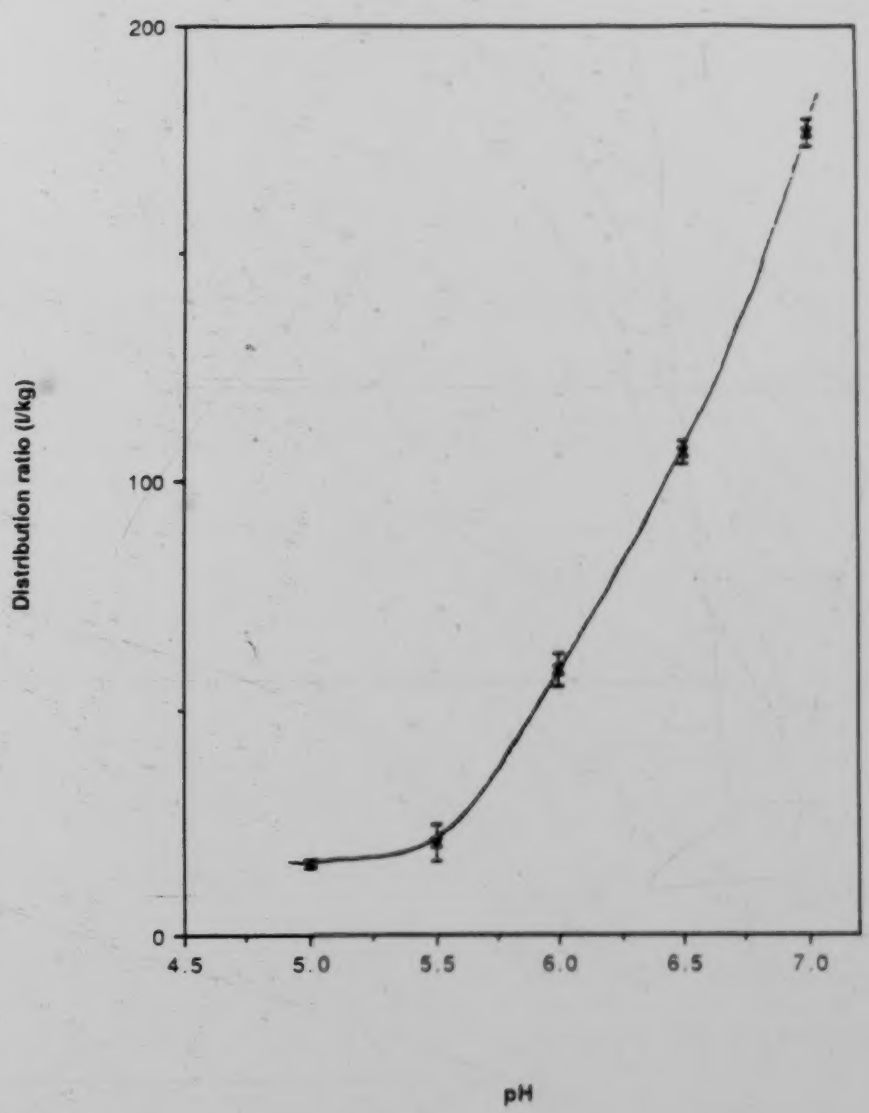

Fig 3.16: The effect of solution pH on the distribution ratio using only the points form 4.11×10^{-6} M Mg^{+2} in Fig 3.15.

charge, then iterate to find the true surface charge, this method cannot work because the XAD-2 surface has "natural" surface charge which is difficult to estimate (85).

As expected, experiments done without washing yielded the same kind of non-linear isotherm as observed for the with washing experiments. For this reason, the dependence of λ_o on pH was measured using one [Mg^{+2}] simply to demonstrate the expected behavior as shown in Fig 3.17.

The large changes in λ_o with increasing pH suggests that the application of XAD-oxine to real samples will require that exact pH matching of the Mg^{+2} in the standards and samples. As calculated in section 3.3.6 above, a 1% loading corresponds to 400,000 counts, thus from Fig 3.15, typical working ranges would be: 1×10^{-5} M at pH 7, 2.5×10^{-5} M at pH 6 and 1×10^{-4} M at pH 5. In anticipation for the application of XAD-oxine to determine Mg^{+2} in real samples e.g. urine, a pH 6.00 was chosen for most studies.

3.3.8 Ionic strength

Although chloride slightly complexes Mg^{+2}, $K_{MgCl^+} = 0.1$ (86), sodium chloride was still chosen for ionic strength adjustments mainly because of the anticipated application of this method for the determination of Mg^{+2} in urine. The chloride ion in urine averages 0.17 M and is the ion in the highest concentration (87). Later on in this section, it will be seen that the sorption of Mg^{+2} is dependent on ionic strength. Therefore, it would be necessary to adjust the ionic strength of all samples to 0.25 M in order to have the standards and samples of the same ionic strength. At a [NaCl] concentration of 0.25 M, the [$MgCl^+$] : [Mg^{+2}] ratio will be 0.025. The error of 2.5% resulting from the neglect of $MgCl^+$ species is small compared to the 5-10% r.s.d. from the column equilibration method. This was verified by determining isotherms using NaCl and non-complexing $NaNO_3$ for ionic strength adjustments. As can be seen in Fig 3.18, the signals for the same [Mg^{+2}] were the same in both electrolytes. Similarly, the choice of univalent cation for

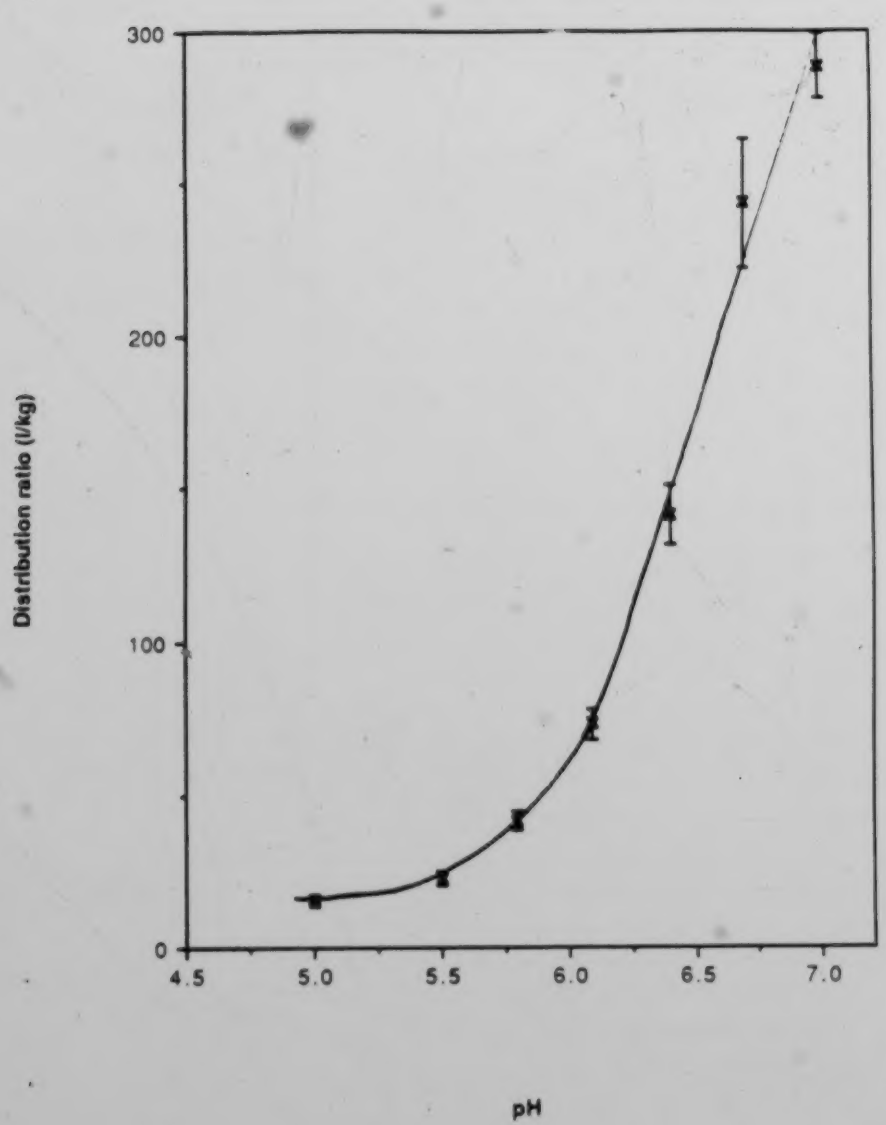

Fig 3.17: The effect of solution pH on the distribution ratio using the without washing procedure. Conditions: PIPES = 0.001 M, μ = 0.25 M, load = 20 min and elute = 2 min with 1 M HNO_3.

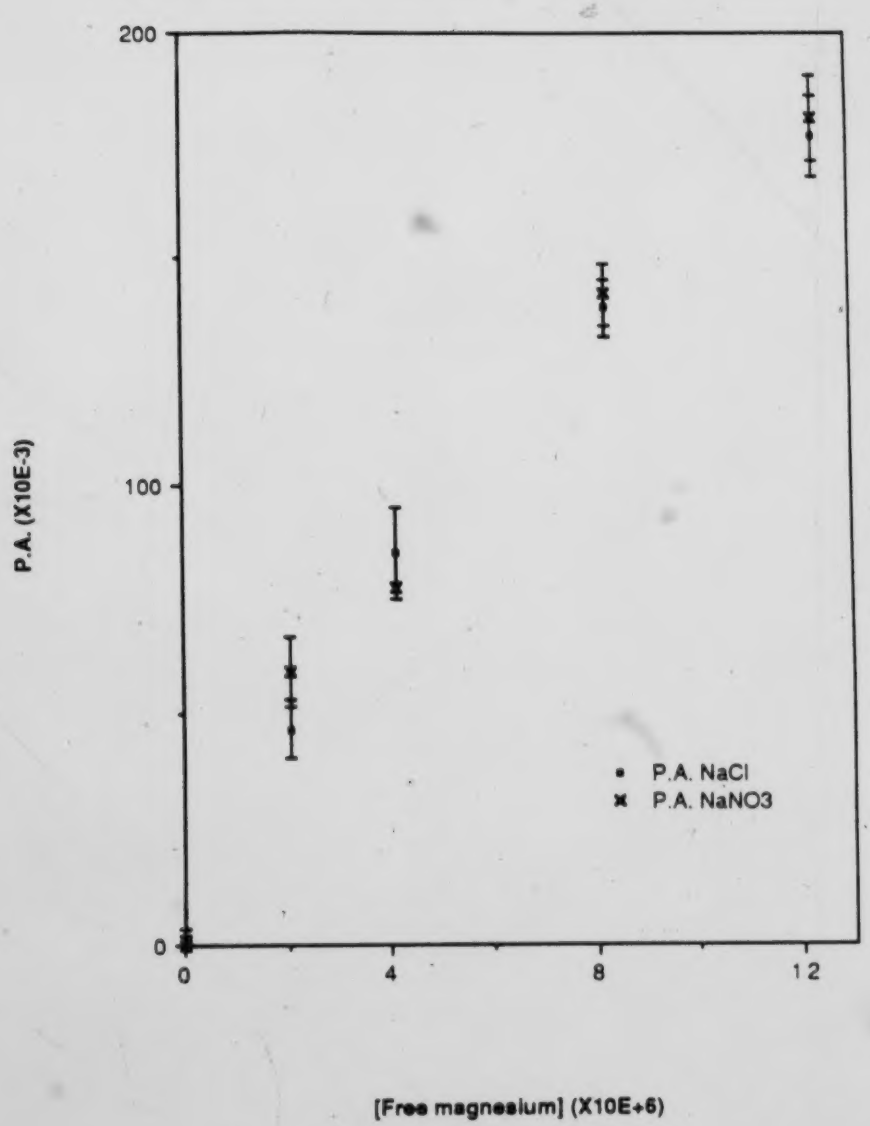

Fig 3.18: With washing isotherms using NaCl (•) and $NaNO_3$ (x) for ionic strength adjustment. Conditions: PIPES = 0.01 M, μ = 0.10 M, pH = 6.00, load = 5 min, wash = 2 min, elute = 1 min with 0.1 M HNO_3 and wash = 2 min.

the inert electrolyte had no effect on λ_o. This is shown by the similarity of the isotherms measured when when only NaCl (0.25 M) was used, to that measured when a mixture of 0.20 M NaCl and 0.05 M KCl were used for ionic strength adjustment (Fig 3.19).

Previous experiments with 5-phenylazo-8-hydroxyquinoline immobilized on CPG showed that Mg^{+2} sorption was strongly influenced by the ionic strength of the solution (38). Therefore, experiments were carried out in which the ionic strength was the only parameter varied. A typical plot to show the effect of ionic strength on the distribution ratio, using the with washing procedure, is presented in Fig 3.20. In Fig 3.20, the data points were done at a $[Mg^{+2}]$ of 4.11×10^{-6} M where they are in the non-linear region of the Mg^{+2} isotherm. Thus, as discussed in section 3.3.7, Fig 3.20 will only illustrate the effect of μ on λ_o for the with washing procedure. Fig 3.21 gives a better representation of the effect of μ on λ_o using the without washing procedure, because all the data points were done as close as possible to the linear region of the Mg^{+2} isotherm. The first two data points were measured at $[Mg^{+2}]$ of 4.02×10^{-7} M and the other points were done at 2.01×10^{-6} M. Both curves (Figs 3.20 and 3.21) show that the λ_o of Mg^{+2} on XAD-oxine decreases as μ increases.

To understand the observed effect of μ on λ_o, we invoke the "ionizable surface group model" that was previously used to relate these two parameters for CPG-oxine (38). This model assumes the surface is charged, and 1:1 complexation occurs between the charged anionic oxine sites, Ox^- and free metal. By analogy, the relationship between λ_o and μ is given by:

$$\lambda_o = \alpha_{Ox^-} \gamma_{Mg^{+2}} v K_{MgOx^+} \exp\left(-\frac{2F\Psi_x}{RT}\right) + \frac{k \gamma_{Mg^{+2}}}{\mu^{0.5}} \quad \text{.....3.15}$$

where α_{Ox^-} is the fraction of anionic oxine sites, $\gamma_{Mg^{+2}}$ is the activity coefficient in solution, v is the resin capacity, K_{MgOx^+} is the formation constant of $MgOx^+$ at the resin

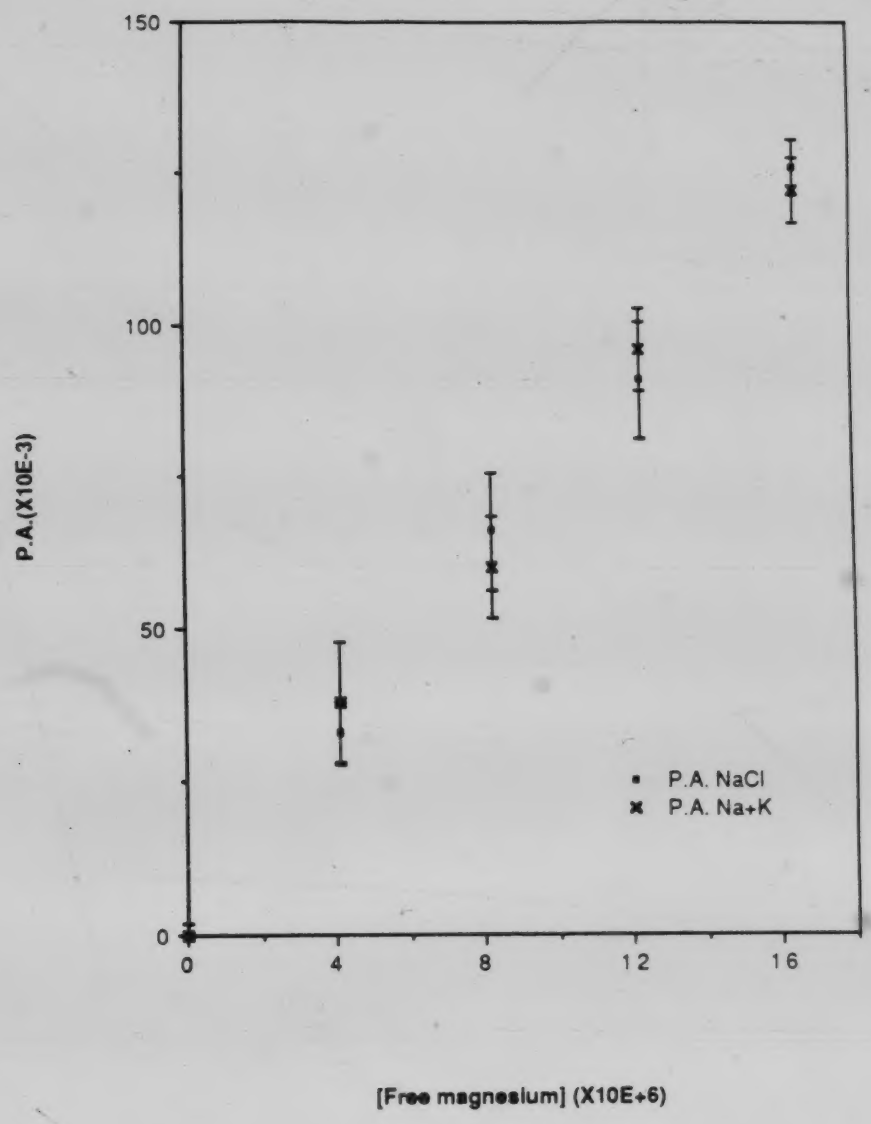

Fig 3.19: With washing isotherms using only 0.25 M NaCl (•) and 0.05 M KCl + 0.20 M NaCl (x) for ionic strength adjustment. Conditions: PIPES = 0.01 M, pH = 6.00, load = 5 min, wash = 2 min, elute = 1 min with 0.1 M HNO_3 and wash = 2 mjn.

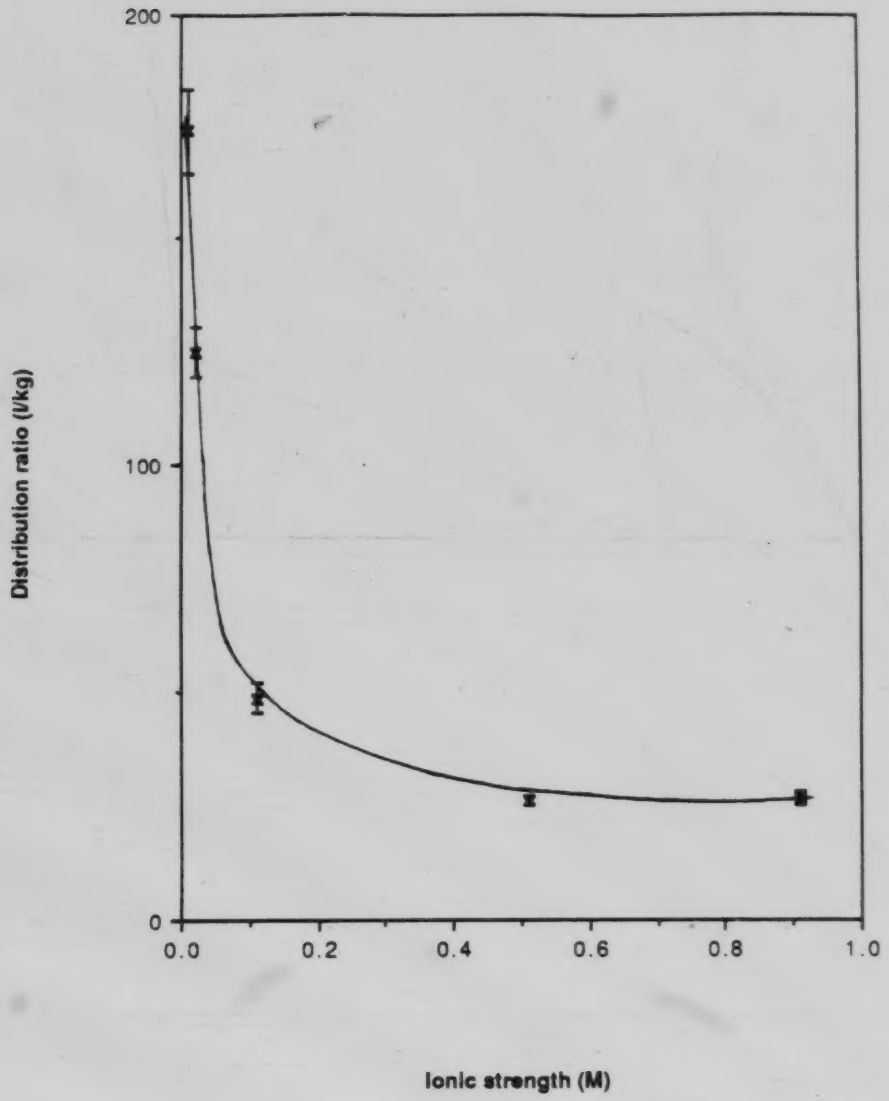

Fig 3.20: The effect of ionic strength on the distribution ratio using the with washing procedure. Conditions: PIPES = 0.01 M, pH = 6.00, load = 5 min, wash = 2 min, elute = 1 min with 0.1 M HNO_3 and wash = 2 min. All data points were done with $[Mg^{+2}] = 4.11 \times 10^{-6}$ M.

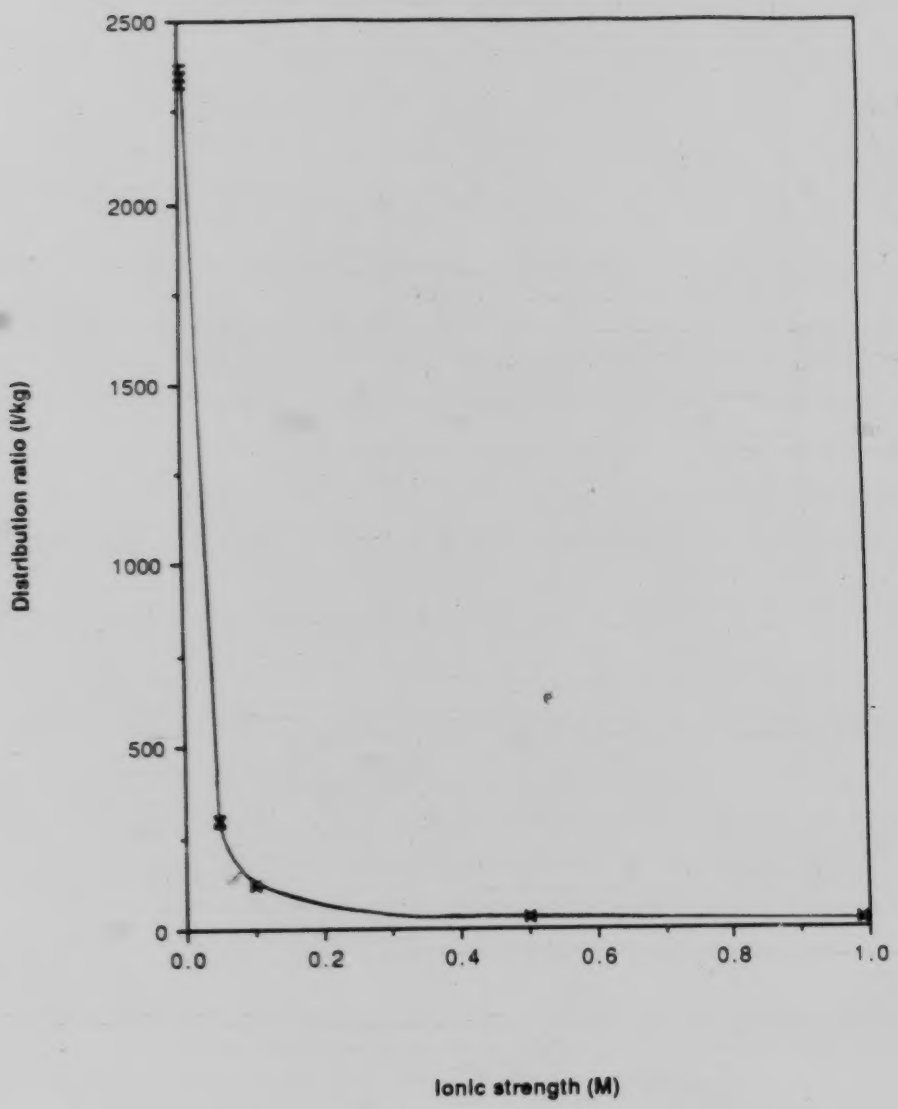

Fig 3.21: The effect of ionic strength on the distribution ratio using the without washing procedure. Conditions: PIPES = 0.001 M, pH = 6.00, load = 20 min, elute = 2 min with 1 M HNO_3. The data points at μ = 0.005 M and 0.05 M were done at $[Mg^{+2}] = 4.02 \times 10^{-7}$ M and the others were done at 2.01×10^{-6} M.

surface, F is the Faraday constant, R is the ideal gas constant, T is the absolute temperature, k is a constant, ψ_x is the surface potential at a distance x cm away from (but close to) the surface charge. Details of the derivation of eq 3.15 are given in reference 38.

An increase in the ionic strength will result in a decrease in ψ_x as well as a decrease in $\gamma_{Mg^{+2}}$. Thus, both terms on the right side of eq 3.15 decreases, causing λ_o to decrease.

Unfortunately the data from Figs 3.20 and 3.21 cannot be readily fit to eq 3.15 because the surface charge is unknown and the isotherms are non-linear (discussed in section 3.3.7).

3.3.9 Effect of other sorbed cations on Mg^{+2} sorption

In homogeneous solution, the log β_1 values between the oxine and Cu^{+2}, Mg^{+2} and Ca^{+2} are 12.56, 4.74 and 3.27 (86). Although the immobilized oxine will be expected to have a slightly different β_1 from that of homogeneous solution, one will expect the relative trend of β_1 with these metals to be similar. Therefore, the more strongly bound Cu^{+2} will be expected to displace the sorbed Mg^{+2}.

Loading curves with washing for standards containing added Cu^{+2} show a decrease in Mg^{+2} signal with increasing load time (Fig 3.22). In contrast, loading curves with solutions containing only Mg^{+2} do not show a decrease in Mg^{+2} sorption with increasing load time (Figs 3.9 and 3.10). Furthermore, the loading curve in Fig 3.22 shows that solution Mg^{+2} quickly reaches equilibrium with the resin, but Cu^{+2} did not. This is advantageous because for real samples e.g. environmental and biological samples, the effect due to the presence of heavy metals will be minimized. Furthermore, heavy metals generally have larger β_1 values than Mg^{+2} with most ligands and one will expect these heavy metals to exist mainly as complexes. The concentration of Cu^{+2} in isotherm standards was estimated to be 2×10^{-8} M when the AAS lamp was changed to determine copper. These trace levels of Cu^{+2} and other heavy metals that will be usually present in

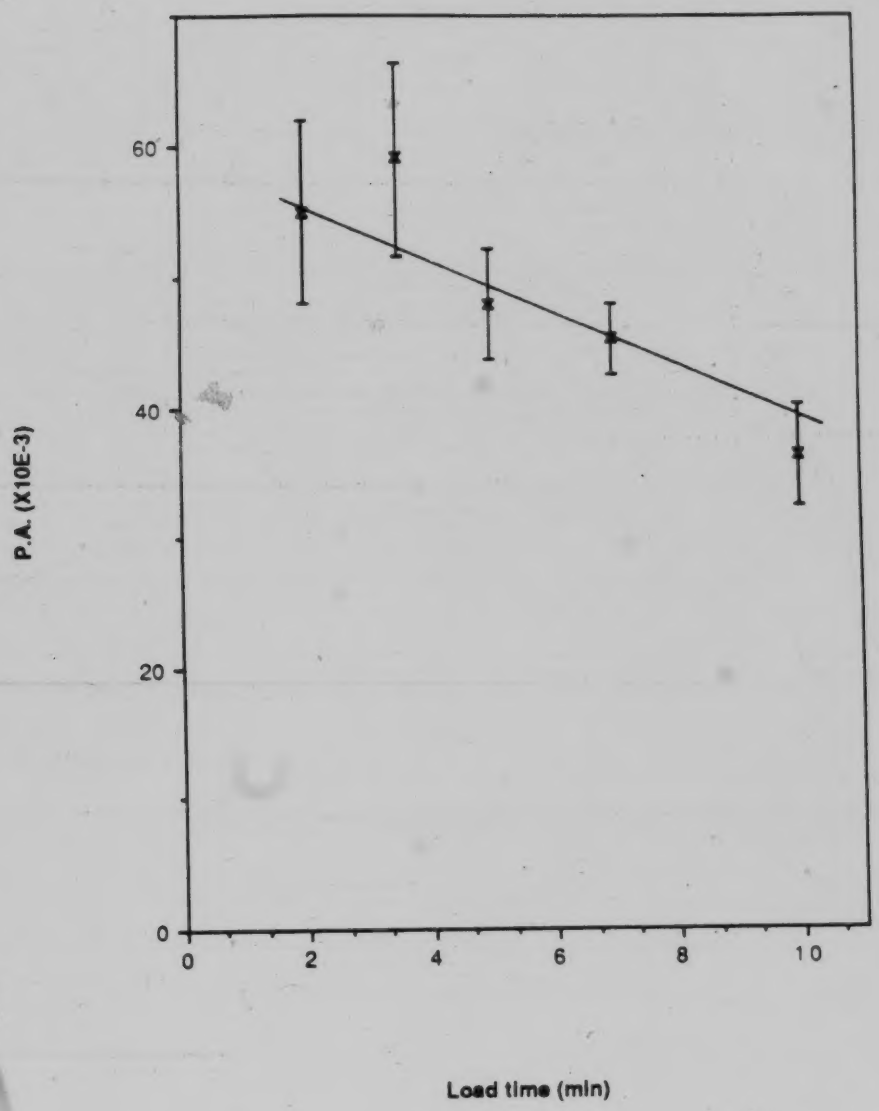

Fig 3.22: Loading curve for a copper containing solution using the with washing procedure. Conditions: C_{Mg} = 1.23 x 10^{-5} M, $[Cu^{+2}]$ = 1.2 x 10^{-5} M, PIPES = 0.01 M, μ = 0.25 M, pH = 6.00, load = varying, wash = 2 min, elute = 1 min with 0.1 M HNO_3 and wash = 2 min.

isotherm standards do not cause a decrease in Mg^{+2} sorption for loading times of up to 2 h (section 3.3.2). Thus, it is reasonable to conclude that XAD-oxine can be used to determine $[Mg^{+2}]$ for samples containing trace levels of free heavy metal.

On the other hand, formation constants for Mg^{+2} and Ca^{+2} with most ligands are comparable in magnitude. Thus, the concentration of both ionic species in real samples will be comparable, hence Ca^{+2} can be a potential problem (as in other methods to determine Mg^{+2}). Figure 3.23 shows that at 1% column loading, Ca^{+2} : Mg^{+2} ratios of up to 3.5 to 1 did not affect the eluted Mg^{+2} signal with washing experiments. Similarly, for without washing experiments, the eluted Mg^{+2} signals did not show significant differences for ratios of up to 5:1 (Fig 3.24). This figure also shows that concentrations of up to 1×10^{-4} M Ca^{+2} do not significantly decrease the Mg^{+2} signal obtained from a solution containing 1×10^{-5} M of Mg^{+2}. A $[Mg^{+2}]$ of 1×10^{-5} M corresponds to a column loading of 0.5% (using the procedure in section 3.3.6).

3.3.10 **Overloaded column conditions with washing**

The average pH and total magnesium concentration for biological samples (87) and environmental e.g. river, lake or ground water are both higher ($\sim 10^{-3}$ M). In section 3.3.7 (Fig 3.15), the upper limit for Mg^{+2} for 1% column loading was 2.5×10^{-5} M at pH = 6.00. As such, the application of XAD-oxine for the determination of $[Mg^{+2}]$ in real samples will require working at high % column loading (i.e. with overloaded columns). Thus experiments were carried out where the $[Mg^{+2}]$ varied up to 3.3×10^{-3} M, corresponding to 4-10 % column loading. Furthermore, in anticipation of a possible application to real samples, Ca^{+2} at concentrations of up to 1×10^{-2} M was added into the test solutions.

Using a shorter 2 mm column bed to maintain the eluted Mg^{+2} signal within the linear region of the AAS, the standard 5 min load time was found to be enough to reach equilibrium. As predicted, under overloaded conditions, the presence of Ca^{+2} will affect

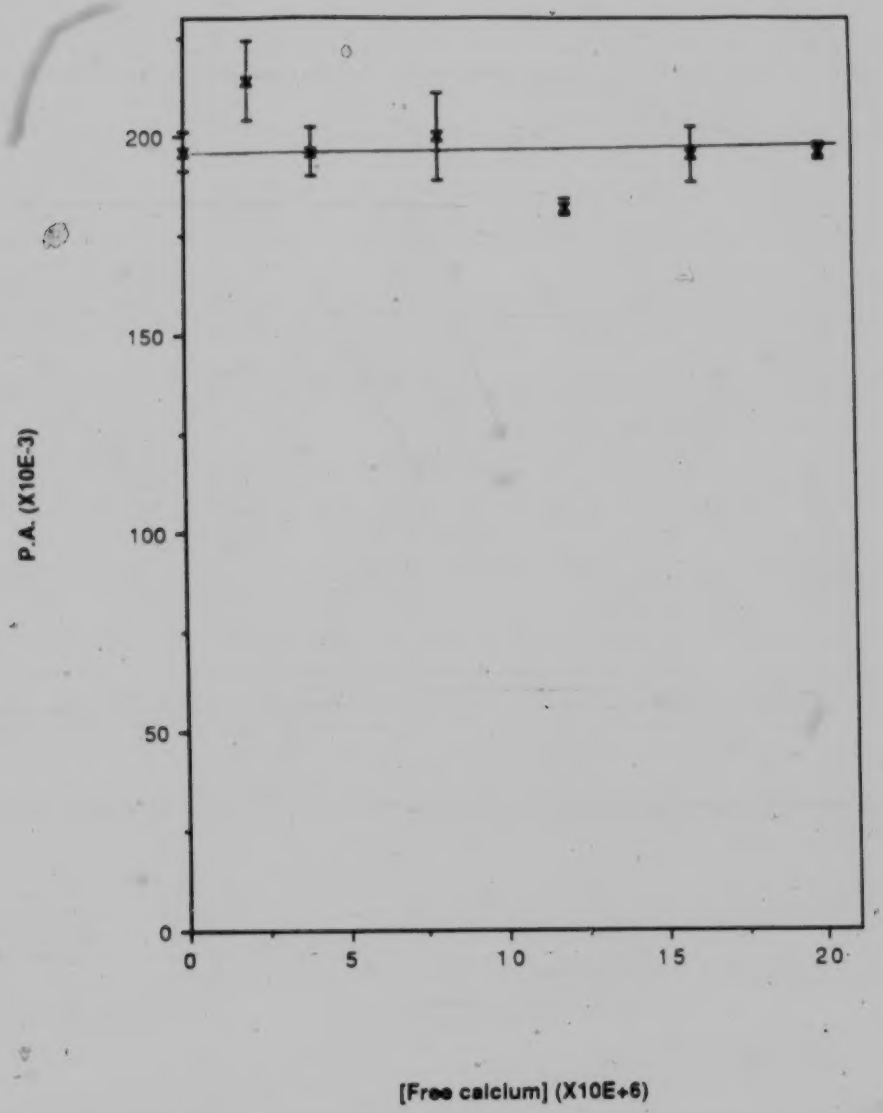

Fig 3.23: Effect of varying concentration of Ca^{+2} on Mg^{+2} sorption using the with washing procedure. Conditions: C_{Mg} = 8.23 x 10^{-6} M, PIPES = 0.01 M, μ = 0.25 M, pH = 6.00, load = 5 min, wash = 2 min, elute = 1 min with 0.1 M HNO_3 and wash = 2 min.

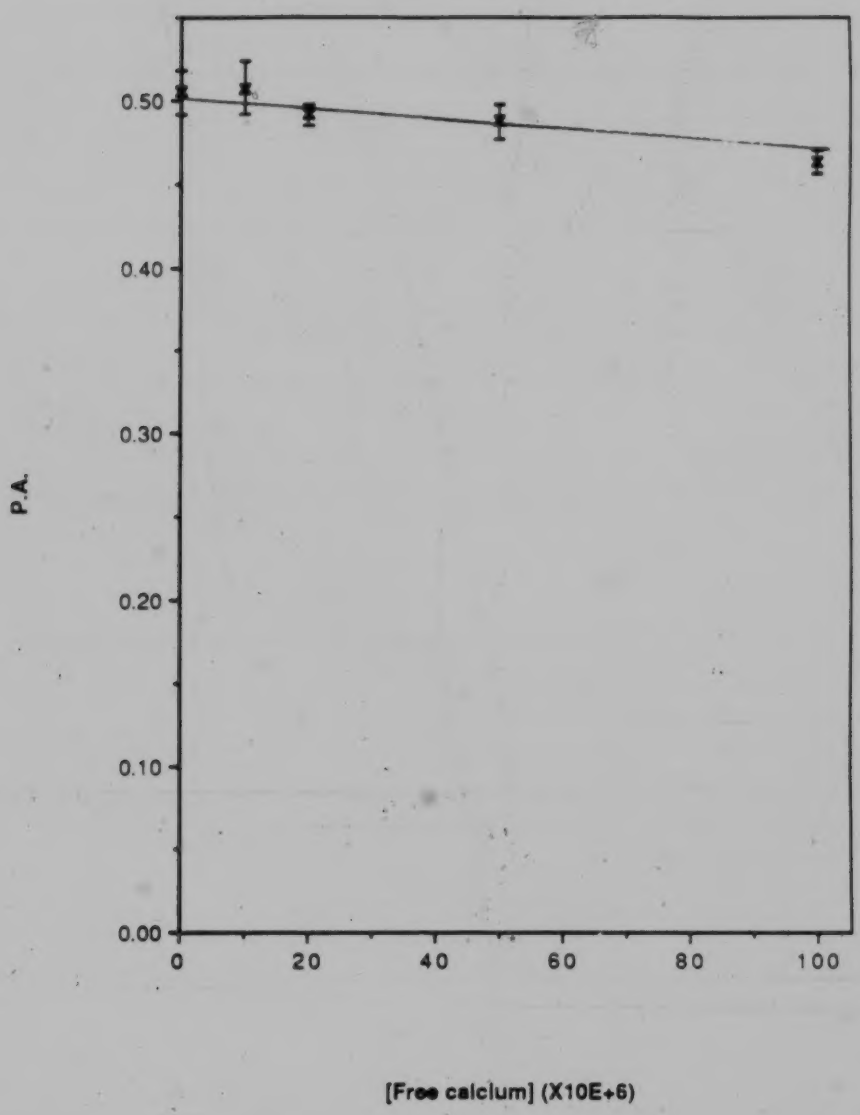

Fig 3.24: Effect of varying concentration of Ca^{+2} on Mg^{+2} sorption using the without washing procedure. Conditions: C_{Mg} = 1.00 x 10^{-5} M, PIPES = 0.001 M, μ = 0.25 M, pH = 6.00, load = 20 min and elute = 1 min with 1 M HNO_3.

the amount of Mg^{+2} sorbed. Mg^{+2} isotherms containing varying quantities of added Ca^{+2} are presented in Fig 3.25. In order to compare the effect of Ca^{+2} at low column loadings (Fig 3.24), the data points for $[Mg^{+2}]$ of 1.65×10^{-3} M in Fig 3.25 were used for Fig 3.26, which is a plot of P.A. vs $[Ca^{+2}]$. On the basis of Fig 3.25, the application of XAD-oxine under overloaded column conditions to determine $[Mg^{+2}]$ will also require the determination of $[Ca^{+2}]$ in order to prepare appropriate standards.

Column equilibration experiments without washing could not be performed under overloaded column conditions mainly because of the high signal contribution due to magnesium in the void volume.

3.4 Summary

In this chapter, two slightly different procedures i.e. with washing and without washing were used to characterize the sorption of $[Mg^{+2}]$ on XAD-oxine. The optimized system and experimental conditions obtained in this chapter will be used in the next chapter to determine $[Mg^{+2}]$ in the presence of other magnesium-containing species. At this point, both procedures appear to be suitable for use in determining the $[Mg^{+2}]$.

Isotherms from both procedures were non-linear, and the upper limit (i.e. low % column loading) occurred at $[Mg^{+2}]$ of 2.5×10^{-5} M at pH 6.00 which is well below the $[Mg^{+2}]$ in real samples. The effect of solution pH and μ were qualitatively accounted for, but attempts to quantitatively relate the amount of Mg^{+2} sorbed to the other variables proved unsuccessful. At 1% column loading, the observed effect with other sorbed cations was consistent to that expected i.e. weakly sorbed Ca^{+2} does not affect the sorption of Mg^{+2}, but strongly sorbed Cu^{+2} causes displacement of the sorbed Mg^{+2}.

Studies of XAD-oxine under overloaded column conditions were done to investigate the feasibility and limitations of matching samples with those of standards. The procedure without washing could not be applied to overloaded columns because of the large magnesium signal contributions due to the void volume. Thus, overloaded conditions were investigated

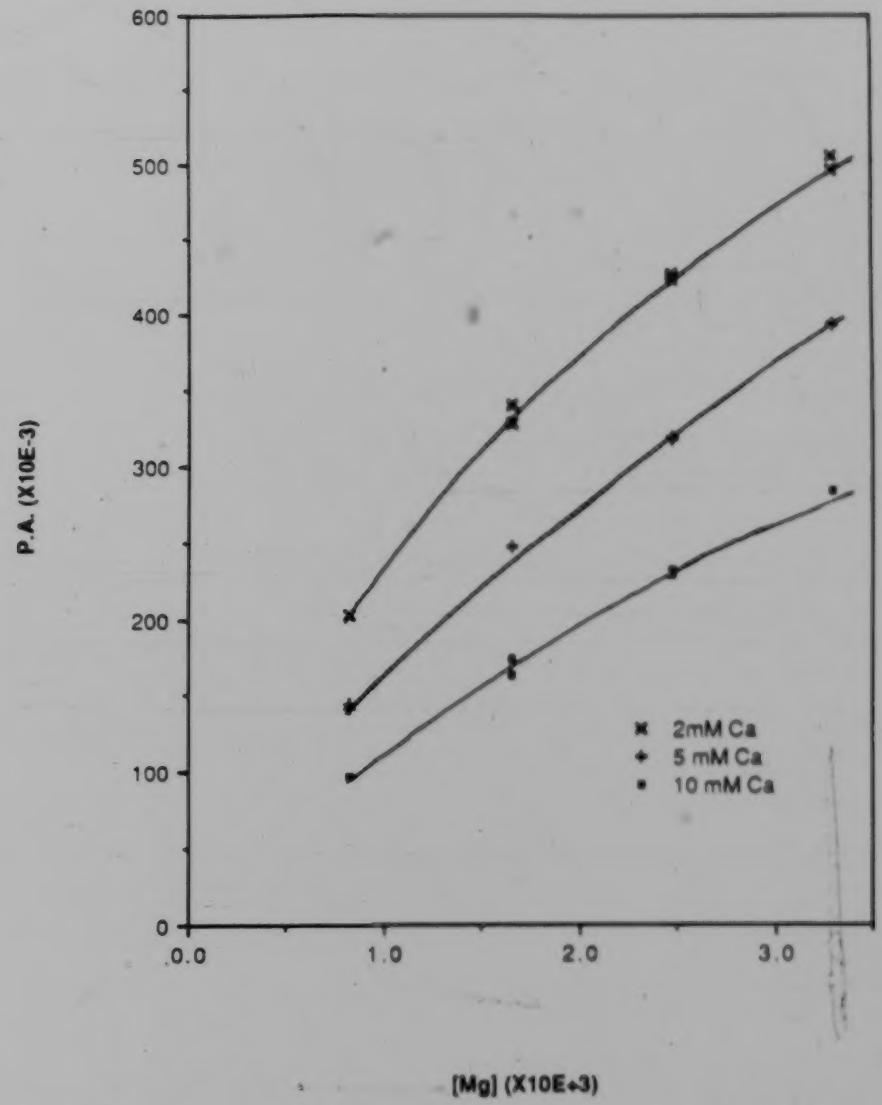

Fig 3.25: Effect of 2.0×10^{-3} M (x), 5.0×10^{-3} M (+) and 1.0×10^{-2} M (■) added Ca^{+2} on Mg^{+2} isotherm using the with washing procedure. Conditions: PIPES = 0.01 M, μ = 0.25 M, pH = 6.00, load = 5 min, wash = 2 min, elute = 1 min with 0.1 M HNO_3 and wash = 2 min.

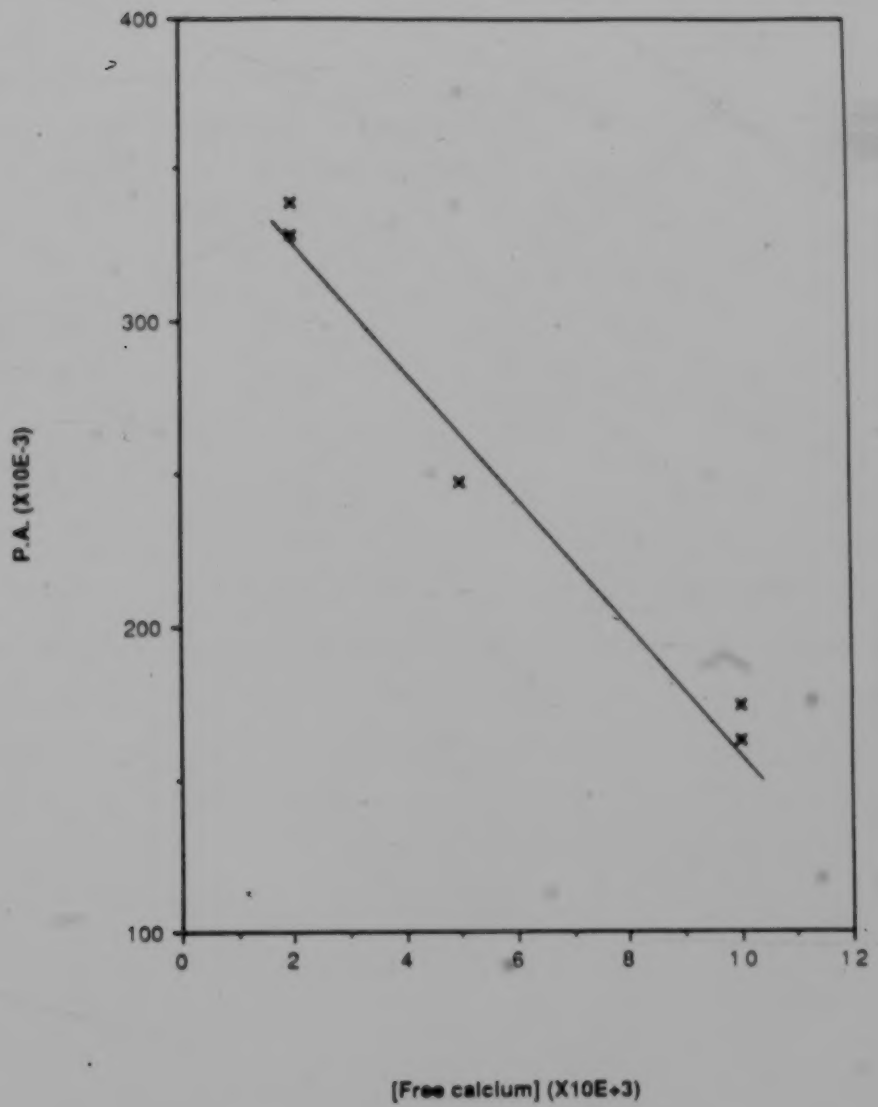

Fig 3.26: Plot of P.A. vs $[Ca^{+2}]$ for the points when $[Mg^{+2}] = 1.65 \times 10^{-3}$ M from Fig 3.25.

using the with washing procedure. Sorption of Mg^{+2} was strongly dependent on $[Ca^{+2}]$. Thus for successful application of XAD-oxine for $[Mg^{+2}]$ determination on overloaded columns, the pH, μ and $[Ca^{+2}]$ will have to be determined for preparation of appropriate standards. The determination of $[Ca^{+2}]$ itself has not been very successful (see summary in ref 68).

CHAPTER 4
SPECIATION OF Mg^{+2} WITH XAD-OXINE

4.1 Introduction

Addition of a solution containing ligand to one containing Mg^{+2} will result in the formation of one or more magnesium complexes and a decrease in $[Mg^{+2}]$ in the resulting solution. A dynamic equilibrium exists between the Mg^{+2} and its complexes. The column equilibration technique can be used to determine $[Mg^{+2}]$ in this solution. Successful use of this technique however, requires that only the free metal ion is selectively sorbed onto the resin while the complexes are not.

The column equilibration technique using sulfonated ion exchange resins (32,37) and CPG-oxine (38) has been previously used for free metal determination. The sulfonated resins did not show the desired high selectivity because cationic metal complexes were sorbed (32). Furthermore, in the presence of neutral complexes, the measured free metal ion concentration was slightly higher than the calculated values, suggesting a slight sorption of these neutral metal complexes (32,77). On the other hand, the use of CPG-oxine was extremely successful in measuring $[Ca^{+2}]$ in the presence of cationic, neutral and anionic complexes of calcium. This suggests that the oxine group shows the desired high selectivity. Thus, one would expect that the oxine group in XAD-oxine would show better selectivity than do sulfonated ion exchange resins for the determination of $[Mg^{+2}]$.

The column equilibration technique used in the above mentioned studies involved a water wash step. The procedure was the same as that described in Chapter 3 as the with washing procedure. Apparently, no difficulties were observed with that procedure on the cation exchange resin and on CPG-oxine. Furthermore, in Chapter 3, both the with washing and without washing procedures show the same behavior when XAD-oxine was used. In contrast, in this Chapter it will be shown that the with washing procedure yields

an erroneously value for [Mg^{+2}] when XAD-oxine is used, apparently because of dissociation of the complexes during dilution in the water wash step. Furthermore, it will be shown that XAD-oxine can be non-specific to some magnesium complexes. This Chapter also investigates the non-specificity of XAD-oxine, in order to understand the fundamental sorption process.

4.2 Experimental

4.2.1 Chemicals and Reagents

0.1 M Oxalic acid (Fisher Certified Reagent) was used as supplied.

1 M Picolinic acid (2-pyridinecarboxylic acid) was used as supplied from Sigma Chemical Co.

Distilled water, Hydrochloric acid, Nitric acid, NaOH and XAD-2 resin were the same as in section 2.2.2.

NaCl, PIPES, EDTA and magnesium stock solutions were the same as section 3.2.1.

XAD-oxine was prepared as described in section 2.2.4.

4.2.2 Apparatus

The apparatus used for column equilibrium experiments with washing was the same as described in section 3.2.2.1, and that used for the without washing procedure was the same as in section 3.2.2.2. Construction of the column packed with either XAD-2 resin or XAD-oxine was described in section 3.2.4. Measurements of pH were performed in the same manner as described in section 2.2.1. Nylon membrane filters (0.45 μm) were manufactured by Ultipor, Pall Trinity Micro Corp., Cortland, NY.

4.2.3 Column equilibration procedure

The procedures for experiments with washing and without washing after column equilibration were described in sections 3.2.3.1 and 3.2.3.2 respectively.

4.2.4 Preparation of test solutions

Standards of varying [Mg^{+2}] but of fixed pH and ionic strength were prepared as described in section 3.2.5. These were used for isotherm measurements.

As described in section 3.2.5, the pH and ionic strength were accurately controlled in all test solutions. Since EDTA, oxalic acid and picolinic acid are highly dissociated at pH 6.00, sample solutions containing these acids as well as the PIPES buffer were corrected for their ionic strength contributions. With the tetraprotic EDTA, consideration was given to the fraction of each multivalent species. For example, at a pH of 6.00 and an ionic strength of 0.1 M, the fractional contribution from the main EDTA species are: $\alpha_{HY^{-3}} = 0.41$ and $\alpha_{H_2Y^{-2}} = 0.59$. Thus the ionic strength contribution from EDTA is 3.02 C_{EDTA} as shown in eq 4.1

$$\mu = \frac{1}{2}\sum z_i^2 C_i = \frac{C_{EDTA}}{2}\sum 9(0.41) + 4(0.59) = 3.02\, C_{EDTA} \quad \text{.....4.1}$$

where z_i is the charge of the ion and C_i is the concentration of the species. Final adjustment to the desired ionic strength was made with 1 M NaCl solution. The solution pH was controlled with PIPES buffer. The final concentration of PIPES in the test solution was 0.01 M for the with washing procedure and 0.001 M for the without washing procedure.

When ligand-containing solutions with a desired $\alpha_{Mg^{+2},\,Expt}$ were prepared, the concentration of ligand was first theoretically calculated. Also the concentration of total magnesium added to the ligand-containing solution was such that the final [Mg^{+2}] in the solution was below the concentration required for 1% column loading.

4.2.5 Experimental determination of $\alpha_{Mg^{+2},Expt}$ in ligand containing solutions

For experimentally determining $\alpha_{Mg^{+2},Expt}$ it was necessary to determine the $[Mg^{+2}]$ in the ligand-containing solution. This was done by measuring the eluted P.A. after column equilibration experiments were performed on these ligand-containing solutions. The $[Mg^{+2}]$ in the ligand-containing solution was found by interpolation from a Mg^{+2} isotherm of P.A. against $[Mg^{+2}]$. The standard Mg^{+2} solutions, that were used to generate the isotherm, were run on columns in alternation with the ligand-containing solutions in every experiment. Running solutions for the Mg^{+2} isotherm on the same day as the ligand-containing solutions eliminates errors that may arise from day-to-day variation of experimental parameters.

As discussed in section 3.3.6, all test solutions contained traces of Mg^{+2} from the NaCl and PIPES stock solution. In speciation studies where ligands were added, the measurement of $\alpha_{Mg^{+2}}$ required correction for the amount of Mg^{+2} in the blank. Rather than doing an individual blank for each ligand-containing solution, it was more convenient to sum the magnesium concentration found in the blank with that which was added to the ligand-containing solution in order to obtain C_{Mg}. The same was done for the standards used for the Mg^{+2} isotherm i.e. Mg^{+2} isotherms were plotted as P.A. vs ($[Mg^{+2}]$ in blank + $[Mg^{+2}]$ added to standard). The concentration of Mg^{+2} in the blank was obtained by direct aspiration of all the prepared Mg^{+2} standard solutions used for the isotherm. Linear regression of the absorbance values of these standards allowed extrapolation to obtain the concentration of magnesium in the blank. Furthermore, directly aspirating the standards into the AAS to determine the concentration of magnesium in the blank also provides a check on the AAS linearity for every experiment.

4.2.6 Calculation of $\alpha_{Mg^{+2},Calc}$ from theory

Calculation of theoretical values of $\alpha_{Mg^{+2},Calc}$ in all ligand containing solutions was based on simultaneous calculations of multiple equilibria (88-90). In calculating the $\alpha_{Mg^{+2},Calc}$ all the metal-ligand equilibria are taken into consideration. However, since hydrolysis of magnesium does not occur significantly at pH 6-7 (86,91), it was neglected. Also, as discussed in section 3.3.8, complexation between Mg^{+2} and the Cl^- is small and was not taken into consideration. Formation constants used for calculations were all taken from the critical compilation of Smith and Martell (86). The values used are listed in Table 4.1. If necessary, formation constants were corrected for ionic strength from activity coefficients calculated from the Davies equation (92).

To understand the general procedure, the calculation with the largest number of equilibria will be presented. Consider a sample solution containing EDTA and magnesium in a NaCl electrolyte. The equilibria that are present, and their respective concentration stability constants are:

$$Y^{-4} + H^+ \leftrightarrow HY^{-3} \qquad K_{HY} = \frac{[HY^{-3}]}{[H^+][Y^{-4}]} \qquad \text{.....4.2}$$

$$HY^{-3} + H^+ \leftrightarrow H_2Y^{-2} \qquad K_{H_2Y} = \frac{[H_2Y^{-2}]}{[H^+][HY^{-3}]} \qquad \text{.....4.3}$$

$$H_2Y^{-2} + H^+ \leftrightarrow H_3Y^{-3} \qquad K_{H_3Y} = \frac{[H_3Y^{-3}]}{[H^+][H_2Y^{-2}]} \qquad \text{.....4.4}$$

$$H_3Y^{-3} + H^+ \leftrightarrow H_4Y \qquad K_{H_4Y} = \frac{[H_4Y]}{[H^+][H_3Y^{-3}]} \qquad \text{.....4.5}$$

Table 4.1: Values of formation constants used in this chapter to calculate the fraction of individual species in metal-ligand solutions. These values were taken from Smith and Martell (86). Uncertainties in parenthesis were obtained from all values compiled in the literature (86,95-97) and those not in parenthesis were from Smith and Martell.

Equilibrium	log K_f	Temp(°C), μ(M)
$H^+ + Y^{-4} \rightleftharpoons HY^{-3}$	10.17 (± 0.09)	25, 0.1
$H^+ + HY^{-3} \rightleftharpoons H_2Y^{-2}$	6.11 (± 0.07)	25, 0.1
$H^+ + H_2Y^{-2} \rightleftharpoons H_2Y^-$	2.68 (± 0.03)	25, 0.1
$H^+ + H_3Y^- \rightleftharpoons H_4Y$	2.0 (± 0.07)	25, 0.1
$Na^+ + Y^{-4} \rightleftharpoons NaY^{-3}$	1.64 (± 0.13)	25, 0.1
$Mg^{+2} + Y^{-4} \rightleftharpoons MgY^{-2}$	8.83 (± 0.10)	25, 0.1
$H^+ + MgY^{-2} \rightleftharpoons MgHY^-$	3.85 (± 0)	20, 0.1
$H^+ + Ox^{-2} \rightleftharpoons HOx^-$	4.266 ± 0.001	25, 0.1
$H^+ + HOx^- \rightleftharpoons H_2Ox$	1.252 (± 0)	25, 0.1
$Mg^{+2} + Ox^{-2} \rightleftharpoons MgOx$	2.76 (± 0.14)	25, 0.1
$Mg^{+2} + 2Ox^{-2} \rightleftharpoons MgOx_2$	4.25 (± 0.24)	25, 0.1
$H^+ + P^{-2} \rightleftharpoons HP^-$	5.21 ± 0.01	25, 0.1
$H^+ + HP^- \rightleftharpoons H_2P$	1.03 (± 0.09)	25, 0.1
$Mg^{+2} + P^{-2} \rightleftharpoons MgP^+$	2.20 (± 0.05)	25, 0.1
$Mg^{+2} + 2P^{-2} \rightleftharpoons MgP_2$	3.95 (± 0)	25, 0.0

$$Mg^{+2} + Y^{-4} \leftrightarrow MgY^{-2} \qquad K_{MgY} = \frac{[MgY^{-2}]}{[Mg^{+}][Y^{-4}]} \quad \text{..... 4.6}$$

$$MgY^{-2} + H^{+} \leftrightarrow MgHY^{-} \qquad K_{MgHY} = \frac{[MgHY^{-}]}{[MgY^{-2}][H^{+}]} \quad \text{.....4.7}$$

$$Na^{+} + Y^{-4} \leftrightarrow NaY^{-3} \qquad K_{NaY} = \frac{[NaY^{-3}]}{[Na^{+}][Y^{-4}]} \quad \text{..... 4.8}$$

The fraction of EDTA ligand ($\alpha_{Y^{-4}}$) is given by:

$$\alpha_{Y^{-4}} = \frac{[Y^{-4}]}{[Y^{-4}]+[HY^{-3}]+[H_2Y^{-2}]+[H_3Y^{-3}]+[H_4Y]+[MgY^{-2}]+[MgHY^{-}]+[NaY^{-3}]} \quad \text{..... 4.9}$$

On substituting for the concentration constants of the various species in eq 4.9, by rearranging eqns 4.2 to 4.8 and cancelling out the common terms, $\alpha_{Y^{-4}}$ becomes:

$$\alpha_{Y^{-4}} = (1+K_{HY}[H^{+}]+K_{HY}K_{H_2Y}[H^{+}]^2+K_{HY}K_{H_2Y}K_{H_3Y}[H^{+}]^3+K_{HY}K_{H_2Y}K_{H_3Y}K_{H_4Y}[H^{+}]^4 + K_{MgY}[Mg^{+2}]+K_{MgY}K_{MgHY}[Mg^{+2}][H^{+}]+K_{NaY}[Na^{+}])^{-1} \quad \text{..... 4.10}$$

Equation 4.10 was used to get a first estimate of $\alpha_{Y^{-4}}$ by neglecting $[MgY^{-2}]$ and $[MgHY^{-}]$. The concentration of ligand $[Y^{-4}]$ from EDTA, is estimated from the total concentration, C_{EDTA} by

$$[Y^{-4}] = \alpha_{Y^{-4}} C_{EDTA} \quad \text{.....4.11}$$

The fraction of free Mg^{+2}, $\alpha_{Mg^{+2}}$ is given by:

$$\alpha_{Mg^{+2}} = \frac{[Mg^{+2}]}{C_{Mg}} = \frac{[Mg^{+2}]}{[Mg^{+2}] + [MgY^{-2}] + [MgHY^{-2}]} \quad \text{..... 4.12}$$

Substituting for $[MgY^{-2}]$ and $[MgHY^{-}]$ in eq 4.12 by rearranging eqns 4.6 and 4.7, and cancelling out common terms, $\alpha_{Mg^{+2}}$ becomes

$$\alpha_{Mg^{+2}} = (1 + K_{MgY}[Y^{-4}] + K_{MgY}K_{MgHY}[Y^{-4}][H^{+}])^{-1} \quad \text{..... 4.13}$$

Using the first estimate of $[Y^{-4}]$ from eq 4.11, the first value of $\alpha_{Mg^{+2}}$ was calculated. The first value of $\alpha_{Mg^{+2}}$ was used to calculate the first value of $[Mg^{+2}]$ in the ligand-containing solution using eq 4.12. The $[Mg^{+2}]$ was then used in eq 4.10 to get a more accurate value of $\alpha_{Y^{-4}}$ and the steps outlined above were repeated (iteration) until two successive estimates of $[Mg^{+2}]$ agreed within 1% of each other.

The above calculations of species distribution were checked by computer calculations (University of Alberta Amdahl) using a slightly modified version of the speciation program COMICS (93). Species distribution values obtained by this computer program agreed within 2% of those obtained from the above calculations. The modification is an additional subroutine which provides the fraction of each species distribution in a tabular form. A detailed description and input procedures is given in the appendix of reference 68.

Uncertainties in the theoretically calculated values were obtained by the standard procedures for error propagation (88,90,94) using all the reported values of the formation constants. The uncertainty of the formation constants was based on all values compiled in the literature (86,95-97). Where uncertainties for formation constants

were reported, more weight (x3) was given to them in calculating the standard deviation. If necessary, the stability constants were corrected for ionic strength. Uncertainties obtained by this procedure are presented in parenthesis in Table 4.1. The uncertainties not in parenthesis in Table 4.1 were taken from Smith and Martell (86).

4.3 Results and Discussion

4.3.1 Selectivity in the presence of EDTA

EDTA is a hexadentate chelating ligand that forms the species MgY^{-2} and $MgHY^{-}$ with Mg^{+2}. The formation formation constant of MgY^{-2} which was given by eq 4.6 is 6.76×10^{8} and that of $MgHY^{-}$ given by eq 4.7 is 7.08×10^{3} (86). At a pH of 6.00 and at the highest [EDTA] used, the fraction of the various species in the presence of Mg^{+2} are $\alpha_{Mg^{+2}} \sim 0.056$; $\alpha_{MgY^{-2}} \sim 0.94$ and $\alpha_{MgHY^{-}} \sim 0.007$. Because $\alpha_{MgHY^{-}}$ is very small, MgY^{-2} can be considered as the only complex species formed. Solutions were prepared with varying concentrations of EDTA and magnesium to give values of $\alpha_{Mg^{+2},Calc}$ ranging from 0.005 to 0.6. The corresponding values of $[Mg^{+2}]$ all yield column loading of <1% using the with washing procedure. The experimentally observed $\alpha_{Mg^{+2},Expt}$ and calculated $\alpha_{Mg^{+2},Calc}$ are presented in Table 4.2 which shows that in all cases, the experimentally observed $\alpha_{Mg^{+2},Expt}$ values were greater than the calculated $\alpha_{Mg^{+2},Calc}$ values. Table 4.2 also shows that at high values of $\alpha_{Mg^{+2},Calc}$ (~ 0.6), the calculated and experimental values were statistically the same, but as the values of $\alpha_{Mg^{+2},Calc}$ get lower (~ 0.005), the experimental values become increasingly greater than calculated values. Observations of this kind were previously obtained with other metal-ligand systems (77) but no further studies were done. Previous workers attributed this uncertainty to the sorption of other metal containing species (77) or to the high uncertainty in the published values of the formation constants (98). For a well characterized system like

Table 4.2: Effect of varying [EDTA] on the fraction of free metal using the with washing procedure. Solution conditions: μ = 0.10 M, [PIPES] = 0.01 M, pH = 6.00, load = 5 min, water wash = 2 min, elute with 0.1 M HNO_3 = 1 min and wash = 2 min.

C_{EDTA} $\times 10^{-3}$ M	C_{Mg} $\times 10^{-6}$ M	$\alpha_{Mg^{+2},Calc}$	$\alpha_{Mg^{+2},Expt}$
10.0	411	0.00518 ± 0.00149	0.0145 ± 0.0003
10.0	823	0.00539 ± 0.00153	0.0141 ± 0.0008
10.0	123	0.00567 ± 0.00159	0.0131 ± 0.0005
0.16	12.3	0.249 ± 0.054	0.452 ± 0.003
0.12	12.3	0.309 ± 0.061	0.511 ± 0.038
0.080	12.3	0.406 ± 0.068	0.612 ± 0.032
0.040	12.3	0.588 ± 0.069	0.727 ± 0.026

EDTA, it is unlikely that the published values have large errors associated with the formation constants.

In this work, a systematic investigation was done to determine why the experimentally observed $\alpha_{Mg^{+2}}$ values were always greater than the calculated values. Before it was discovered that the wash step was the cause for the difference between $\alpha_{Mg^{+2},Expt}$ and $\alpha_{Mg^{+2},Calc}$, five possible reasons were investigated:

1) Is the 5 min loading time sufficient to achieve equilibration in the ligand-containing solution? The loading curve in Fig 4.1 shows that complete equilibrium was achieved within 3 min for a solution containing a high concentration of EDTA (0.001 M).

2) The possibility of resin sorption of other species such as MgY^{-2} was investigated. Assuming that the acidity constants of the immobilized oxine are close to those in homogeneous solution, then using equations similar to eq 3.14, the fraction of various species of the oxine at pH 6.00 are $\alpha_{Ox^-} = 6.7 \times 10^{-4}$; $\alpha_{HOx} = 0.97$ and $\alpha_{H_2Ox^+} = 0.031$. Since the oxine has a net positive charge, the possibility exists for sorption of the anionic MgY^{-2} by a ion exchange process as shown by eq 4.14.

$$2(ROH_2^+Cl^-)_R + MgY^{-2} \rightleftharpoons ((ROH_2^+)_2MgY^{-2})_R + 2\,Cl^- \quad \text{4.14}$$

Increasing the pH of the solution will increase the fraction of anionic oxine sites, α_{Ox^-} and decrease the fraction of cationic sites $\alpha_{H_2Ox^+}$ on the resin. Thus, decreasing the pH of the solution will increase $\alpha_{H_2Ox^+}$ of the resin. If the H_2Ox^+ group on the resin is responsible for MgY^{-2} sorption, then when EDTA solutions of different pH are run on the resin, one should observe more sorption of MgY^{-2} with decreasing pH. Since the measured P.A. will be used to obtain $[Mg^{+2}]$ in the Mg-EDTA solution, and is the sum of $[MgY^{-2}]$ and $[Mg^{+2}]$ sorbed on the resin, then $\alpha_{Mg^{+2},Expt}$ should show an increase with decreasing solution pH. Table 4.3 shows the $\alpha_{Mg^{+2},Expt}$ as well as $\alpha_{Mg^{+2},Calc}$ for Mg-EDTA solutions at different solution pH. As can be seen in Table 4.3, the reverse effect

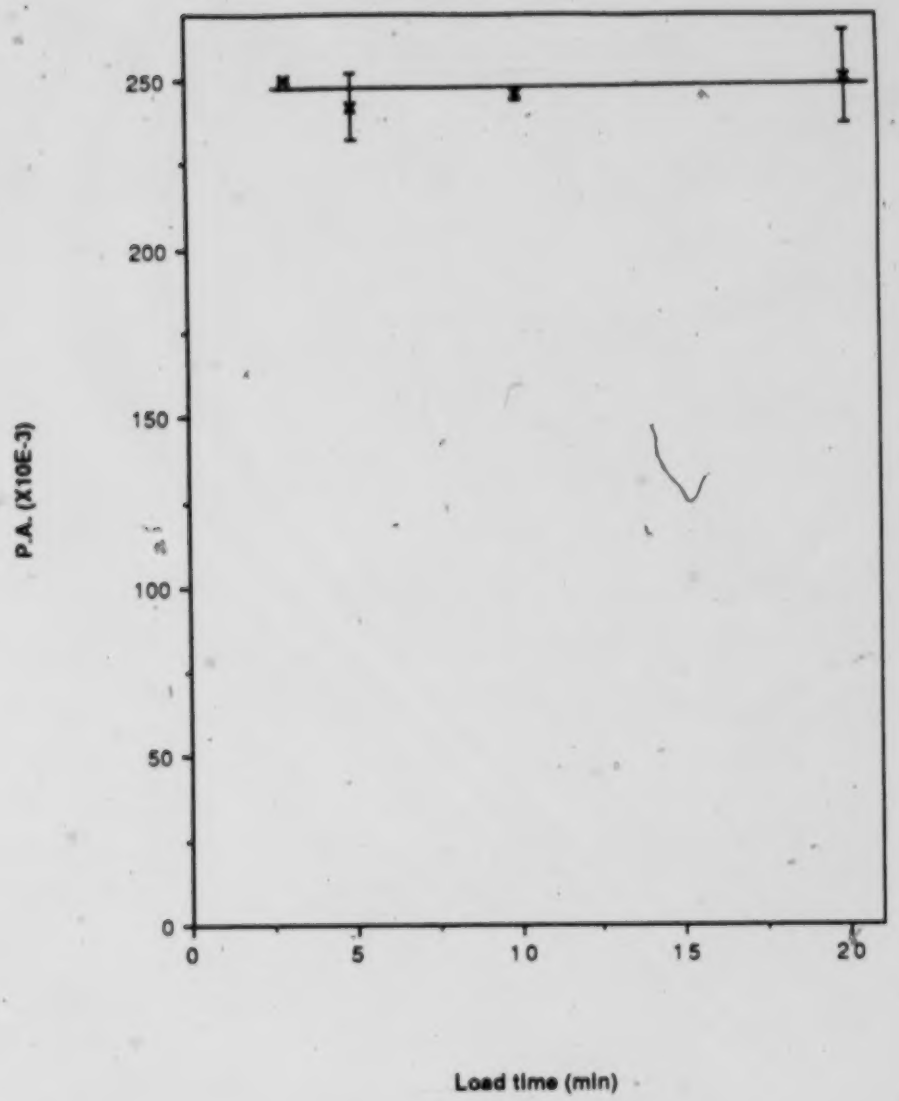

Fig 4.1: Loading curve using the with washing procedure to recheck the loading time required for the column equilibration to be in complete equilibrium with a Mg-EDTA solution. Conditions: C_{Mg} = 8.23 x 10^{-5} M, C_{EDTA} = 1.00 x 10^{-3} M, PIPES = 0.01 M, μ = 0.10 M, pH = 6.00, load = varying, wash = 2 min, elute = 1 min and wash = 2 min.

Table 4.3: Effect of EDTA at various pH on the fraction of free metal using the with washing procedure. Solution conditions: μ = 0.10 M, [PIPES] = 0.01 M, pH = specified, load = 5 min, water wash = 2 min, elute with 0.1 M HNO_3 = 1 min and wash = 2 min.

C_{EDTA} $\times 10^{-3}$ M	C_{Mg} $\times 10^{-6}$ M	pH	$\alpha_{Mg^{+2},Calcc}$	$\alpha_{Mg^{+2},Expt}$
1.0	11.5	5.50	0.258	0.546 ± 0.004
1.0	32.1	5.50	0.260	0.474 ± 0.012
1.0	52.7	5.50	0.263	0.441 ± 0.001
1.0	104	5.50	0.271	0.402 ± 0.006
1.0	42.7	6.00	0.0494 ± 0.0136	0.125 ± 0.013
1.0	83.9	6.00	0.0512 ± 0.0141	0.109 ± 0.004
1.0	125	6.00	0.0537 ± 0.143	0.112 ± 0.005
1.0	166	6.00	0.0558 ± 0.0147	0.107 ± 0.004
1.0	42.5	6.50	0.0101	0.0482±0.0020
1.0	125	6.50	0.0109	0.0407±0.0001
1.0	207	6.50	0.0121	0.0376±0.0006
1.0	289	6.50	0.0133	0.0366±0.0001

was observed i.e. $\alpha_{Mg^{+2},Expt}$ gets closer to $\alpha_{Mg^{+2},Calc}$ when the solution pH decreases. Therefore, sorption of MgY^{-2} by the cationic form of the immobilized oxine can be eliminated from consideration.

3) Sorption of charged species on the hydrophobic XAD-2 surface had been previously observed (99), and was investigated in this study. The possibility of sorption onto the XAD-2 surface is based on the fact that the immobilized oxine covers only a small fraction (< 5%) of the hydrophobic surface (99). The amount of magnesium sorbed from the same EDTA containing solutions were determined on similar size XAD-2 and XAD-oxine columns. The raw data of P.A. on these two XAD columns are presented in Table 4.4. The sorption of Mg-EDTA complexes on the two glass frits was found to be negligible from a solution containing 1.65×10^{-4} M magnesium and 0.001 M EDTA ($\alpha_{Mg^{+2}} \sim 0.05$) performed on a column containing 12 mm of only glass frits. Assuming that the amount of magnesium sorption on the XAD-2 resin and glass frits would be the same as that of the XAD-oxine column, the quantity of magnesium eluted from the XAD-2 column was subtracted from the quantity eluted on the XAD-oxine column. Using these data the $\alpha_{Mg^{+2},Expt}$ were calculated and are presented in Table 4.4. Comparison of the calculated and experimental values of $\alpha_{Mg^{+2}}$ suggests that sorption of MgY^{-2} onto XAD-2 and glass frits does not totally account for the difference between the experimental and calculated values of $\alpha_{Mg^{+2}}$.

4) Another sorption possibility that was considered was the sorption of MgY^{-2} by a mechanism shown in equations 4.15 and 4.16 i.e the sorbed Mg^{+2} becomes another site for MgY^{-2} sorption i.e.

$$(RO^{-}Na^{+})_R + Mg^{+2} \rightleftharpoons (RO^{-}Mg^{+2})_R + Na^{+} \quad \text{.....4.15}$$

$$2(ROMg^{+2}Cl^{-})_R + MgY^{-2} \rightleftharpoons ((ROH_2^{+})_2MgY^{-2})_R + 2\,Cl^{-} \quad \text{.....4.16}$$

Table 4.4: The sorption of Mg-EDTA solutions on columns packed with 1 cm of XAD-2 and XAD-oxine. Also, the effect of varying [EDTA] on the fraction of free metal after correcting for sorption on a blank XAD-2 column, using the with washing procedure. Solution conditions: μ = 0.10 M, [PIPES] = 0.01 M, pH = 6.00, load = 5 min, wash = 2 min, elute = 1 min and wash = 2 min.

C_{EDTA} x 10^{-3} M	C_{Mg} x 10^{-6} M	P.A.(XAD-Oxine) x 10^3	P.A.(XAD-2) x 10^3	$\alpha_{Mg^{+2},Calc}$	$\alpha_{Mg^{+2},Expt}$
6.0	496	348 ± 4.2	62.8 ± 10.3	0.00895 ± 0.00253	0.0210 ± 0.004
6.0	14.4	23.3 ± 0.7	8.2 ± 1.0	0.00825 ± 0.0024	0.0392 ± 0.0018
0.60	51.4	244 ± 5.7	29.2 ± 2.1	0.0820 ± 0.0217	0.155 ± 0.004
0.60	14.4	82 ± 4.9	13.0 ± 1.5	0.0784 ± 0.0210	0.173 ± 0.013
0.080	14.4	240 ± 3.5	18.2 ± 0.5	0.410 ± 0.069	0.560 ± 0.008
0.012	14.4	364 ± 13	17.8 ± 4.0	0.837 ± 0.038	0.874 ± 0.034

Attempts to fit the raw data of Table 4.4 to equations 4.15 and 4.16 proved fruitless.

5) The possibility that a 2 min water wash after column equilibration is involved in producing the high $\alpha_{Mg^{+2},Expt}$ values was investigated. Initially, a similar experiment to that described in section 3.3.3 was done. Using a solution containing 0.001 M EDTA and 8.23×10^{-5} M C_{Mg}, columns were brought to equilibrium and then water washed for varying times. The results are shown in Fig 4.2, which shows that the water wash completely removes the interstitial solution and there was no decrease in sorbed magnesium for water washing of between 1 to 20 min. These results are similar to those in Fig 3.11 in that the water wash does not remove sorbed Mg^{+2}. However, these results do not reveal what is happening at the start of the water wash step before 1 min, and thus can be misleading.

The procedure described as "without washing" was specifically designed to observe the effect with the absence of a water wash after column equilibration. Table 4.5 shows the values of $\alpha_{Mg^{+2},Calc}$ and $\alpha_{Mg^{+2},Expt}$ obtained with the without washing procedure for Mg-EDTA solutions, using the same experimental conditions (given in Fig 4.5 caption) as those used for the with washing procedure. Although these were not the optimum experimental conditions, Table 4.5 shows there is considerable agreement between the calculated and experimental values. Because all experimental variables were the same except the elimination of the water wash, these results suggest that the inclusion of a wash step affects $\alpha_{Mg^{+2},Expt}$.

As discussed in section 3.3.4, optimization of the without washing procedure required reduction of the [PIPES] to 0.001 M. The optimum conditions with this procedure were: load = 20 min and eluent concentration = 1 M HNO_3. Table 4.6 shows results obtained after optimization of all the variables for the without wash procedure. The results in Table 4.6 demonstrate that the water wash step was the main reason for

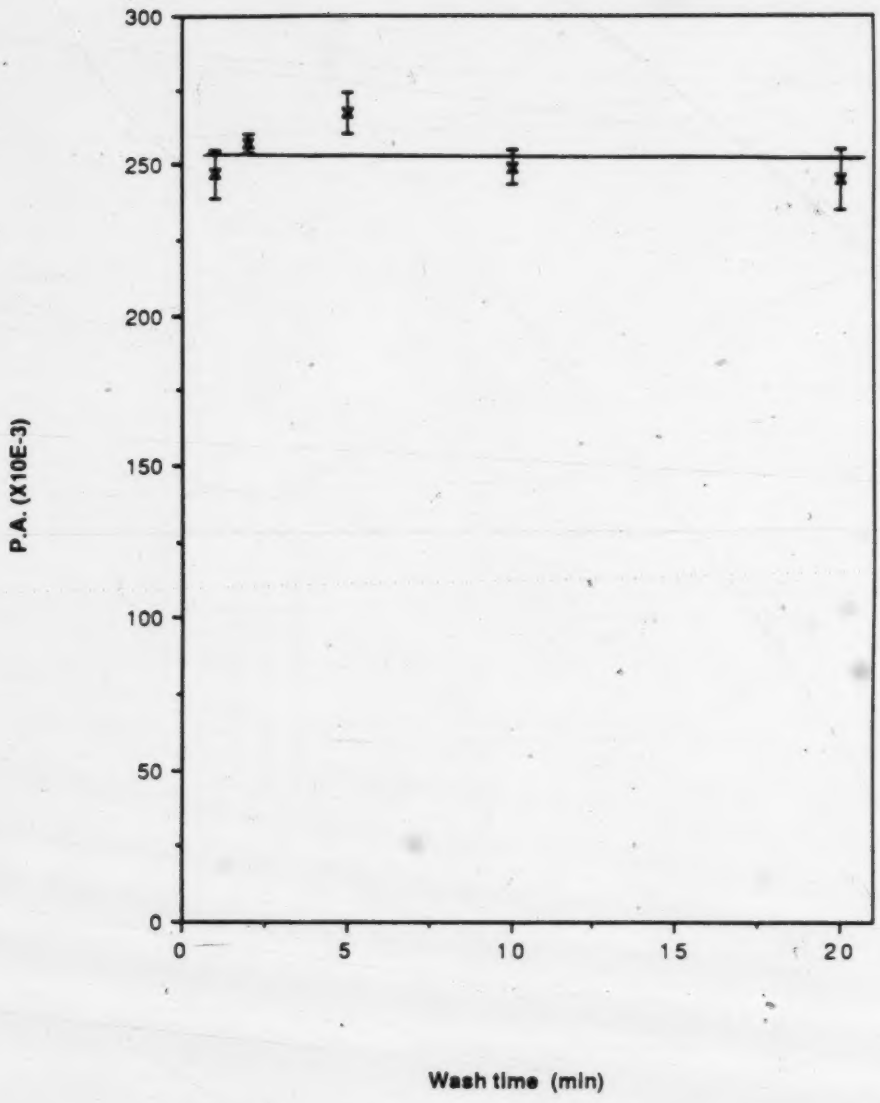

Fig 4.2: Washing conditions. Conditions: C_{Mg} = 8.23 x 10^{-5} M, C_{EDTA} = 1.00 x 10^{-3} M, PIPES = 0.01 M, μ = 0.10 M, pH = 6.00, load = 5 min, wash = varying, elute = 1 min and wash = 2 min.

Table 4.5: Effect of EDTA on the fraction of free metal immedately on using the without washing procedure. Conditions were not optimized, but were the same as those used in the with washing procedure. Solution conditions: μ = 0.10 M, [PIPES] = 0.01 M, pH = 6.00, load = 5 min and elute with 0.1 M HNO_3 = 1 min.

C_{EDTA} x 10^{-3} M	C_{Mg} x 10^{-6} M	$\alpha_{Mg^{+2},Calc}$	$\alpha_{Mg^{+2},Expt}$
0.20	43.2	0.230 ± 0.049	0.174 ± 0.015
0.20	22.7	0.215 ± 0.048	0.222 ± 0.013
0.50	43.2	0.0975 ± 0.0112	0.0914 ± 0.0112
0.50	22.7	0.0941 ± 0.025	0.106 ± 0.021

Table 4.6: Effect of EDTA on the fraction of free metal using the without washing procedure. Conditions were optimized: μ = 0.25 M, [PIPES] = 0.001 M, pH = 6.00, load = 20 min and elute with 1 M HNO_3 = 2 min.

C_{EDTA} x 10^{-3} M	C_{Mg} x 10^{-6} M	$\alpha_{Mg^{+2},Calc}$	$\alpha_{Mg^{+2},Expt}$
0.010	5.15	0.941 ± 0.019	1.00 ± 0.016
0.10	5.15	0.613 ± 0.081	0.651 ± 0.014
0.20	10.0	0.441 ± 0.084	0.520 ± 0.060
0.40	16.1	0.280 ± 0.070	0.342 ± 0.030
0.50	20.6	0.243 ± 0.060	0.273 ± 0.040
1.0	10.36	0.135 ± 0.040	0.154 ± 0.009
5.0	20.37	0.030 ± 0.010	0.0515 ± 0.0012

the higher value of $\alpha_{Mg^{+2},Expt}$ than $\alpha_{Mg^{+2},Calc}$. Furthermore, these results suggest that the XAD-oxine is specific for Mg^{+2} in the presence of Mg-EDTA species. In section 4.3.2, the same specificity for Mg^{+2} will be observed in the presence of oxalate ligand.

This observation that the water wash step immediately after column equilibration perturbs the resin-solution equilibrium was surprising because the with washing procedure was successfully used with ion exchange resins for speciation studies(37,98). To explain why the wash step causes erroneously high $\alpha_{Mg^{+2},Expt}$ with XAD-oxine but not with ion exchangers, one will have to consider what happens upon switching an equilibrated resin-solution system to the water wash.

For the sulfonated resin at equilibrium between the resin and metal-ligand solution, anionic species e.g. MgY^{-2} are excluded by the Donnan potential from entering the resin particles (100). Furthermore, the ionic strength within the sulfonated resin is very high and relatively constant because the constant surface charge requires counter ions to be present for charge balance. On changing to the wash step, the metal-ligand solution outside of the resin is removed almost instantaneously in the flow system. Within the resin, no more free metal sorption or dissociation of metal-complexes occurs, because the ionic strength will remain almost constant.

By contrast, at equilibrium between XAD-oxine and the metal-ligand solution, the solution inside the resin is almost the same composition as that outside the resin. This is because the surface of XAD-oxine is almost neutral at pH 6 ~ 7, and thus Donnan exclusion of co-ions (i.e. MgY^{-2}) is very small. On switching to the wash step, the metal-ligand solution outside of the resin can be considered to be removed almost instantaneously. However, the composition of the solution within the XAD-oxine particles does not change as fast as the external solution because all species (including electrolyte) inside will have to diffuse out of the resin. As discussed in section 3.3.8, one would expect to see more sorption of Mg^{+2} as the ionic strength in the resin solution

decreases. Furthermore, the change in ionic strength will cause dissociation of magnesium complexes to occur.

4.3.2 Selectivity in the presence of oxalate

Mg^{+2} ion complexes oxalate ion (Ox^{-2}) to form species of the type MgOx and $MgOx_2^{-2}$. At a pH of 6.0 and ionic strength of 0.10, the fraction present as the ligand oxalate ion is 0.99, and the conditional formation constants of MgOx and $MgOx_2^{-2}$ are 5.75×10^2 and 1.74×10^4 respectively. Solutions were prepared for which the $\alpha_{Mg^{+2},Calc}$ varied from 0.17 to 0.82, and the column loading was always less than 1%. The calculated fractions of Mg^{+2}, MgOx and $MgOx_2^{-2}$ in these solutions are given in Table 4.7. The fraction of Mg^{+2} were determined by the with washing procedure as described in section 4.2.5. These experimentally observed $\alpha_{Mg^{+2},Expt}$ values and the calculated $\alpha_{Mg^{+2},Calc}$ are presented in Table 4.7. These results are similar to the effect of EDTA observed when using the with washing procedure (Table 4.2), in that the $\alpha_{Mg^{+2},Expt}$ were always larger than $\alpha_{Mg^{+2},Calc}$.

Prior to identification of the wash step as the cause for the discrepancies between the observed and calculated values of $\alpha_{Mg^{+2}}$, two possibilities were ruled out:

1) The possibility of sorption of Mg-oxalate complexes on the hydrophobic XAD-oxine surface was ruled out by replacing the XAD-oxine column with a similar sized column packed with XAD-2, and then using Mg^{+2} solutions with and without added oxalate to determine the amount of Mg^{+2} sorption. The procedure used for the determination of Mg^{+2} sorption is the with washing procedure. Peak areas for sorption of magnesium onto XAD-2 from the magnesium solutions with and without oxalate were of the same magnitude and very small.

2) The possibility of colloid formation by Mg-oxalate complexes was investigated because $MgOx.2H_2O$ is relatively insoluble (101). If these colloidal complexes formed, then during the loading step, these particles will be filtered out of solution, and would

Table 4.7: Effect of varying [Oxalic acid] on the fraction of various species using the with washing procedure. Solution conditions: μ = 0.10 M, [PIPES] = 0.01 M, pH = 6.00, load = 5min, wash = 2 min, elute with 0.1 M HNO_3 = 1 min and wash = 2 min.

C_{Oxalic} x 10^{-3} M	C_{Mg} x 10^{-6} M	α_{MgOx}	α_{MgOx_2}	$\alpha_{Mg^{+2},Calc}$	$\alpha_{Mg^{+2},Expt}$
10.0	32.9	0.623	0.204	0.173 ± 0.056	0.219 ± 0.008
10.0	12.3	0.642	0.210	0.151 ± 0.037	0.294 ± 0.016
2.0	12.3	0.446	0.029	0.525 ± 0.078	0.696 ± 0.021
0.5	12.3	0.174	0.003	0.825 ± 0.005	> 1.0

subsequently be detected by the column during the elution step because of decomposition of the colloid by the acid eluent. To determine the presence of colloid, the amount of Mg^{+2} sorbed on the XAD-oxine was determined by the with washing procedure first in a solution containing 2.0×10^{-3} M oxalate and 1.65×10^{-4} M C_{Mg}, and then again after the same solutions were filtered through 0.45 μm membrane. In both cases, the eluted P.A. due to Mg^{+2} were the same before and after filtration of the solutions. Furthermore, if colloidal particles form, then during the loading step, the amount of particles retained will increase with load time. A loading study similar to that described in section 3.3.2, using Mg-oxalate solution, showed that complete equilibrium was achieved within 3 min, and there was no increase in the amount of Mg sorbed when the load time was increased.

As concluded for the Mg-EDTA system, the washing step is the main reason for the discrepancy between the experimental and calculated $\alpha_{Mg^{+2}}$. In Table 4.8, the results for the oxalate solutions containing various fraction of $\alpha_{Mg^{+2}}$, are presented using the without washing procedure. The observed and calculated $\alpha_{Mg^{+2}}$ agree with each other, and thus, it can be concluded that XAD-oxine is selective to Mg^{+2} in the presence of MgOx and $MgOx_2$ species.

4.3.3 Selectivity in the presence of picolinic acid

Based on the results of EDTA and oxalate systems, only the without washing procedure was used for picolinic acid studies. At a pH of 6.00, 84% of picolinic acid exists as the picolinate ion (P^-) which complexes Mg^{+2} to form species of the type MgP^+ and MgP_2. The conditional formation constants, at a pH of 6.00 and μ of 0, are 3.80×10^2 and 8.91×10^3 for MgP^+ and MgP_2 respectively. Using picolinic acid, solutions were prepared to contain $\alpha_{Mg^{+2},Calc}$ values ranging from 0.06 to 0.9, and the $[Mg^{+2}]$ was determined using the without washing procedure. Column 4 in Table 4.9 shows the raw data (i.e. P.A.). The amount of magnesium eluted (i.e. P.A.) increases as the

Table 4.8: Effect of varying [Oxalic acid] on the fraction of free metal using the without washing procedure. Solution conditions: μ = 0.25 M, [PIPES] = 0.001 M, pH = 6.00, load = 20 min and elute with 1 M HNO_3 = 1 min.

C_{Oxalic} x 10^{-3} M	C_{Mg} x 10^{-6} M	$\alpha_{Mg^{+2},Calc}$	$\alpha_{Mg^{+2},Expt}$
1.0	10.0	0.766 ± 0.058	0.721 ± 0.041
5.0	10.0	0.545 ± 0.066	0.487 ± 0.017
10.0	10.0	0.204 ± 0.047	0.202 ± 0.025

Table 4.9: Table shows the amount of magnesium sorption (i.e. P.A.) with solutions of varying picolinic acid concentration done on XAD-oxine and XAD-2 using the without washing procedure. Solution conditions: μ = 0.25 M, [PIPES] = 0 001 M, pH = 6.00, load = 20 min and elute with 1 M HNO_3 = 1 min. **Note**: All P.A. were corrected for the P.A. due to the void volume as discussed in section 3.2.3.2.

C_{HP} x 10^{-3} M	C_{Mg} x 10^{-6} M	$\alpha_{Mg^{+2},Calc}$	P.A. on XAD-Oxine	P.A. on XAD-2
0	10.0	1.0	0.430 ± 0.008	
1.00	10.0	0.906 ± 0.010	0.469 ± 0.021	0.021± 0.003
6.00	10.0	0.573 ± 0.025	0.552 ± 0.002	-
10.0	10.0	0.416 ± 0.020	0.615 ± 0.005	0.168 ± 0.015
50.0	10.0	0.0624 ± 0.005	0.694 ± 0.013	0.803 ± 0.078

concentration of picolinic acid increases, i.e. the P.A. increases as $\alpha_{Mg^{+2},Calc}$ decreases. The same observations of increasing P.A. with decreasing $\alpha_{Mg^{+2},Calc}$ on XAD-oxine were obtained using the with washing procedure. These observations suggest that Mg-picolinate complexes are sorbed on the XAD-oxine. To determine whether the Mg-picolinate complexes are sorbed by the hydrophobic XAD surface, the same solutions used on XAD-oxine column were repeated on a blank XAD-2 column. These results for XAD-2 sorption are presented in column 5 of Table 4.9. The same type of observations were made i.e. Mg-picolinate complexes are sorbed on XAD-2, because Mg^{+2} does not sorb (section 4.3.2). Also, the amount of magnesium sorption (i.e. P.A.) increases with increasing picolinic acid concentration.

However, these observations do not reveal what species are sorbed, and by what mechanism. To answer these questions, the approach taken will be to study the sorption of Mg-picolinate complexes on XAD-oxine and XAD-2 when pH, C_{Mg} and $C_{picolinic\ acid}$ are varied. Fig 4.3 shows the calculated species distribution of Mg^{+2}, MgP^{+} and MgP_2 when the pH and concentration of picolinic acid are varied, and will be used to design experiments to determine what species are sorbed on the XAD-2. Specifically:

1) Fig 4.3 shows that above pH 6.00, the distribution of species is dependent on $C_{picolinic\ acid}$. At a fixed pH, there is no linear relationship between $C_{picolinic\ acid}$ and the ratio of MgP^{+} to MgP_2 and thus experiments with varying $C_{picolinic\ acid}$ will reveal which of Mg-picolinate complexes are sorbed.

2) Above pH 6.00 and at a constant $C_{picolinic\ acid}$, Fig 4.3 shows that the fractions of the 3 species remains relatively constant. Thus experiments performed on XAD-2 and XAD-oxine, using solutions of varying pH but constant C_{Mg} and $C_{picolinic\ acid}$, will show the effect of pH on the sorption of these 3 species.

3) In Fig 4.3, $C_{picolinic\ acid}(1.0 \times 10^{-3}\ M) >> C_{Mg}(1.0 \times 10^{-5}\ M)$ for $\alpha_{MgP^{+}}$ above 0.10 and α_{MgP_2} above 0.01. Thus, if C_{Mg} is varied, but the pH and $C_{picolinic\ acid}$ are held constant, then an additive isotherm will be obtained on XAD-oxine. The isotherm

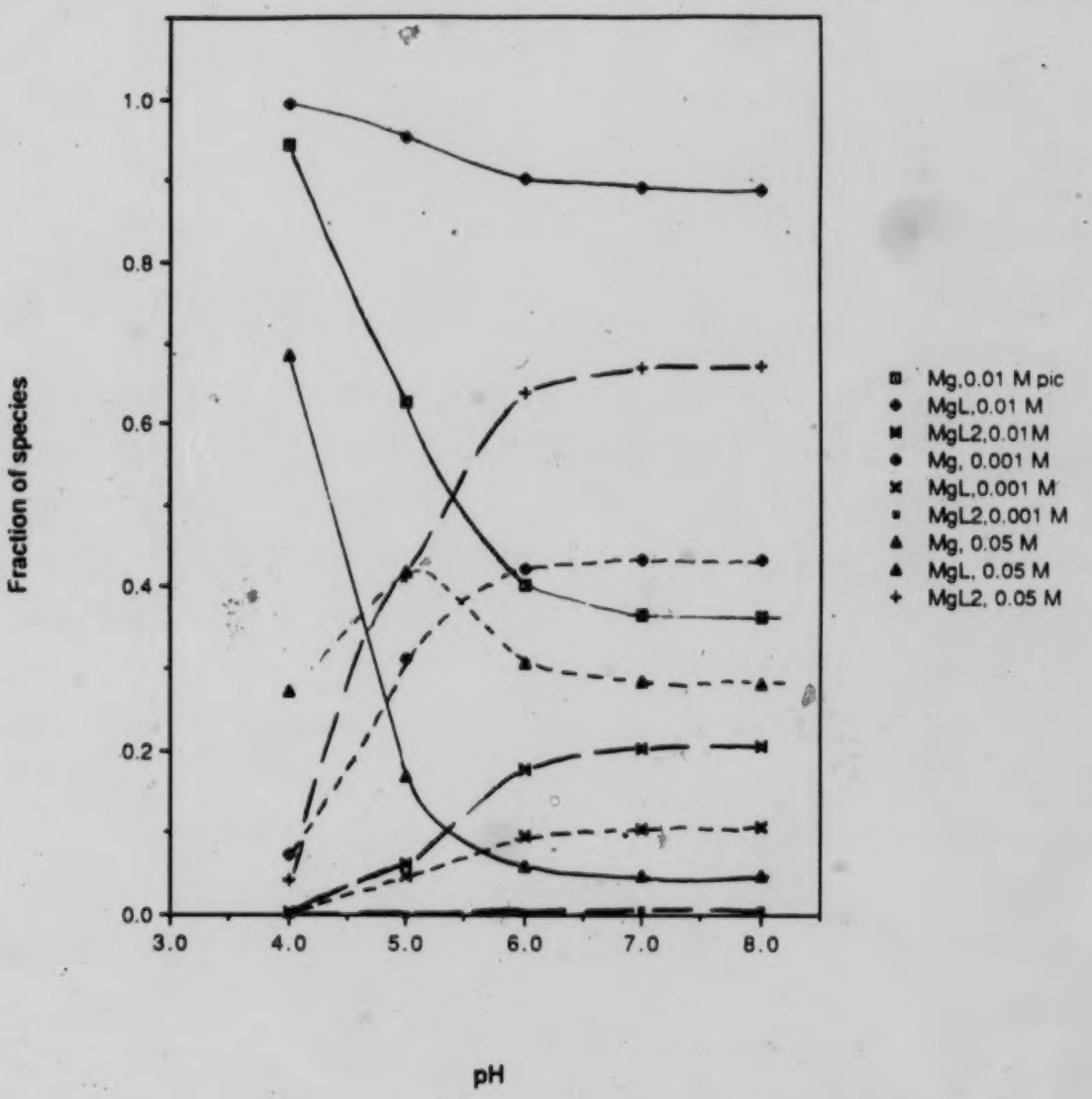

Fig 4.3: Species distribution of Mg^{+2}, MgP^{+} and MgP_2 at various pH and $C_{picolinic\ acid}$ (0.001 M, 0.01 M and 0.05 M). These data points were generated with the speciation program (COMICS) using $C_{Mg} = 1.00 \times 10^{-5}$ M and formation constants corrected to $\mu = 0.25$ M.

is additive because the eluted P.A. will be due to Mg^{+2}, MgP^{+} and MgP_2 sorption. Furthermore by performing the same experiment on XAD-2, the isotherm for Mg-complexes on XAD-2 can be subtracted from the isotherm on XAD-oxine to give an isotherm due to sorption of only the immobilized oxine.

4.3.3.1 Sorption on XAD-2 as a function of C_{HP} i.e. [picolinic acid]

As discussed in section 4.3.3, the species distribution of Mg^{+2},MgP^{+} and MgP_2 is dependent on $C_{picolinic\ acid}$ at a fixed pH. Furthermore, the ratio of MgP^{+} : MgP_2 changes as $C_{picolinic\ acid}$ changes. For example, when 0.01 M picolinic acid is present, the ratio of MgP^{+} : MgP_2 is 0.4 to 0.2 but when 0.05 M picolinic acid is present, the ratio of MgP^{+} to MgP_2 is 0.3 to 0.6 as can be seen in Fig 4.3. XAD-2 does not sorb Mg^{+2} as shown in section 4.3.2. Thus, when column equilibration experiments are done on XAD-2 resin with solutions of varying $C_{picolinic\ acid}$, the amount of magnesium sorbed (i.e. P.A. sorb) can be correlated to $[MgP^{+}]$ and $[MgP_2]$.

Table 4.10 shows the amount of magnesium sorbed on an XAD-2 column for solutions containing varying $C_{picolinic\ acid}$ at two different pH. Also presented on Table 4.10 are the concentration of the various species in the solutions used. The amount of magnesium sorbed (represented as P.A. sorb) is plotted against the calculated $[MgP_2]$ at pH 6.00 and 7.50 respectively (Figs 4.4 and 4.5). Linear regression analysis of the data in Fig 4.4 gives : slope = 0.129 ± 0.010; intercept = -0.0104 ± 0.037 and a correlation coefficient of 0.997. For the data in Fig 4.5, linear regression analysis gives: slope = 0.144 ± 0.015; intercept = -0.020 ± 0.030 and a correlation coefficient of 0.989. In contrast, linear regression analysis of P.A. sorb on $[MgP^{+}]$ gave correlation coefficients of 0.37 at pH 6.00 and 0.78 at pH 7.50 (plots not shown). These results suggests that: (a) the hydrophobic XAD surface in XAD-oxine is responsible for some sorption of Mg-picolinate complexes (b) the good linear correlation between the P.A. sorb and $[MgP_2]$ shows that MgP_2 is the main species sorbed (c) the slope at pH 6.00

Table 4.10: Effect of varying [picolinic acid] on XAD-2 using the without washing procedure. Table also shows the calculated concentration of the various species. Solution conditions: μ = 0.25 M, [PIPES] = 0.001 M, pH = specified, load = 20 min and elution with 1 M HNO_3 for 2 min.

C_{HP} x 10^{-3} M	C_{Mg} x 10^{-6} M	$[Mg^{+2}]$ x 10^{-6} M	$[MgP^{+}]$ x 10^{-6} M	$[MgP_2]$ x 10^{-6} M	P.A. XAD-2	pH
1.00	10.0	9.06 ± 0.10	0.906 ± 0.109	0.04 ± 0.004	0.021 ± 0.003	6.00
10.0	10.0	4.16 ± 0.25	4.18 ± 0.56	1.66 ± 0.20	0.168 ± 0.015	6.00
50.0	10.0	0.624 ± 0.05	3.13 ± 0.48	6.24 ± 0.86	0.803 ± 0.078	6.00
6.00	4.78	2.49	1.78	0.507	0.077 ± 0.001	7.50
10.0	4.78	1.73	2.07	0.978	0.112 ± 0.001	7.50
20.0	4.78	0.846	2.02	1.92	0.228 ± 0.011	7.50
50.0	4.78	0.225	1.35	3.20	0.464 ± 0.026	7.50

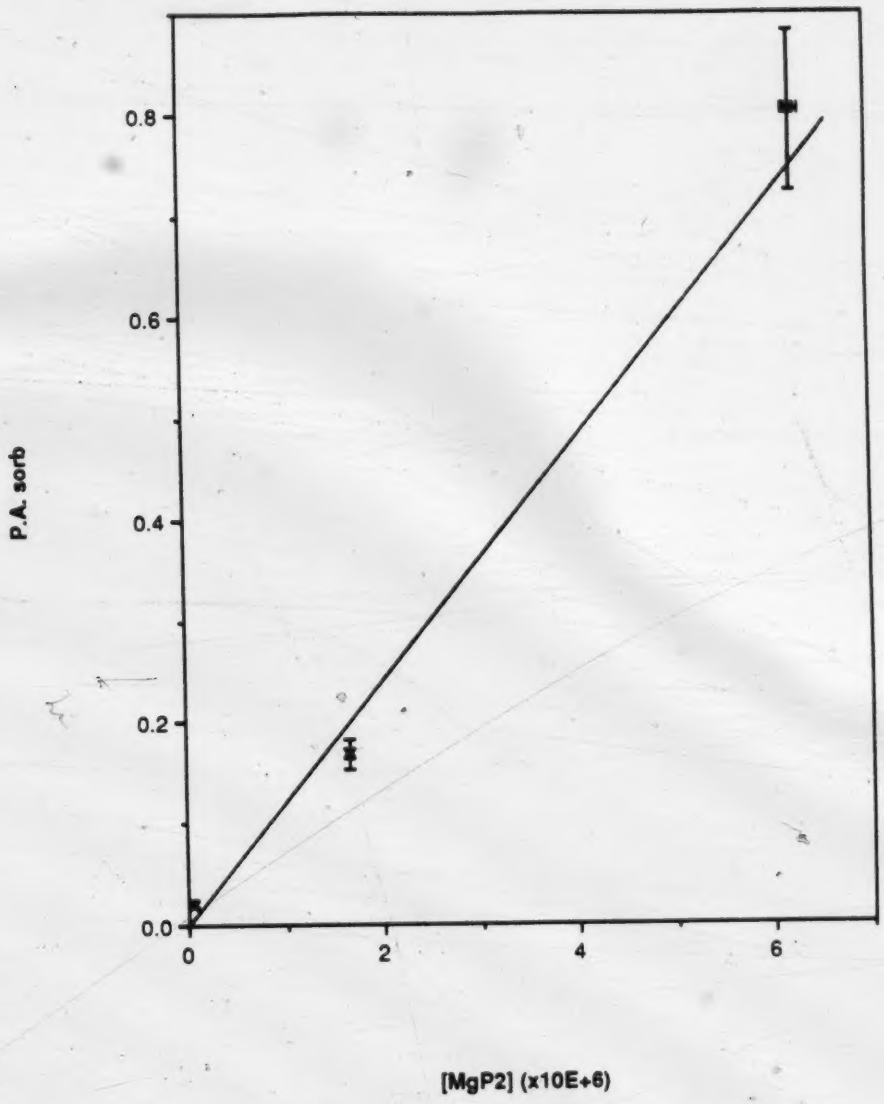

Fig 4.4: The amount of Mg-picolinate complexes sorbed at a pH of 6.00 on XAD-2 vs the calculated [MgP_2] in solution. Conditions: PIPES = 0.001 M, μ = 0.25 M, load = 20 min and elute = 2 min with 1 M HNO_3.

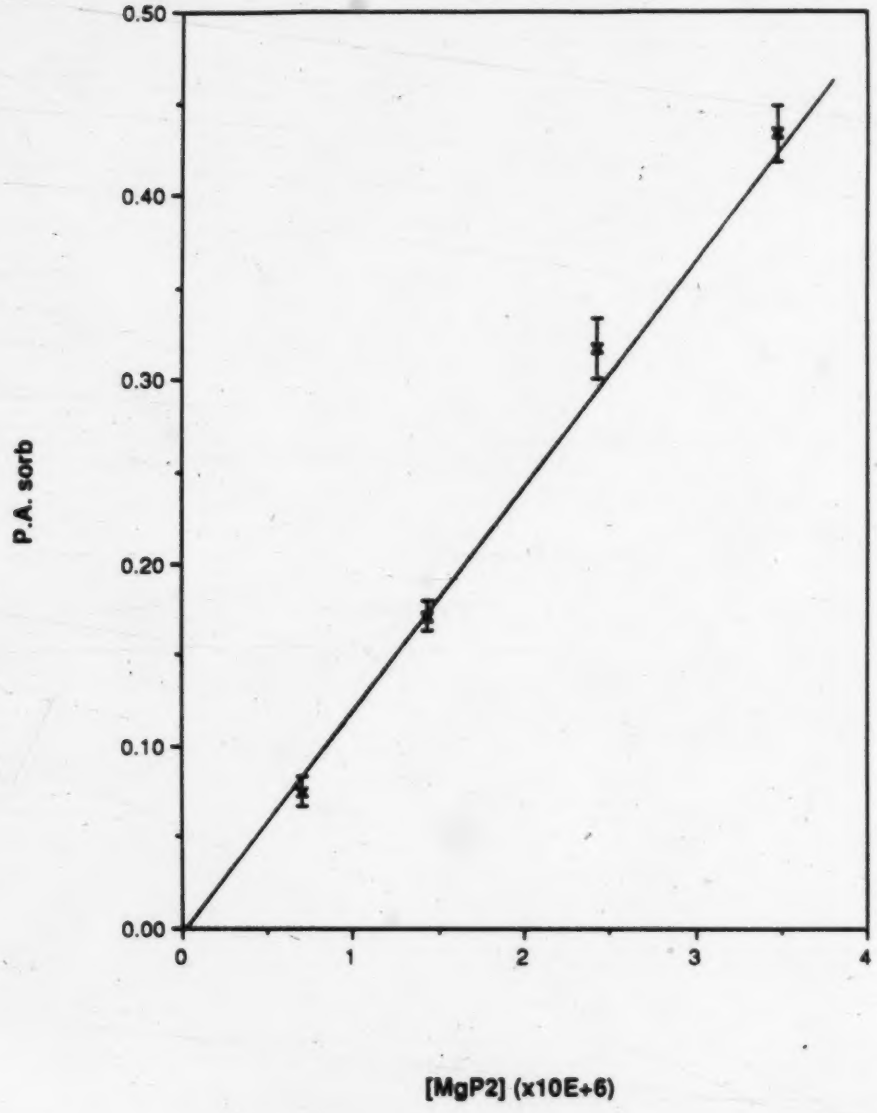

Fig 4.5: The amount of Mg-picolinate complexes sorbed at a pH of 7.50 on XAD-2 vs the calculated [MgP_2] in solution. Conditions are the same as Fig 4.4.

and 7.50 are statistically the same which shows that the sorption of MgP_2 is independent of solution pH (in the next section, these results will be reconfirmed).

The surface of XAD-2 is highly hydrophobic, and its use for adsorption of large organic molecules is popular (102). Therefore, the above results are not unreasonable when one considers that the picolinate ion (2-pyridinecarboxylate ion) has a large, flat hydrophobic pyridine ring. When P^- complexes with Mg^{+2} to form MgP_2, the resulting structure is neutral, large, flat and hydrophobic. Thus, it has the ideal properties for adsorption on the hydrophobic XAD-2 surface.

4.3.3.2 Sorption on XAD-2 as a function of solution pH

In Fig 4.3, it is seen that for a specific $C_{picolinic\ acid}$, the fraction of each species remains relatively constant at pH above 6.00. Solutions were prepared with fixed C_{Mg} and $C_{picolinic\ acid}$ but having different pH above 6.00, and contain the same $[MgP_2]$. When column equilibrium equilibrium experiments <u>without washing</u> were performed on XAD-2 using such solutions at various pH > 6.00, the sorption of magnesium was nearly constant (i.e. nearly horizontal plot, Curve A in Fig 4.6). As expected, MgP_2 is the only species sorbed.

These conclusions that XAD-2 sorbs mainly MgP_2 and is independent of solution pH is reasonable when one considers the surface of XAD-2 and the properties of MgP_2. XAD-2 is a macroporous polymer made exclusively from styrene and divinyl benzene. Thus, the surface is expected to be relatively independent of pH.

4.3.3.3 Sorption on XAD-oxine as a function of solution pH

In section 4.3.3.1 and 4.3.3.2, it was shown that for Mg-picolinate solutions, the MgP_2 species is sorbed on the hydrophobic XAD-2 surface but the MgP^+ was not sorbed. XAD-oxine has only a small fraction of its surface covered by the oxine groups. Therefore, one would expect that the underivitized portion of the XAD-oxine surface to

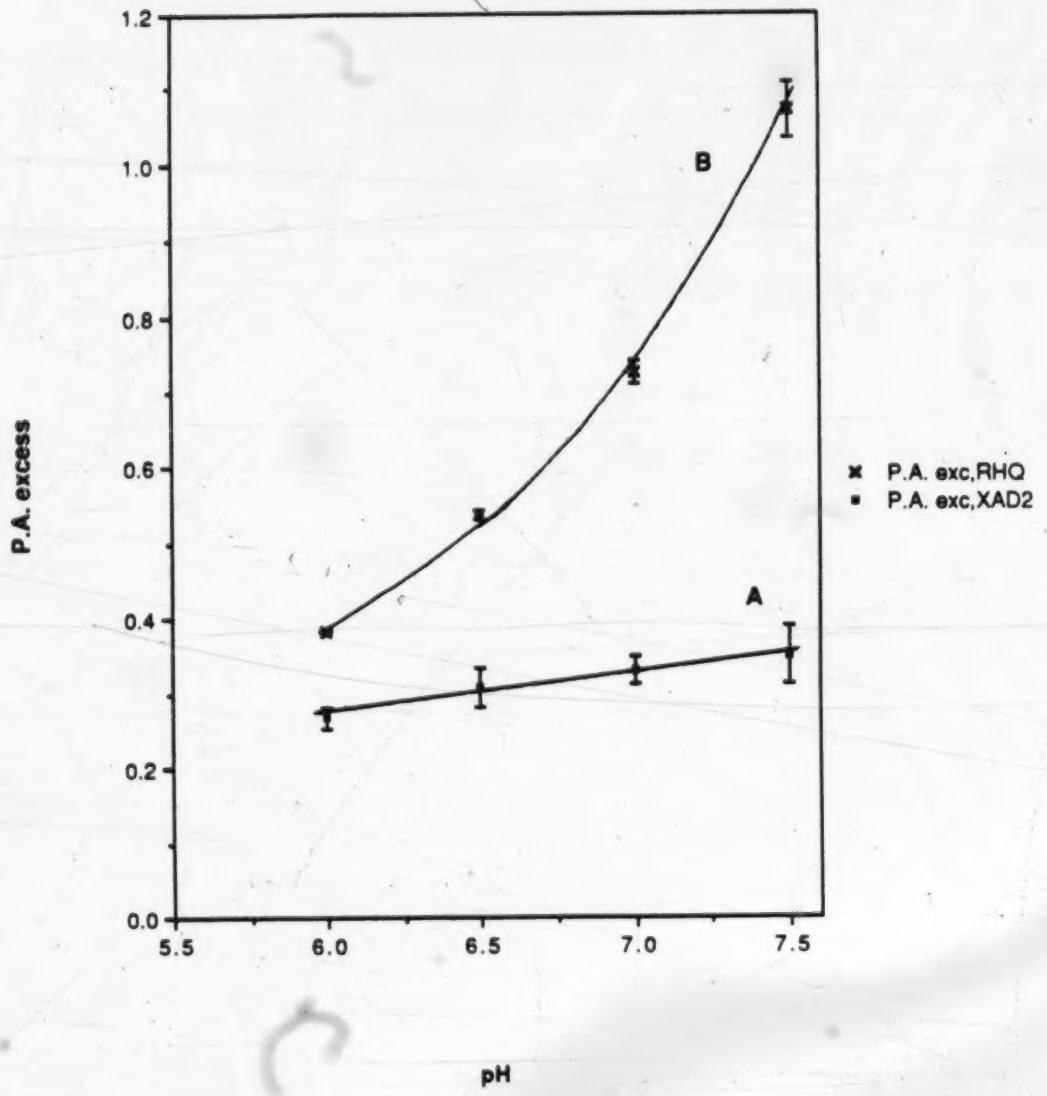

Fig 4.6: The excess amount of Mg-picolinate complex sorbed (i.e. P.A. excess) as a function of solution pH on columns packed with XAD-2 (curve A) and XAD-oxine (curve B). Conditions: C_{Mg} = 4.62 x 10^{-6} M, $C_{picolinic\ acid}$ = 0.05 M, PIPES = 0.001 M, μ = 0.25 M, load = 20 min, and elute = 1 min with 1 M HNO_3.

behave like XAD-2 and adsorb MgP_2 but not MgP^+. However, the question arises whether the oxine groups can sorb the cationic MgP^+ species. It is the anionic form of the immobilized oxine, Ox^-, that is responsible for sorbing the cation Mg^{+2} and it might be expected that it could also sorb the cation MgP^+. If this is possible, its sorption behavior should be similar to that discussed in section 3.3.7 i.e. an increase in solution pH will increase the fraction of Ox^- sites, and thus column equilibration experiments with solutions containing the same $[MgP^+]$ will show increasing sorption with increasing solution pH.

To determine the sorption of MgP^+ on XAD-oxine, column equilibrium experiments using the same solutions as in section 4.3.3.2 (i.e. fixed C_{Mg} and $C_{picolinic\ acid}$ but having different pH above 6.00) were run on this column. Since the sorption of MgP_2 would be constant, independent of pH, it is possible to measure the sorption of MgP^+ on XAD-oxine if one also runs experiments on the XAD-oxine, using solutions containing only Mg^{+2}, without picolinic acid, over the same pH range and subtracts the amount of Mg^{+2} sorbed from the total amount of magnesium sorbed. Determination of the P.A. due to Mg^{+2} sorption at a particular pH was done by preparing standard solutions with $[Mg^{+2}]$ within 80% to the calculated $[Mg^{+2}]$ in the Mg-picolinate solutions. The $[Mg^{+2}]$ in both the standard and Mg-picolinate solution were very small (2.93×10^{-7} M at a $C_{picolinic\ acid}$ of 0.05 M) and would thus be in the linear region of the Mg^{+2} sorption isotherm. The amount of magnesium (i.e. P.A.) sorbed as Mg^{+2} from the Mg-picolinate solution was calculated on the basis of this linear relationship (Table 4.11). As seen in Table 4.11, the P.A. contribution due to Mg^{+2} sorption is very small compared to the total P.A. due to sorption of all species.

In Fig 4.6, curve B is a plot of P.A. excess for Mg-picolinate solutions on XAD-oxine against the solution pH. The P.A. excess is the difference between the total P.A. due to sorption of all species and the measured P.A. due to Mg^{+2} sorption. The P.A. excess increases rapidly as the solution pH increases. Since the sorption of MgP_2 does not

Table 4.11: Effect of varying solution pH on XAD-oxine using the without washing procedure. Solution conditions: μ = 0.25 M, [PIPES] = 0.001 M, C_{Mg} = 4.62 x 10^{-6} M, pH = specified, load = 20 min and elution with 1 M HNO_3 for 2 min. **Note**: P.A. due to void volume = 0.069

pH	Total P.A.	P.A.due to Mg^{+2}	Excess P.A.
6.00	0.471 ± 0.001	0.018	0.384 ± 0.004
6.50	0.649 ± 0.003	0.043	0.537 ± 0.005
7.00	0.864 ± 0.016	0.070	0.725 ± 0.016
7.50	1.23 ± 0.037	0.094	1.07 ± 0.037

increase with solution pH, these results are consistent with the idea that MgP^+ sorption occurs, and is dependent on the fraction of anionic oxine sites on the XAD-oxine.

4.3.3.4 Sorption on XAD-oxine as a function of C_{Mg}

At a constant large excess concentration of picolinic acid and constant pH, Fig 4.3 shows that the fractions of Mg^{+2}, MgP^+ and MgP_2 are constant. Thus, the concentration of these 3 species will be directly proportional to C_{Mg} (eq 4.12). In column equilibration experiments using Mg-picolinate solutions on XAD-oxine, the magnesium sorbed is the sum of all three species. Thus, when C_{Mg} is varied, a plot of the total amount of magnesium sorbed (i.e. Total P.A.) against C_{Mg} can be considered as an isotherm that is the sum of isotherms due to all species. Table 4.12 shows the Total P.A. on XAD-oxine after column equilibration experiments were performed on two groups of solutions with varying C_{Mg} but at fixed $C_{picolinic\ acid}$ of 0.05 M and at two different pH. Figs 4.7 and 4.8 show the overall isotherm of Total P.A. against C_{Mg}. Both Figs 4.7 and 4.8 were linear and will be discussed later on in this section.

The Total P.A. for Mg-picolinate solution on XAD-oxine is given by:

$$\text{Total P.A.} = \text{P.A.}_{Mg^{+2}} + \text{P.A.}_{MgP^+} + \text{P.A.}_{MgP_2} \quad \text{.....4.17}$$

The P.A._{MgP^+} at the various C_{Mg} on XAD-oxine can be obtained by subtraction of the $\text{P.A.}_{Mg^{+2}}$ and P.A._{MgP_2}.

The $\text{P.A.}_{Mg^{+2}}$ can be obtained by interpolation from a Mg^{+2} isotherm on XAD-oxine at the particular pH. In Table 4.12, the interpolated values of $\text{P.A.}_{Mg^{+2}}$ corresponding to various calculated $[Mg^{+2}]$ are presented. Figs 4.9 and 4.10 show the isotherms at pH 6.00 and 7.50 from which the $\text{P.A.}_{Mg^{+2}}$ values were interpolated. Although Mg^{+2} isotherms were presented earlier, Figs 4.9 and 4.10 are necessary because they were done simultaneously with experiments for the overall isotherms

Table 4.12: Effect of varying C_{Mg} on XAD-oxine and XAD-2 using the without washing procedure. Solution conditions: μ = 0.25 M, [PIPES] = 0.001 M, pH = specified, load = 20 min and elution with 1 M HNO_3 for 2 min.

C_{Mg} x10^{-6} M	pH	Total P.A. XAD-oxine	P.A.$_{MgP_2}$ on XAD-2	P.A.$_{Mg^{+2}}$ (interpolated)	P.A.$_{MgP^+}$
0.82	6.00	0.118±0.001	0.042±0.004	0.015±0.001	0.061±0.00
4.39	6.00	0.683±0.007	0.261±0.003	0.034±0.003	0.388±0.009
7.98	6.00	1.18±0.01	0.485±0.038	0.065±0.005	0.632±0.038
11.5	6.00	1.72±0.03	0.725±0.021	0.086±0.007	0.910±0.033
1.04	7.50	0.379±0.001	0.075±0.001	0.060±0.005	0.043±0.10
2.14	7.50	0.794±0.037	0.171±0.008	0.090±0.007	0.533±0.038
3.62	7.50	1.25±0.04	0.317±0.016	0.127±0.010	0.810±0.038
5.18	7.50	1.78±0.06	0.433±0.015	0.182±0.015	1.16±0.06

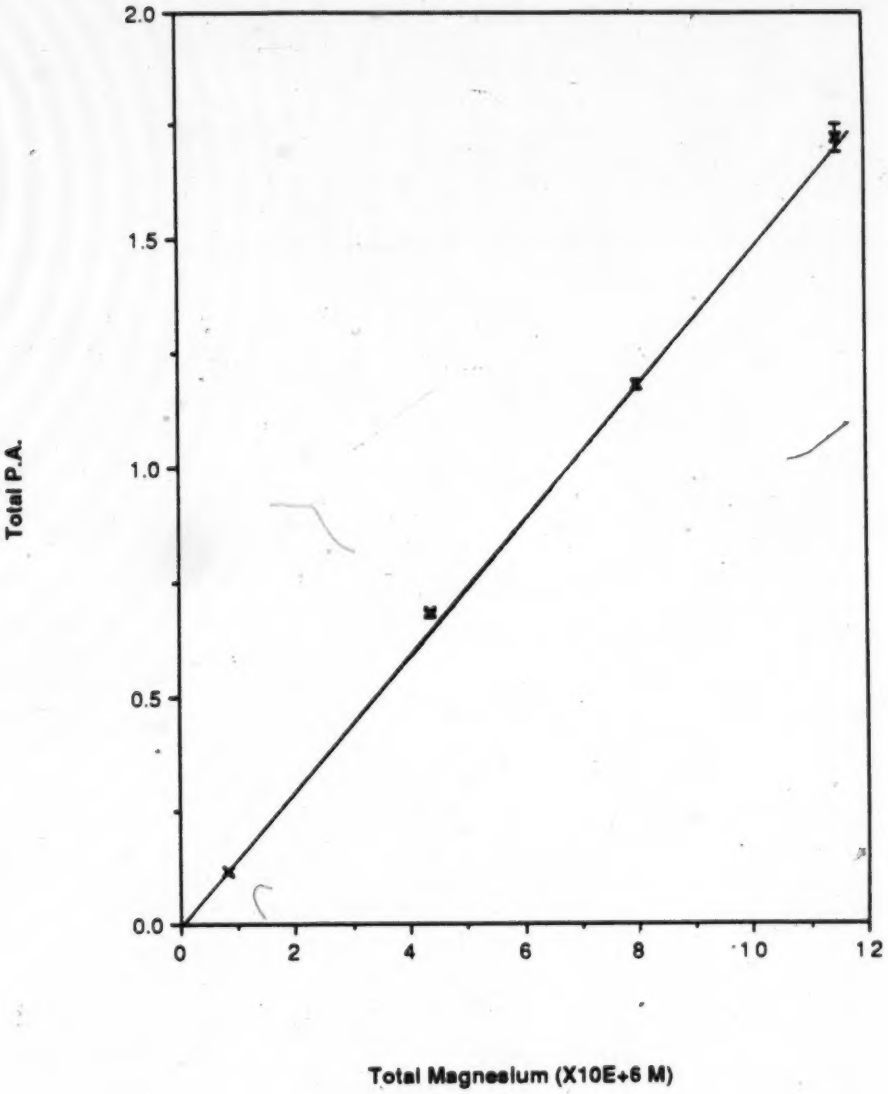

Fig 4.7: Overall Mg-picolinate isotherm without washing at a pH of 6.00. Conditions: PIPES = 0.001 M, μ = 0.25 M, load = 20 min, and elute = 1 min with 1 M HNO_3.

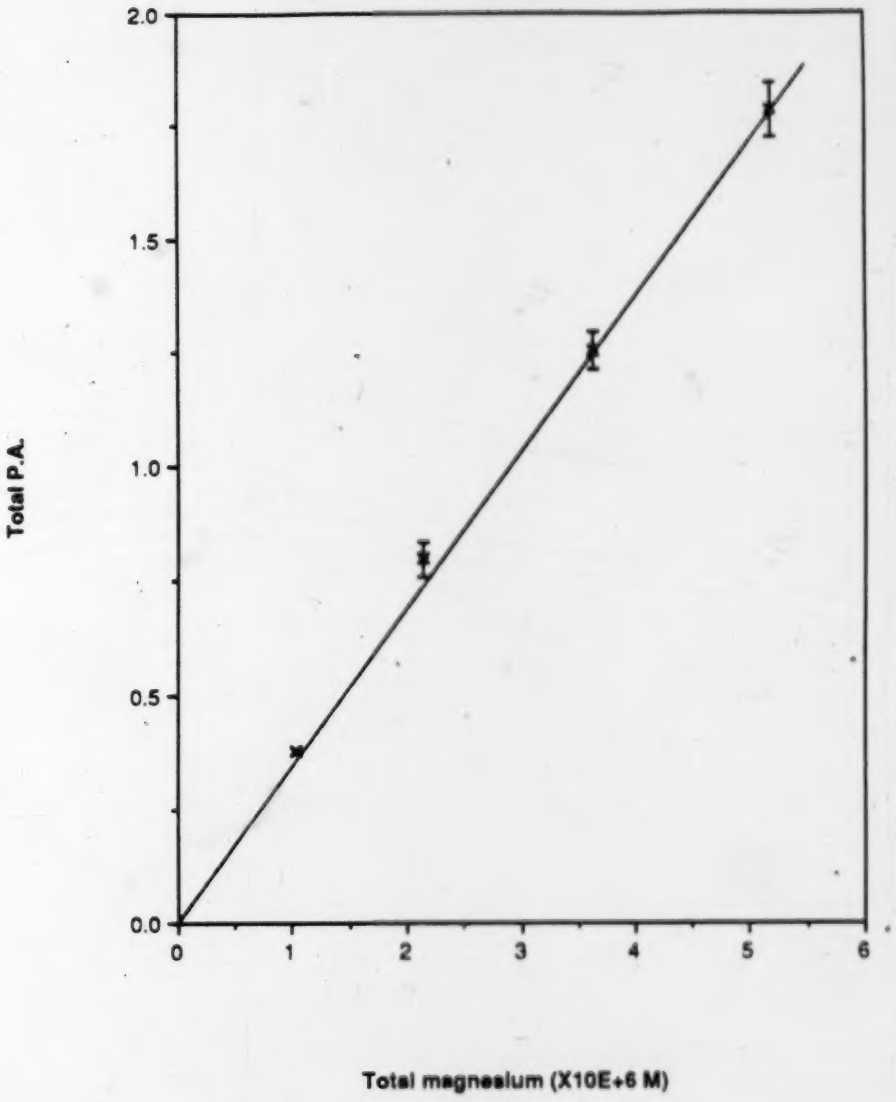

Fig 4.8: Overall Mg-picolinate isotherm without washing at a pH of 7.50. Conditions are the same as Fig 4.7.

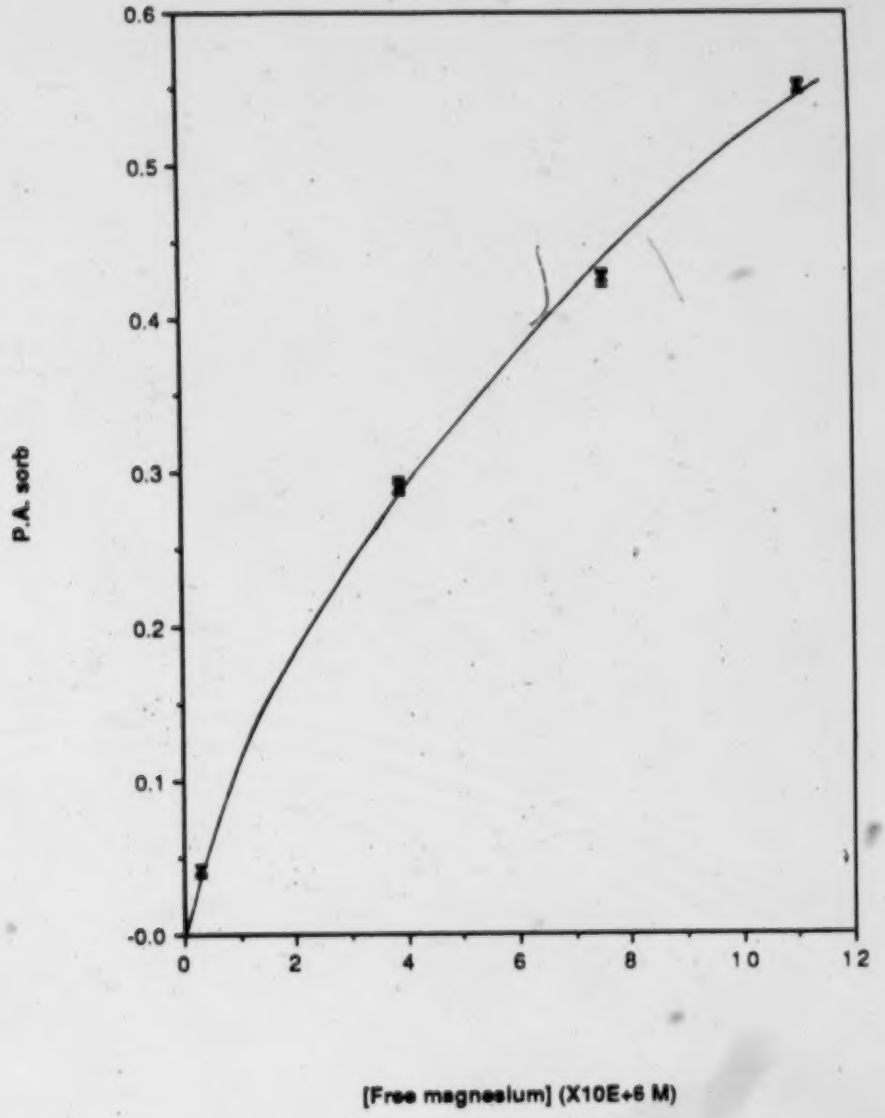

Fig 4.9: Mg^{+2} isotherm without washing at a pH of 6.00. Conditions: PIPES = 0.001 M, μ = 0.25 M, load = ~~20~~ min, and elute = 1 min with 1 M HNO_3.

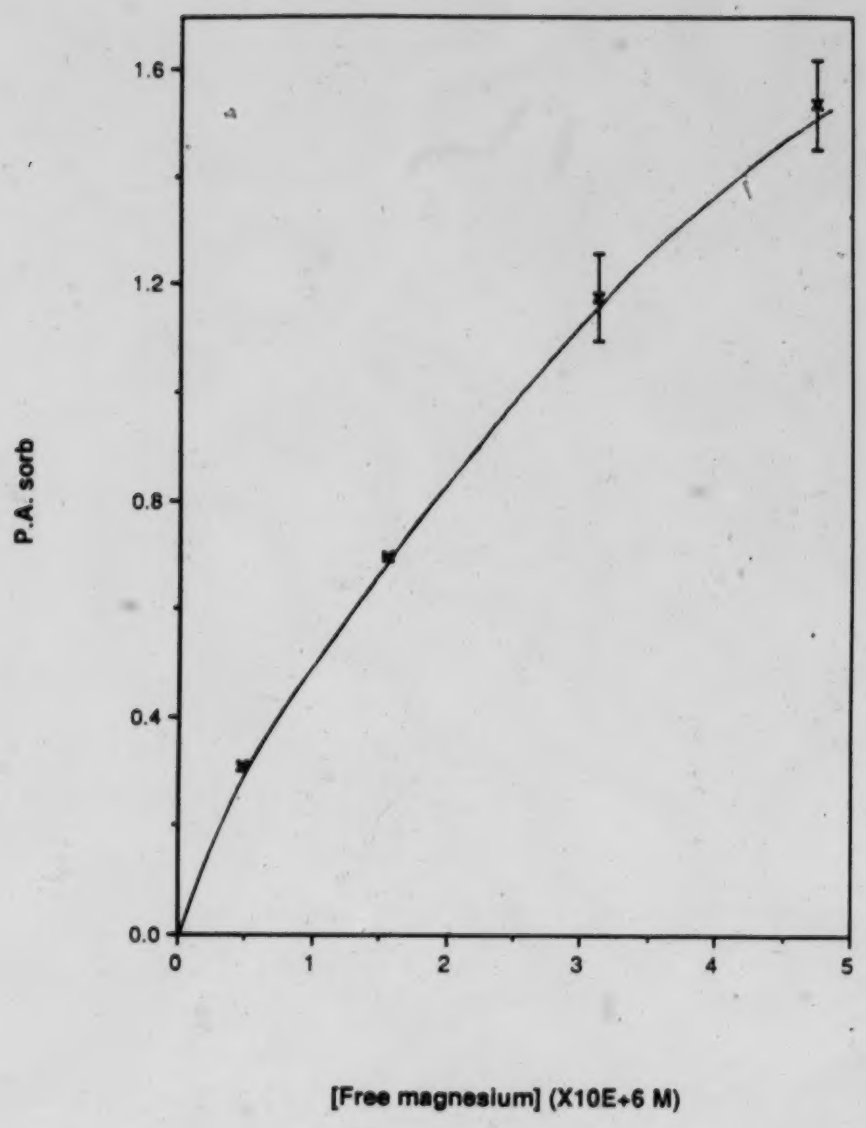

Fig 4.10: Mg^{+2} isotherm without washing at a pH of 7.50. Conditions are as Fig 4.9.

(Figs 4.7 and 4.8). Both Figs 4.9 and 4.10 are consistent with earlier Mg^{+2} isotherms (see section 3.3.6).

The $P.A._{MgP_2}$ due to sorption of MgP_2 on XAD-oxine was obtained by measuring the sorption on an XAD-2 column using the same solutions used to obtain the overall isotherms. As mentioned previously, the XAD-oxine surface would be expected to have the same properties as XAD-2 surface, and thus the distribution ratio of MgP_2 on these two resins would be the same. Values of $P.A._{MgP_2}$ due to MgP_2 sorption on XAD-2 are presented in Table 4.12.

The $P.A._{MgP^+}$ due to sorption of MgP^+ on XAD-oxine at the various C_{Mg} are also presented in Table 4.12. Figs 4.11 and 4.12 show isotherms of $P.A._{MgP^+}$ versus the calculated $[MgP^+]$ at pH 6.00 and 7.50 respectively. All the data points in Table 4.12 as well as the Mg^{+2} isotherms were performed under the same instrumental sensitivity, and thus, the scales can be intercompared. Several key points from Figs 4.4 through 4.12 are illustrated:

1) Both MgP^+ isotherms are linear. This may seem surprising in light of the fact that previous Mg^{+2} isotherms were non-linear. However, with MgP^+ species, the oxine can only complex in a 1:1 ratio to give R-OxMgP (both are univalent) as compared to the sorption of Mg^{+2} where 1:1 and 1:2 ratio of Mg^{+2} : oxine are both possible. Previous workers have assumed that, for synthetic methods normally used, the functional groups on poystyrene surfaces were evenly spread out on the solid surface (99), and thus for the XAD-oxine, one would expect the oxine groups to be evenly spread out on the XAD surface and, thus, the possibility that 2 oxine groups are in close proximity to form exclusively 2:1 complex would be remote. However, for the XAD-oxine used in this work, the synthetic method of Warshswsky *el al.* (45) was used, in which the reagent was $Al(oxine)_2$. It has been proposed (45) that the reaction mechanism involves an intermediate in which two oxine groups are chelated to aluminium (III) and, thus, the possibility exists for two oxine groups to be immobilized

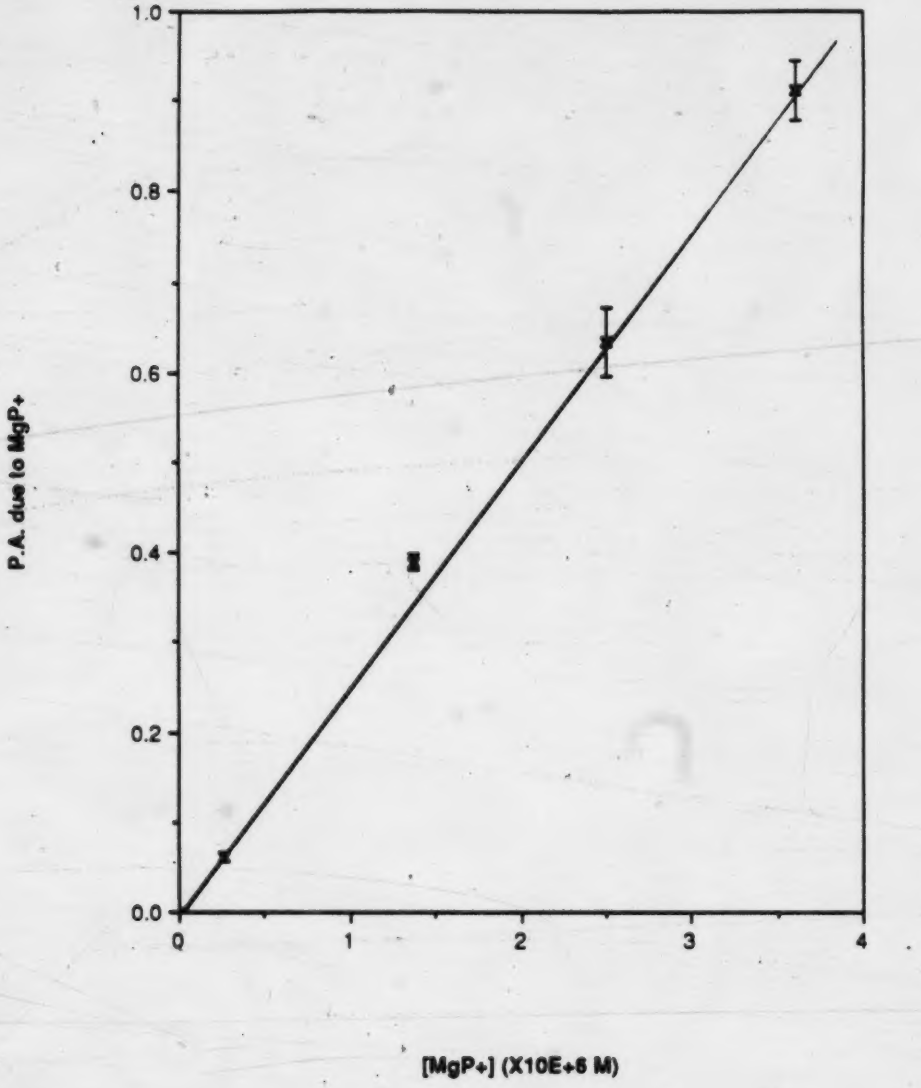

Fig 4.11: MgP^+ isotherm without washing after subtraction of the P.A. contribution due to Mg^{+2} and MgP_2 at a pH of 6.00. Conditions: $C_{picolinic\ acid}$ = 0.05 M, PIPES = 0.001 M, μ = 0.25 M, load = 20 min, and elute = 1 min with 1 M HNO_3.

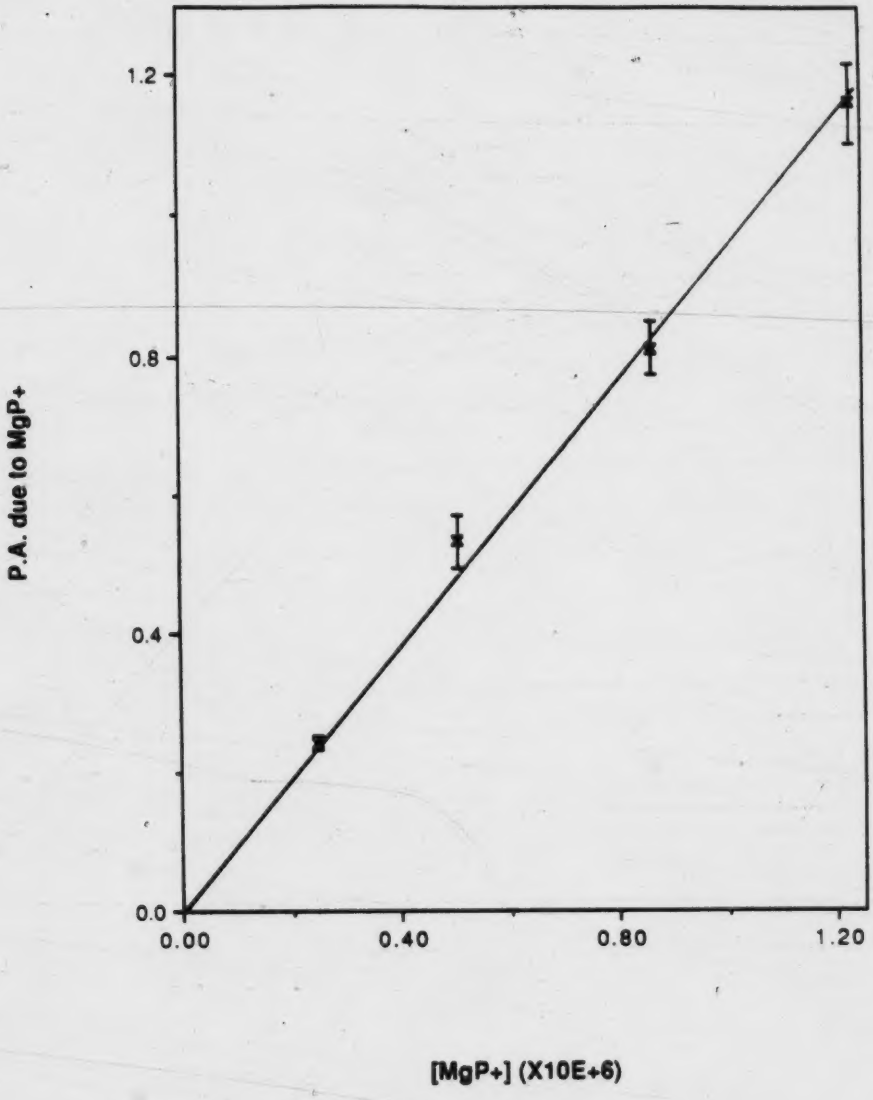

Fig 4.12: MgP^+ isotherm without washing after subtraction of the P.A. contribution due to Mg^{+2} and MgP_2 at a pH of 7.50. Conditions are the same as Fig 4.11.

in close proximity to each other. If this is so then the probability of forming a 2:1 complex with Mg^{+2} is greater here than for XAD-oxine prepared by other synthetic methods.

2) At a pH of 6.00, the slope is 0.25 ± 0.01 (Fig 4.11) while at a pH of 7.50, it is 0.92 ± 0.04 (Fig 4.12). This is consistent with the model that at a higher pH, more anionic oxine sites are formed, hence more sorption of MgP^+. In other words, the distribution ratio of MgP^+ is higher at higher solution pH.

3) The slopes of Figs 4.4 to 4.12 can be used to determine the relative strengths to which the various species are sorbed. In summary, the slope for sorption of MgP_2 is 0.13 ± 0.01 (Fig 4.4), that of MgP^+ are 0.25 ± 0.01 at pH 6.00 and 0.92 ± 0.04 at pH 7.50 (Fig 4.11 and 4.12), and although its isotherm is non-linear, the slope for the sorption of Mg^{+2} is 0.05 at pH 6.00 (Fig 4.7) and 0.3 at pH 7.50 (Fig 4.8). These data shows that the relative strength of sorption by the oxine group on XAD-oxine is $MgP^+ > Mg^{+2}$. Furthermore, the MgP_2 species is sorbed on the XAD-2 surface of about the same strength as Mg^{+2}.

4.3.3.5 Mechanism of sorption of MgP^+ on XAD-oxine

Since the isotherms for MgP^+ and MgP_2 are linear, the data in Table 4.11, showing the influence of pH on the sorption of these species, can be qualitatively analyzed. The sorption of MgP_2 on the XAD-surface is purely by adsorption, and it was shown in section 4.3.3.1 that the concentration of MgP_2 in the resin phase, $[MgP_2]_R$ is directly proportional to $[MgP_2]$ in solution. The distribution ratio of MgP_2 is given by

$$\lambda_{MgP_2} = \frac{[MgP_2]_R}{[MgP_2]} \quad \text{..... 4.18}$$

However, the sorption of MgP^+ might be explained by one or more of 3 different models viz:

1) Complexation of MgP^+ on to the anionic oxine sites, ROx^-, as given by eq 4.19

$$(ROx^-)_R + MgP^+ \rightleftharpoons (ROxMgP)_R \quad \text{.....4.19}$$

This model was successfully used to explain the sorption behavior of Ca^{+2} on CPG-oxine (38). This model requires that the surface potential be known, which is not available for XAD-oxine (discussed in section 3.3.7).

2) Surface adsorption of MgP^+. Surface adsorption of charged species has previously been reported (103,104,99). Application of this model also requires knowledge of the surface potential. Attempts to fit the data of Table 4.11 to a simplified version of this model, which ignores the surface potential, failed to give constants for λ_{MgP^+} and λ_{MgP_2} in eq 4.20

$$\text{P.A. Excess} = \lambda_{MgP^+}[MgP^+] + \lambda_{MgP_2}[MgP_2] \quad \text{.....4.20}$$

where λ_{MgP^+} is the ratio of $[MgP^+]_R$ to $[MgP^+]$. The dependence of λ_{MgP^+} implied in Fig 4.6 also is inconsistent with eq 4.20.

3) Sorption of MgP^+ by an ion exchange model as given by eq 4.21

$$(RO^-Na^+)_R + MgP^+ \rightleftharpoons (RO^-MgP^+)_R + Na^+ \quad \text{.....4.21}$$

Derivation of the equation for this model proceeds as follows: The excess P.A. given by eq 4.22 is the sum of the P.A. contribution due to MgP_2 and MgP^+ sorption

$$\text{P.A.}_{\text{excess}} = \text{P.A.}_{MgP_2} + \text{P.A.}_{MgP^+} \quad \text{.....4.22}$$

The ion exchange constant, K_{IEX} for eq 4.21 is given by:

$$K_{IEX} = \frac{[RO^- Mg^+]_R\,[Na^+]}{[RO^- Na^+]_R\,[MgP^+]} \quad \text{.....4.23}$$

The P.A. is directly proportional to the concentration of the magnesium species in the resin phase i.e.

$$\text{P.A.} = k\ [\text{magnesium species}]_R \quad \text{.....4.24}$$

Substituting for $[MgP_2]_R$ and $[MgP^+]_R$ in eq 4.22 gives

$$\text{P.A.}_{excess} = k\,\lambda_{MgP_2}[MgP_2] + k\,K_{IEX}\frac{[RO^- Na^+]_R\,[MgP^+]}{[Na^+]} \quad \text{.....4.25}$$

The $[MgP_2]$ and $[MgP^+]$ can be expressed in terms of C_{Mg} and are given as (α_{MgP_2}) $(C_{Mg})$and (α_{MgP^+}) (C_{Mg}) respectively. Similarly $[RO^-Na^+]_R$ can be expressed as (α_{Ox^-}) (v) where v is the capacity of the resin. Substituting for $[MgP_2]$, $[MgP^+]$ and $[RO^- Na^+]_R$, eq 4.25 takes the form:

$$\text{P.A.}_{excess} = k\,\lambda_{MgP_2}\alpha_{MgP_2}C_{Mg} + k\,K_{IEX}\frac{\alpha_{Ox^-}\,v\,\alpha_{MgP^+}\,C_{Mg}}{[Na^+]} \quad \text{.....4.26}$$

In pH study, k, C_{Mg}, v_{Ox} and $[Na^+]$ were constant, so that a plot of

$$\frac{\text{P.A.}_{Excess}}{\alpha_{MgP_2}} \text{ vs } \frac{\alpha_{MgP^+}\alpha_{Ox^-}}{\alpha_{MgP_2}}$$

should be linear. The fraction of Mg species, α_{MgP_2} and α_{MgP^+} were calculated as described in section 4.2.6. The value of α_{Ox^-} was calculated using eq 3.14 assuming that the proton acidity constants of XAD-oxine are the same as in homogeneous solution and ignoring the effects of surface charge on the ionization of the oxine. As can be seen in Fig 4.13, the plot non-linear, and thus the model that MgP^+ is sorbed by ion exchange is not valid.

4.4 Conclusion

XAD-oxine is selective for the determination of $[Mg^{+2}]$ in the presence of anionic complexes of EDTA (MgY^{-2}) and neutral oxalate complexes (MgOx) using the without washing procedure. Water washing to remove interstitial fluid after column equilibration i.e. the with washing procedure, was found to perturb the resin-solution equilibrium giving higher $\alpha_{Mg^{+2},Expt}$ values. This effect of washing on $\alpha_{Mg^{+2},Expt}$ was not previously observed with sulfonated ion exchange resins.

Free metal speciation requires the separation of one species from all others. Understanding the sorption process of XAD-oxine is critical for future selection of suitable sorbents for free metal determination. Complexes of Mg^{+2} containing hydrophobic moieties (i.e. MgP_2) are sorbed on the hydrophobic XAD surface, and are measured along with sorbed Mg^{+2} during the elution step. Thus, hydrophobic supports are unsuitable as supports on which to immobilize chelating agents for the purpose of free metal speciation because real samples, e.g. river water and urine contain many organics with large hydrophobic residues.

The species MgP^+ was also sorbed only on XAD-oxine and its sorption was found to be dependent on the solution pH. In other words, the sorption of MgP^+ is dependent on the degree of ionization of the immobilized oxine. Three models were discussed but the lack of information on the electrical properties of the XAD-surface prevents any

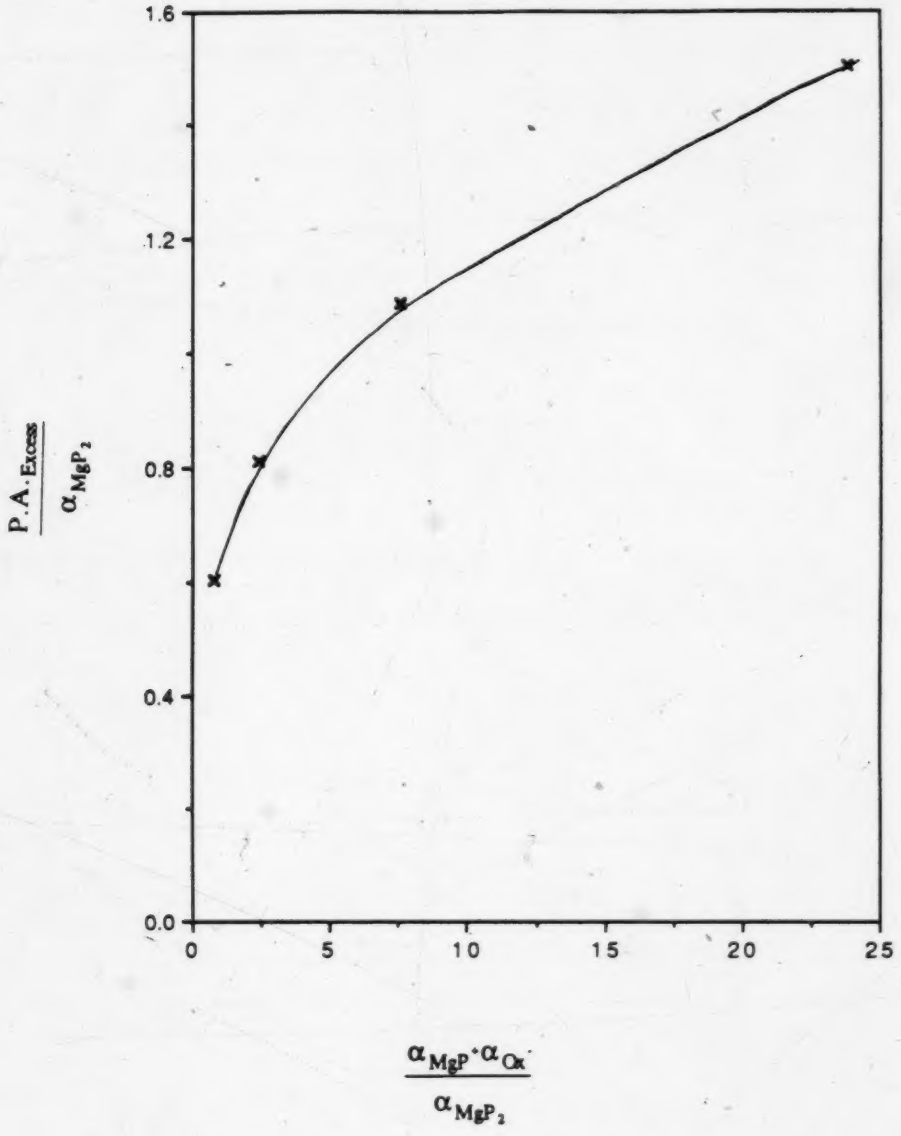

Fig 4.13: Plot of

$$\frac{P.A._{Excess}}{\alpha_{MgP_2}} \quad vs \quad \frac{\alpha_{MgP}*\alpha_{Ox}}{\alpha_{MgP_2}}$$

extensive application of these models. Attempts to use a simplified ion exchange model (i.e. neglecting all electrical properties on the XAD-surface) proved unsuccessful. As such, further work on the electrical properties on the XAD-oxine surface will be required to explain the pH dependence on MgP^+ sorption.

CHAPTER 5

CONCLUSIONS OF PART I AND SUGGESTIONS FOR FUTURE WORK

The use of XAD-oxine as a sorbent for speciation of Mg^{+2} using the column equilibration technique showed a number of difficulties. These were:

a) Too high sensitivity for application to most real samples

b) Non-linear Mg^{+2} sorption isotherm for low column loading (~ 1%)

c) pH sensitivity which requires matching of standards and samples

d) Sorption of neutral magnesium complexes, containing a large hydrophobic part, on the hydrophobic surface of XAD-oxine

e) Sorption of cationic magnesium complexes (MgP^{+}) by XAD-oxine

f) A water wash step after column equilibration cannot be used.

These difficulties were all due to the immobilized ligand and the support. Therefore, for successful use of the column equilibration technique to determine $[Mg^{+2}]$, the choice of the ligand and support should be the major consideration. From this work, it would appear that a weaker chelating agent than 8-hydroxyquinoline bound to a hydrophilic support would be a suitable sorbent for Mg^{+2}.

With a weaker chelating agent, less Mg^{+2} will be sorbed for a given $[Mg^{+2}]$, and trace loading conditions will be achieved at higher $[Mg^{+2}]$ which would go closer to the desired range for application into real samples. Also, the chelating agent should not show a high pH sensitivity in the pH range of real samples (i.e. pH 6-8). Possible chelating agents are amino acids, which are not highly ionized at the desired range. Another chelating agent that shows pH independence above 6 is picolinic acid.

Changing the support to hydrophilic supports (water wetted) will eliminate the problem of sorption of complexes containing hydrophobic parts. Hydrophilic supports

are well known in the literature and include porous glass, silica, cellulose, naturally occurring chitins (104a) and synthetic resins e.g. Fractogel KSK. Functionalization of these hydrophilic supports was discussed in many reviews (46-50). Many of these supports with a particular chelating agent are commercially available (50). In fact, the naturally occurring chitins show metal sorption properties without any modification (104a) and therefore their sorption properties to Mg^{+2} should be investigated.

The non-linear sorption isotherms for Mg^{+2} appear to be due to sorption of more than one type of oxine complex by the sorbent (i.e. $ROxMg^{+}$ and $(ROx)_2Mg$). Introducing a long spacer arm (e.g. alkyl or polyether groups) between the chelating agent and the support will allow the chelating group to move around to completely form the 2:1 ligand to metal ion complex.

Finally, the with washing column equilibrium procedure should be used with caution, because it was successfully used for sulfonated resins and CPG-oxine but not with XAD-oxine. Consideration has to be given to perturbation of the solution-ligand equilibrium at the start of the washing step. The without washing procedure eliminates the problem of perturbation of the solution-resin equilibrium, but will have the limitation from the void volume signal contribution.

PART II

CHAPTER 6

BEHAVIOR OF SOLUTE ADSORBED AT THE LIQUID-LIQUID INTERFACE DURING SOLVENT EXTRACTION WITH POROUS MEMBRANE PHASE SEPARATORS

6.1 Introduction

The concept of "interfacial tension separation" of two immiscible liquids, which utilizes a porous membrane that is preferentially wetted by one of the liquids, has been known for some time (105,106). The principle is based on the fact that when the porous membrane is wetted by one of the liquid phases, it will only allow the phase that wets the membrane to pass through. For example, if filter paper is wetted with water, then it will only allow water to flow through from a chloroform-water dispersion. On the other hand, Teflon is wetted by chloroform and thus will allow only chloroform through. The principle has been used effectively for phase separation in analytical solvent extraction (107-112) and in physico-chemical measurements of the equilibrium (113-117) and kinetics (118-122) of solvent extraction. It is observed in such systems that when the solute involved is interfacially active (i.e. adsorbed at the liquid-liquid interface) then the concentration of solute in the liquid phase flowing through the porous membrane decreases when the degree of agitation is increased (107,110,115,116,119,123-124). This is a consequence of the increase in interfacial area, which in turn adsorbs more solute from the bulk phases with increasing agitation. Observation of this phenomenon has led to the inference that the liquid flowing through the porous membrane has the composition of the bulk liquid in

the dispersion, i.e. that solute in the interfacial phase is "excluded" from the membrane and does not enter the bulk liquid phases during membrane-induced phase separation.

However, the validity of this inference is not immediately obvious. For example, before the bulk liquid from the dispersed phase (droplets) can flow through the membrane it is necessary for droplets to coalescence with the thin film of solvent on the outer surface of the membrane. One might suspect that upon the disappearance of the droplet interface during the process of coalescence some of the adsorbed solute would dissolve into the adjacent bulk liquid phases thereby raising their solute concentrations locally. The locally enriched liquid would flow through the membrane. Thus the concentration of solute in the liquid flowing through the membrane would be higher than that in the bulk phase in the agitated system.

Since porous membrane phase separators are now being used for physicochemical studies such as the measurement of interfacial area in rapidly stirred liquid-liquid systems (116), it is desirable to examine more rigorously the fundamental assumption upon which these studies are based. In this part of the thesis, two membrane phase separators, one for the organic phase and the other for the aqueous phase, are used simultaneously. Comparison of experimentally measured distribution isotherms obtained with and without agitation is found to be consistent with the conclusion that interfacially adsorbed solute does not enter the bulk phases during membrane-induced phase separation. In the discussion, it is shown that this conclusion is predictable from hydrodynamic and surface-chemical principles.

6.2 Experimental

6.2.1 Apparatus

The extraction apparatus shown in Fig 6.1 is based on a previously described two-phase titration cell (126). The "spoiler", which does not rotate, serves to minimize vortex formation and increase shearing forces. Stirring is accomplished with

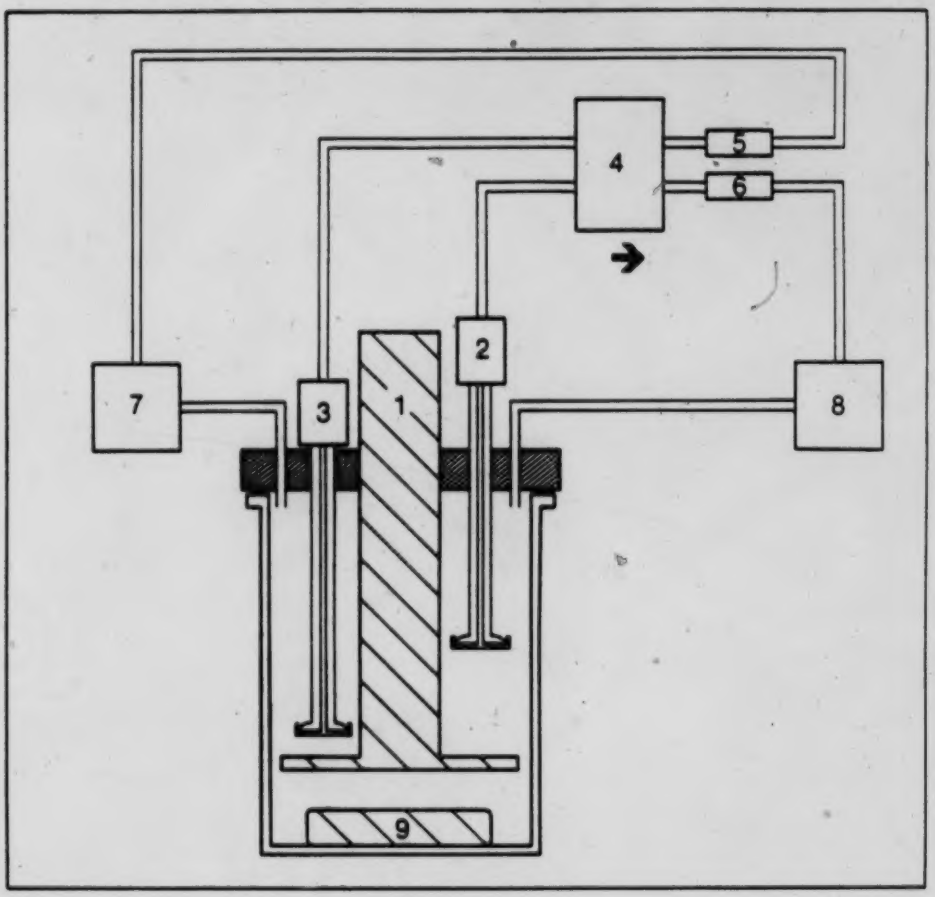

Fig 6.1: Diagram of the apparatus. 1 - spoiler; 2 - "filter probe" with paper membrane; 3 - "filter probe" with Teflon membrane; 4 - peristaltic pump; 5 and 6 - in-line filters; 7 and 8 - spectrophotometers and 9 - stirring bar.

a 1.5 inch magnetic stirring bar and a heavy duty magnetic stirrer (Cole-Parmer Co.). There are two porous membrane phase separators of the "filter probe" type. The "filter probe" is made by fusing a 1 mm capillary tube to a 13 mm glass disc (Fig 6.2). A grooved Teflon washer is placed on the glass disc, and the membrane phase separator is stretched over the washer and held in place by a Teflon sleeve. The organic-membrane phase separator is made with three layers of porous Teflon (Zitex Filter Membrane, 10-20 μm pore size, No. E249-122, Chemplast Inc., Wayne, N.J.) and is positioned slightly lower than the other probe so that during non-stirring, it is immersed in the heavier chloroform phase. The aqueous-permeable membrane phase separator is made with two layers of Whatman No. 2 filter paper and is positioned slightly higher than the other phase separator so that it is immersed in the lighter water layer during non-stirring. The in-line filters for the aqueous and organic phases are made of the same filter media as the corresponding phase separators and placed downstream of the peristaltic pump in order to prevent tiny particles of the pump material from reaching the flow cells. All connecting tubing is 0.8 mm i.d. Teflon except the return lines from the detectors to the extraction beaker which are 0.3 mm i.d.. The 170 mL extraction beaker is thermostated at 26 ± 1 ^{o}C by placing it in a glass jacketed beaker and circulating water from a water bath. The apparatus is then placed on top of a magnetic stirrer (126). Absorbance of the chloroform phase is monitored with a Cary 115 spectrophotometer (Cary Instruments, Monrovia, Ca.) fitted with an 80 μL flow cell (Hellma Corp., Toronto) and absorbance of the aqueous phase is monitored with a Varian UV-50 liquid chromatography detector with a 8 μL flow cell (Varian Assoc., Palo Alto, Ca).

6.2.2 Chemicals and reagents

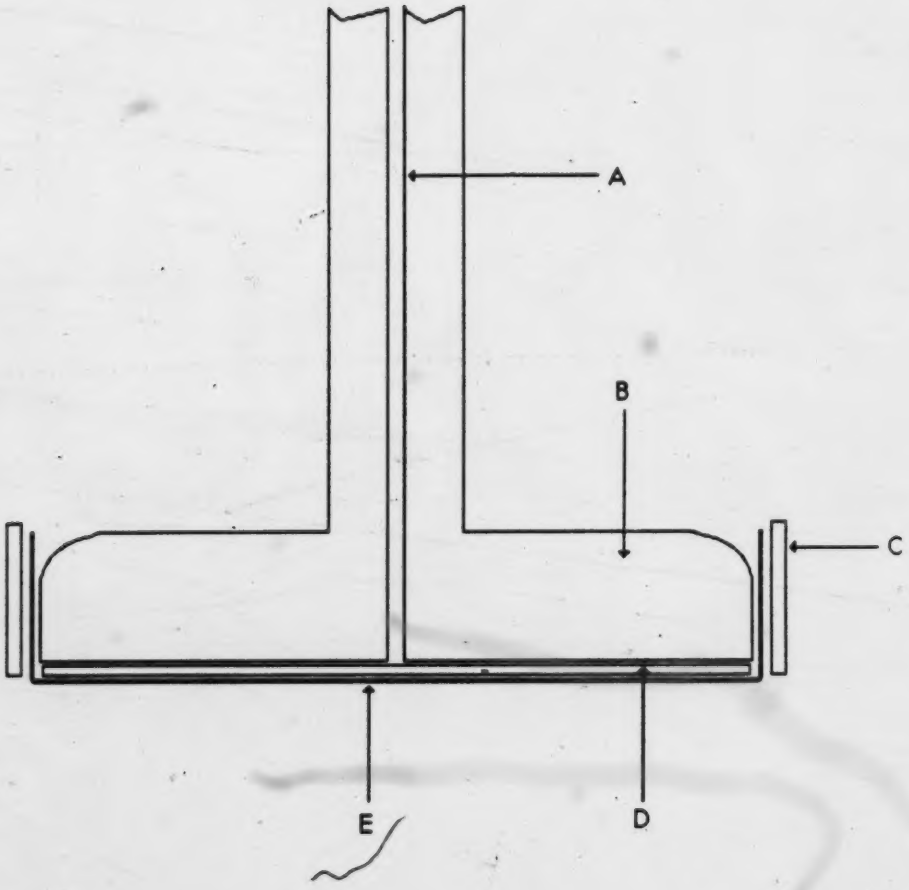

Fig 6.2: Exploded view of the end of the filter probe. A - 1 mm i.d. capillary tube; B - 13 mm diameter glass disc; C - Teflon sleeve; D - grooved Teflon washer, and; E - membrane phase separator.

Methylene blue chloride (U.S.P. equivalent, Fisher Scientific Co.) was purified by repeatedly extracting a 0.4 % aqueous solution with chloroform until the chloroform phase was colorless (127).

Methylene blue perchlorate ($MB.ClO_4$) stock solution in chloroform was prepared by combining aqueous solutions of methylene blue chloride and potassium perchlorate, filtering out the precipitate of $MB.ClO_4$ (**CAUTION**: do not dry the precipitate completely) and dissolving it in chloroform. The $MB.ClO_4$ concentration in the stock solution was determined spectrophotometrically using a published molar absorptivity of 1.00×10^5 at a wavelength of 654 nm (128).

Chloroform to be used for extraction was reagent grade and was washed three times with water before use.

Water was demineralized, distilled and finally distilled from alkaline permanganate. Before use, the water was presaturated with chloroform.

Potassium perchlorate was reagent grade (Fisher Scientific Co.)

6.2.3 Measurement of the distribution isotherms

To the extraction beaker were added the following: X.00 mL of 1.53×10^{-5} M $MB.ClO_4$ stock solution in chloroform (where X = 0 to 6); 60.0 - X.00 mL of chloroform; and 55.0 mL of 1.01×10^{-3} M aqueous potassium perchlorate. Next, the membrane phase separators were wetted with the desired phases that will flow through them. The mixture was rapidly stirred and both the aqueous and organic phases were pumped at 0.5 mL/min via the membrane phase separators through the photometric detectors which were set at the wavelengths of maximum absorbance of $MB.ClO_4$ (654 nm in chloroform and 666 nm in aqueous solution). Absorbances were monitored continuously until they remained constant for at least 15 min. The pump and stirrer were then shut off, the phases were allowed to separate in the beaker and the pump was turned on again to measure the absorbances of the unstirred phases.

Experiments were done in order of increasing $MB.ClO_4$ concentration. When changing the concentration of $MB.ClO_4$ the apparatus was emptied, and the beaker and connecting tubing (but not the filter probe) were rinsed with methanol and either water or chloroform before re-use. This was done to remove adsorbed $MB.ClO_4$ from the solid surfaces. The filter-probes were merely rinsed with either pure water or chloroform, as appropriate, between measurements made at different $MB.ClO_4$ concentrations. Both membranes, especially the paper one, were colored by adsorbed $MB.ClO_4$.

6.2.4 **Measurement of the free stream linear velocity**

The linear velocity of liquid, V_{max}, in the so-called free stream, beyond the boundary layer at the membrane was measured by means of an impact device called a pitot tube (129). In Fig 6.3 is a sketch of the device. An L-shaped glass tube with an O.D. of 0.65 mm, i.d. of 0.36 mm with arms about 0.5 cm and 25 cm long was punched through the face of the membrane so that its long arm would extend well above the liquid level in the beaker. The height of the Pitot tube was first measured with no stirring of the liquid in the beaker (H_{NS}); then the stirrer was turned on and the horizontal short arm of the L-shaped capillary was rotated until it was pointing directly at the stream of liquid flowing past the membrane as indicated by the height of liquid in the vertical arm reaching a maximum (H_S). The experiment was performed with both 1:1 chloroform-water mixture in the beaker and with water alone. The results were essentially the same in both cases but the latter gave more steady readings.

6.3 **Results**

6.3.1 **Hydrodynamics**

The interfacial area between 60 mL of chloroform and 60 mL of aqueous phase can be calculated from the diameter of the beaker to be about 20 cm^2 when the mixture

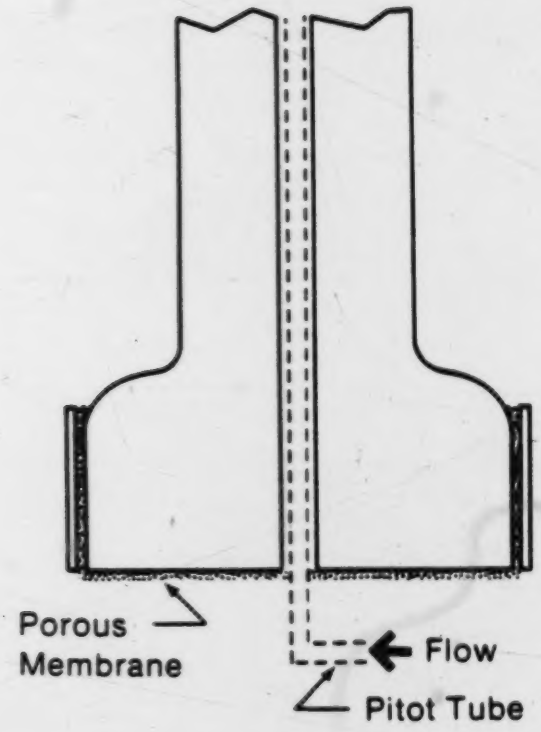

Fig 6.3: Side view of "filter probe" membrane phase separator showing in dashed lines the Pitot tube used to measure free-stream velocity, V_{max}, of liquid flowing past the membrane.

is unstirred and can be calculated from previous studies to be about 5 x 10^4 cm^2 when it is rapidly stirred (116). In the system studied the aqueous phase was the dispersed (droplet) phase and chloroform was the continuous phase. This was shown by withdrawing a small volume of the rapidly stirred mixture and squirting it in either chloroform or water (130). In the former case, droplets of aqueous phase persisted, while in the latter case, coalescence was rapid and no droplets persisted.

The free stream velocity, V_{max}, of the liquid flowing past the membrane phase separator can be calculated from the difference in liquid height in the vertical arm of the L-shaped Pilot tube under stirring, H_S, and non-stirring, H_{NS}, conditions by the following equation which is derived from Bernoulli's Theorem (129,131):

$$V_{max} = c\sqrt{2\,g\,(H_S - H_{NS})} \quad \text{.....} \quad 6.1$$

in which c is a dimensionless coefficient whose value is about 1.00 and g is the gravitational constant whose value is 980 cm/s^2 if H_S and H_{NS} are measured in cm. The measured value of (H_S - H_{NS}) was 1.0 cm, so that V_{max} is 45 cm/s. This value will be used in section 6.4.2 to calculate the time available for the adsorbed solute to desorb/diffuse on coalescence of droplets at the membrane surface.

Calculation of the velocity gradients close to the surface of the membrane in the so-called boundary-layer requires a knowledge of the flow regime in the boundary-layer. At values of the length-Reynolds number, N_{Re}, less than 5 x 10^5 (132) laminar flow prevails. N_{Re} is calculated from the following expression:

$$N_{Re} = \frac{V_{max} \cdot \rho . l}{\eta} \quad \text{.....} \quad 6.2$$

where ρ is the density of the liquid, η is its viscosity, and l is the distance along the membrane in the direction of flow as measured from its upstream edge (l = 1.3 cm). Using density and viscosity values that are averages of the values for chloroform and water (ρ_{Av} = 1.24 g/cm^3 and η_{Av} = 7.1 x 10^{-3} poise), N_{Re} is calculated to be 1 x 10^4 at the downstream edge of the membrane. Thus, flow in the boundary-layer near the membrane is laminar.

6.3.2 Adsorption of $MB.ClO_4$

The key experiment reported in this part of the thesis involves the simultaneous measurement of concentrations of solute in the two immiscible liquid phases under both stirred and non-stirred conditions. To be suitable for use in this study the solute had to meet four criteria. It had to: (i) be readily measured analytically in both phases, preferably by visible absorption spectroscopy; (ii) have a distribution ratio between the two bulk phases of about 1, so that accurately measurable concentrations would be present in both phases and the influence of small amounts of impurity would be minimal; (iii) be adsorbed at the liquid-liquid interface, and; (iv) reach equilibrium fairly quickly after the start or termination of stirring. The chemical system chosen for study involves the organic cation methylene blue (MB^+) and the inorganic perchlorate anion. In dilute aqueous bulk phase methylene blue perchlorate is largely dissociated (133,134), while in the chloroform bulk phase it is present mainly as ion-pairs (133). The form in which it is adsorbed at the chloroform-water interface is not known, though it is probable that the ion-pair predominates (134). Thus, the principal distribution equilibria are the following:

$$(MB^+)_A + (ClO_4^-)_A \rightleftharpoons (MB.ClO_4)_{Int} \rightleftharpoons (MB.ClO_4)_O \quad \text{..... 6.3}$$

where the subscripts indicate the aqueous, interfacial and organic phases. In order to minimize changes in the distribution ratio, D, when $MB.ClO_4$ adsorbs at the interface, $[ClO_4^-]_A >> [MB^+]_A$ at all times. Assuming that $MB.ClO_4$ is largely dissociated in aqueous solution, the relationship between D and $[ClO_4^-]_A$ is given by equation 6.4

$$D = \frac{[MB.ClO_4]_O}{[MB^+]_A} = K_{IP}[ClO_4^-]_A \quad \text{..... 6.4}$$

where

$$K_{IP} = \frac{[MB.ClO_4]_O}{[MB^+]_A\,[ClO_4^-]_A} \quad \text{..... 6.5}$$

where the O and A subscripts represent the organic phase and aqueous phase respectively, and K_{IP} is the ion-pair constant of $MB.ClO_4$ in the aqueous phase. The distribution ratio between the interface and bulk organic phase, $K_{I,O}$, is defined as:

$$K_{I,O} = \frac{\Gamma_{I,MB.ClO_4}}{[MB.ClO_4]_O} \quad \text{..... 6.6}$$

where $\Gamma_{I,MB.ClO_4}$ represents the surface excess of $MB.ClO_4$ at the interface i.e. the number of moles of $MB.ClO_4$ adsorbed at the interface per unit surface area (eq 6.7)

$$\Gamma_{I,MB.ClO_4} = \frac{n_{I,MB.ClO_4}}{A} \quad \text{..... 6.7}$$

Similarly, the distribution ratio between the interface and bulk aqueous phase, $K_{I,A}$, is defined as:

$$K_{I,A} = \frac{\Gamma_{I,MB.ClO_4}}{[MB.ClO_4]_A} \quad \text{..... 6.8}$$

The maximum interfacial concentration (i.e. surface excess) of adsorbed $MB.ClO_4$ encountered in this study (section 6.3.3) was 3.8×10^{-12} moles/cm^2 which corresponds to 4×10^{-13} cm^2/molecule. Since molecular models suggest that in a tightly packed monolayer each $MB.ClO_4$ would occupy about 1×10^{-14} cm^2/molecule (134), it is evident that in this study the reversibly-adsorbed film of $MB.ClO_4$ is loosely packed and can be expected to exhibit the properties of a two-dimensional ideal gas (135-137).

Solutes which adsorb at liquid-liquid interfaces are likely to adsorb at other interfaces as well. Adsorption of $MB.ClO_4$ on interfaces other than the chloroform-water interface, such as glass, paper, Teflon and air-liquid (134), does not cause errors in the observed distribution isotherm between bulk liquid phases if measurements are made by the method used in this study. Nevertheless, the membranes were not rinsed free of adsorbed methylene blue between experiments in order to reduce the adsorptive loss of the dye from the bulk liquid-liquid interface. While adsorption onto other interfaces does not introduce errors in the measurement of the liquid-liquid distribution ratio, it does introduce errors in calculations of the distribution ratios between the liquid-liquid interface and bulk liquid phases since such calculations must involve the mass balance for methylene blue. Thus, in section 6.3.3, the measured distribution ratios of $MB.ClO_4$ between the interface and bulk organic phase ($K_{I,O} = 1.1 \times 10^{-3}$ cm) and between the interface and bulk aqueous phase ($K_{I,A} = 6 \times 10^{-4}$ cm) each have uncertainties of about 10%, relative.

6.3.3 Distribution Isotherm

From eq 6.3 it can be seen that when stirring is started and the interfacial area increases, solute will enter the interface from both bulk phases. A typical example of the effect of stirring is shown in Fig 6.4 which shows the change in absorbance values in both bulk liquid phases on switching from stirring to non-stirring and vice versa. At equilibrium the ratio of solute concentrations in the two bulk phases will be identical to what it would be in non-stirred system containing the same number of moles of solute as are in the bulk phases. That is, equilibrium demands that the distribution ratio, D (eq 6.4), of solute between bulk liquid phases, at the same point on the distribution isotherm, is identical in the stirred and non-stirred mixture. This is true regardless of the shape of the isotherm. Simultaneous use of two membrane phase separators permits measurement of concentrations of solute in the two liquids and thus, an evaluation of D and of distribution isotherms.

Separate experiments performed in chloroform-saturated aqueous $KClO_4$ solution and water-saturated chloroform show that MB^+ and $MB.ClO_4$, respectively, conform to Beer's law. The liquid-liquid distribution isotherm, which is a plot of $[MB.ClO_4]_O$ vs $[MB^+]_A$, is therefore represented in Fig 6.5 by a plot of absorbance in the chloroform phase (A_O) vs absorbance in the aqueous phase (A_A). The open symbols designate the absorbances obtained for various amounts of methylene blue in the absence of stirring. A line through these points corresponds to the liquid-liquid distribution isotherm. The solid symbols designate the absorbances obtained with stirring. Similarly, a line through these points corresponds to the liquid-liquid distribution isotherm. Solid and open symbols having the same shape represent the same solution with and without stirring. For example, the solution represented by the hexagonal symbol had $A_O = 0.500$ and $A_A = 0.236$ when unstirred but these absorbances decreased to $A_O = 0.348$ and $A_A = 0.150$ when the solution was stirred. The data are also presented in Table 6.1. In Table 6.2 are summarized the results of linear least squares regression analysis of the data. Within their 95% confidence limits, both slopes and the

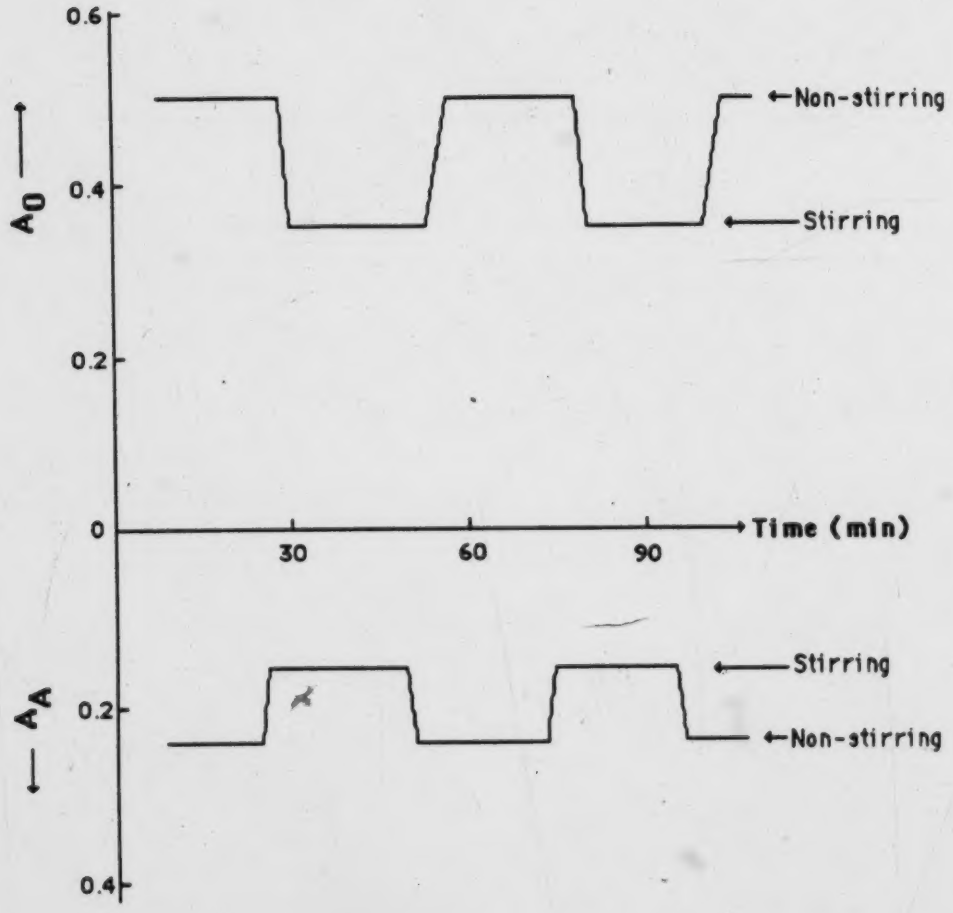

Fig 6.4: Schematic representation of a chart recording that shows the change in absorbance values in both bulk phases on changing from stirring to non-stirring.

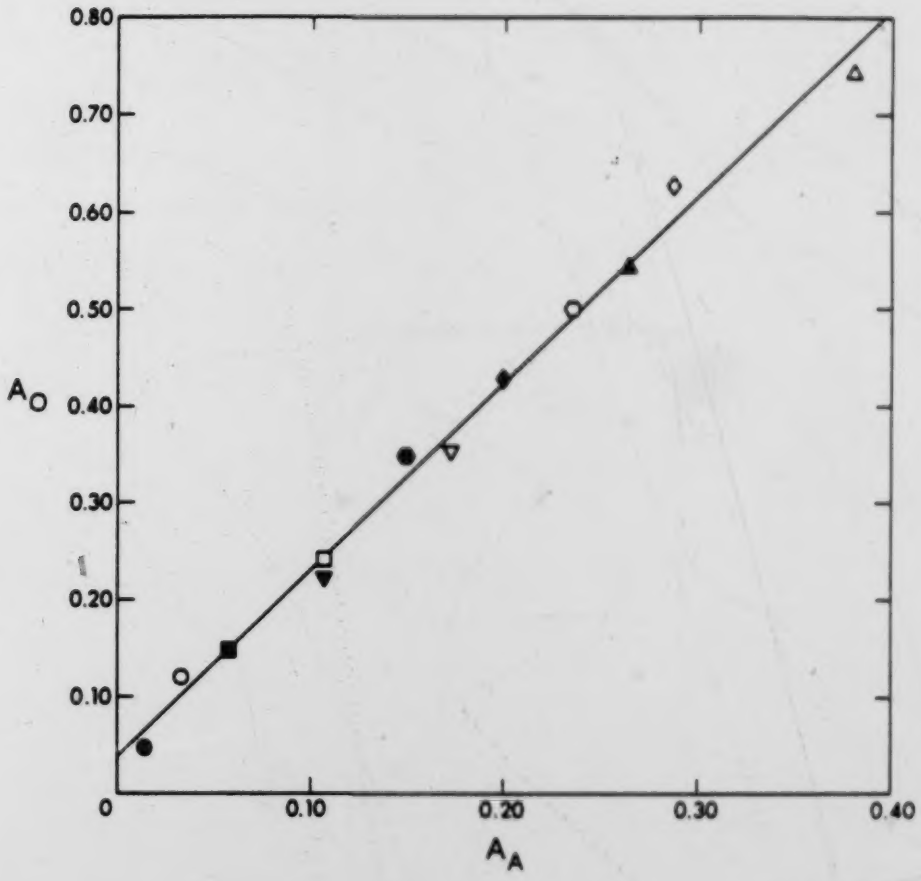

Fig 6.5: Distribution isotherm for methylene blue perchlorate between chloroform and aqueous phases. Open symbols represent non-stirred values and closed symbols represent stirred values. Symbol shapes correspond to total moles of $MB.ClO_4$ present: (○) for 1.53×10^{-7}; (□) for 3.06×10^{-7}; (▽) for 4.59×10^{-7}; (◇) for 6.12×10^{-7}; (◇) for 7.65×10^{-7}; and (△) for 9.18×10^{-7} moles.

Table 6.1: Absorbances of the chloroform phase (A_O) and aqueous phase (A_A) for 60 mL of each phase containing various amounts of methylene blue perchlorate with no stirring (NS) and vigorous stirring (S). Uncertainties are standard deviations for triplicate measurements.

Moles of $MB.ClO_4$ X 10^{-7}	Stirring Condition	A_O	A_A
1.53	NS	0.121 ± 0.008	0.033 ± 0.0006
1.53	S	0.047 ± 0.005	0.014 ± 0.0006
3.06	NS	0.240 ± 0.000	0.107 ± 0.001
3.06	S	0.148 ± 0.008	0.058 ± 0.000
4.59	NS	0.353 ± 0.003	0.173 ± 0.0006
4.59	S	0.221 ± 0.003	0.107 ± 0.001
6.12	NS	0.500 ± 0.010	0.236 ± 0.010
6.12	S	0.348 ± 0.008	0.150 ± 0.011
7.65	NS	0.627 ± 0.013	0.288 ± 0.005
7.65	S	0.428 ± 0.010	0.200 ± 0.004
9.18	NS	0.742 ± 0.009	0.381 ± 0.008
9.18	S	0.542 ± 0.006	0.265 ± 0.010

Table 6.2: Slope and intercept values from linear least squares regression analysis of plots of A_O vs A_A under stirring (S) and non-stirring (NS) conditions. Uncertainties are 95% confidence limits. The number of data points was 18 for NS, 18 for S and 36 for combined data.

Stirring condition	Slope	Intercept	Correlation coefficient
NS	1.86 ± 0.11	0.052 ± 0.026	0.995
S	1.98 ± 0.11	0.027 ± 0.017	0.997
Combined	1.91 ± 0.07	0.039 ± 0.015	0.996

intercepts are the same for stirred and non-stirred conditions which indicates that both sets of data describe the same isotherm. Consequently, at the same point on the distribution isotherm, D is identical for stirring and non-stirring. Regression results are presented in Table 6.2 also for a composite set of data for stirring and non-stirring, and the corresponding regression line is the one shown in Fig 6.5.

Identical isotherms obtained for stirring and non-stirring are consistent with the conclusion that adsorbed solute does not enter the bulk liquids during membrane induced phase separation. However, though it is a necessary condition, it is not a sufficient condition to unequivocally prove this conclusion, for it is conceivable that the fractions of initially adsorbed $MB.ClO_4$ which enter the bulk phases upon coalescence are not zero, but just happen to be proportional to D. For this reason, the matter has also been examined theoretically in the Discussion section later on.

Using the data from Table 6.1, the surface excess, $\Gamma_{I,MB.ClO_4}$, was calculated as follows:

$$\Gamma_{MB.ClO_4} = \frac{(n_{T,NS} - n_{T,S})}{A} \quad \text{..... 6.9}$$

where $n_{T,NS}$ is the sum the of moles in both phases with no stirring, $n_{T,S}$ is the sum of the moles in both phases during stirring and A is the surface area of the interface during stirring (5×10^4 cm^2, ref 116). The surface excess at various concentrations of $MB.ClO_4$ used for the isotherm are presented in Table 6.3.

A plot of $\Gamma_{I,MB.ClO_4}$ vs $[MB.ClO_4]_{O,S}$ gives a value of $(6\pm0.4) \times 10^{-4}$ cm for $K_{I,O}$, the distribution ratio between the interface and the organic phase. Similarly, a plot of $\Gamma_{I,MB.ClO_4}$ vs $[MB.ClO_4]_{A,S}$ gives a value of $(1.1\pm0.08) \times 10^{-3}$ cm for the distribution ratio between the interface and the aqueous phase, $K_{I,A}$.

Table6.3: The surface excess for the various concentrations of both phases used in Table 6.1. The subscripts represent the organic and aqueous phase under stirring and n_{Ads} is the No. of moles of $MB.ClO_4$ adsorbed under stirring (Interfacial area = 5×10^4 cm^2, ref. 116).

$[MB.ClO_4]_{O,S}$ x 10^{-6} M	$[MB.ClO_4]_{A,S}$ x 10^{-6} M	n_{Ads} x 10^{-7} moles	Surface Excess x 10^{-12} mol/cm^2
0.047 ± 0.005	0.14 ± 0.006	0.558 ± 0.009	1.12 ± 0.018
1.48 ± 0.008	0.58 ± 0.000	0.844 ± 0.008	1.69 ± 0.016
2.21 ± 0.003	1.07 ± 0.001	1.19 ± 0.004	2.38 ±0.008
3.48 ± 0.008	1.50 ± 0.011	1.43 ± 0.019	2.86 ± 0.038
4.28 ± 0.010	2.00 ± 0.004	1.72 ± 0.018	3.44 ± 0.036
5.42 ± 0.006	2.65 ± 0.010	1.89 ± 0.017	3.78 ± 0.034

6.4 Discussion

In a rapidly stirred liquid-liquid mixture at equilibrium all three phases are simultaneously at equilibrium with one another. When the concentration of solute at the interface is suddenly increased as a result of droplet coalescence, then distribution equilibrium can be re-established only as a result of transfer of solute from the interface into the two bulk liquid phases. The goal of this theoretical discussion is to predict the extent to which this transfer occurs during membrane-induced phase separation.

In this theoretical discussion, we will first consider the fate of the interfacially adsorbed solute on coalescence of a droplet with the liquid film on the membrane. Next we will consider the residence time that the adsorbed solute from the droplet spends near the membrane surface. Finally, it will be shown that during the residence time only a small fraction of the adsorbed solute diffuses through the Nernst diffusion layer to reach the bulk phase.

6.4.1 Coalescence

Because it is relatively easy to conceptually visualize the coalescence of droplets of dispersed phase with the liquid on the surface of the membrane wetted by that phase, the following discussion will emphasize the behavior of the dispersed phase. It should be remembered, however, that at the surface of the membrane wetted by the continuous phase there is a merging of continuous phase from the liquid-liquid dispersion with the continuous phase on the surface of the membrane which, while it is not properly called coalescence, is analogous to coalescence in the sense that it involves a local loss of liquid-liquid interface. Thus, the conclusions which will be made regarding the fate of interfacially adsorbed solute during coalescence at the surface of the membrane wetted by dispersed phase are equally valid for continuous phase at the other membrane.

In order to allow the passage of one of the liquid phases by flow through its pores while completely excluding the other phase, the membrane must be constructed of a material that is wetted by the liquid to be passed. Both the fibrous Teflon and paper membranes are highly porous: the Teflon, for example, is about 65% pore space (137a). The pores in each type of membrane, which are the spaces between the intertwined fibres, are filled with the wetting phase. The fibres at the surface of the membrane, when they come in contact with the non-wetting phase, remain covered with a thin layer of wetting phase. Under the conditions of rapid stirring which are typically employed (107,113-116,119) the dispersed phase exists as droplets that are only about 0.02 cm in diameter (116). Furthermore, when the liquid phase volume ratio is near one, as in this case, the thickness of the continuous phase between the droplets is also about 0.02 cm.

There is a high frequency of collision with the membrane surface by droplets of dispersed phase from the rapidly moving droplet swarm. Many of the colliding droplets coalesce with the liquid which is on the fibers and in the openings of the pores on the membrane surface, giving rise to a high flow rate of dispersed phase liquid onto the membrane. At the same time the shear force which is created by the tangential flow of the stirred liquid-liquid dispersion across the face of the membrane sweeps the accumulating liquid layer along until, at the downstream edge of the membrane face, it is detached and rapidly dispersed into droplets again. All of these phenomena can be seen by carefully watching the stirred mixture.

Coalescence of droplets with a flat surface has been extensively investigated (138,139). The latter stages of the process, which are of primary interest here, are illustrated in Fig 6.6. The so-called deposition time, which lasts from the time that the droplets has come close enough to the flat surface that rupture of the interface is initiated (Panel B) to the time that the entire liquid contents of the droplet have been emptied into the flat liquid layer is only about 0.02 seconds.

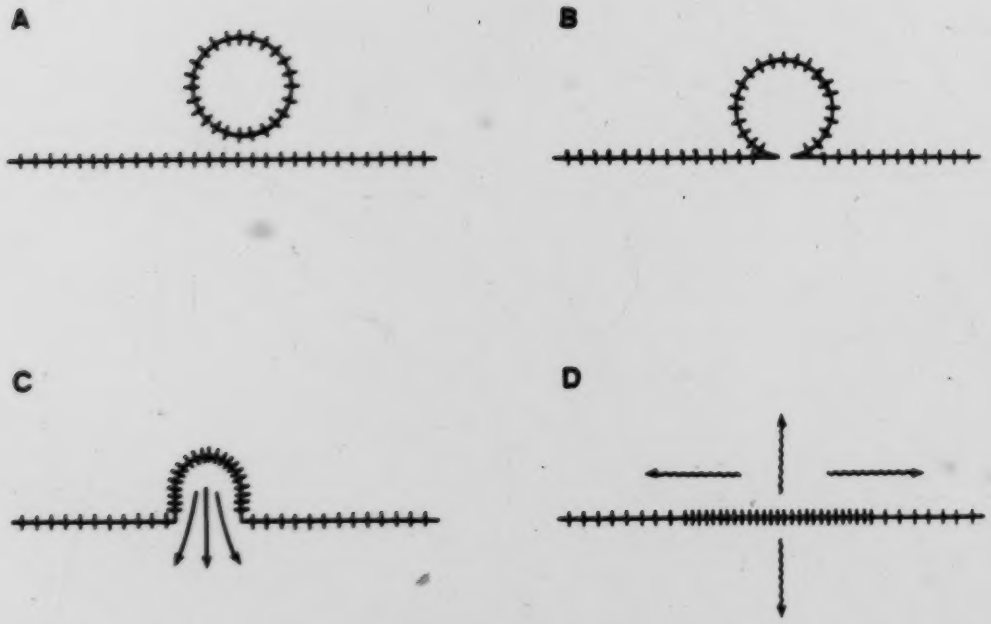

Fig 6.6 : Coalescence of a droplet of dispersed phase with a flat layer of the same phase showing the fate of interfacially adsorbed solute. Solute is represented with short dashes. A - droplet near the membrane surface (equilibrium situation); B - rupture of interface; C - flow of liquid in the droplet into the liquid on the membrane, and; D - the excess solute after the droplet disappears.

In Fig 6.6 the short dashes drawn across the interface represent adsorbed solute molecules. The evenly spaced dashes shown in panel A correspond to the equilibrium adsorption situation which prevails throughout the dispersion in the beaker. The sequence of panels B through D illustrates the fact that during coalescence there is a loss of interfacial area; i.e. the interface which initially surrounded the droplet disappears. The panels also show that solute molecules which were initially adsorbed at the droplet interface are squeezed together as the droplet interface disappears. This local compression of the adsorbed film creates a "patch" of solute whose interfacial concentration is greater than the equilibrium value. (Note in panel D the patch of dashes which are closer together in the region where the droplet has coalesced with the flat layer). The resulting non-equilibrium gives rise to the following process : (i) Desorption of solute from the interface into the very thin equilibrium layers immediately adjacent to the interface and subsequent diffusion of solute away from the equilibrium layers toward the bulk liquids, and (ii) lateral outward spreading of the patch of adsorbed solute in all directions along the interface (135,139,140). Desorption/diffusion is represented in panel D by the vertical wavy arrows, and spreading is represented by the horizontal wavy arrows. Of course, both desorption/diffusion and spreading commence at about the same time that the interfacial area begins to decrease during droplet deposition (140), but for clarity these processes are not represented in panels B and C in Fig 6.6.

Spreading of the adsorbed film along the interface is due mainly to flow induced by the interfacial pressure gradient (135,140,141) and partly to diffusion along the interface (141). In the present case, in which the purpose is to calculate the extent of desorption/diffusion, there is no need to estimate the spreading rate. This is because spreading of the patch of adsorbed solute will simultaneously produce an increase in the interfacial area occupied by the patch and a dilution of its interfacial concentration, with that concentration being inversely proportional to interfacial area occupied. Since

the rate of desorption/diffusion away from the interface is proportional to interfacial area and, for an ideal gas film, it is also proportional to interfacial concentration (141), there is no net effect of spreading on the desorption/diffusion rate (moles/s).

The extent to which solute in the patch at the liquid-liquid interface adjacent to the porous membrane is transferred to the bulk liquids on both sides of the interface is determined by three factors:

(a) The rate of desorption/diffusion, which is related to the diffusion coefficients of solute in the liquid phases and to the distribution ratios between the interface and liquid phases, as will be discussed later.

(b) The thickness (∂X) of the Nernst diffusion layers of liquids through which the desorbed solute must diffuse in order to reach the bulk liquid phases.

(c) The residence time available for diffusion away from the interface to occur: This lasts from the commencement of droplet deposition (e.g. panel B, Fig 6.6) until the region of interface containing the patch of solute has been swept along the membrane to its downstream end, where the wetting phases detaches and becomes re-dispersed.

6.4.2 Residence time

The residence time is governed by the hydrodynamic conditions in the stirred two-liquid phase system. The flow pattern of a two phase liquid near the surface of the porous membrane can be estimated in terms of boundary-layer theory (132,142). When a single phase of relatively low viscosity flows over and parallel to a planer solid surface a thin layer develops in the liquid adjacent to the surface, in which the velocity gradient normal to the surface is large. Across the so-called boundary-layer the linear velocity of the liquid, parallel to the surface, changes from zero at the solid surface to a limiting free stream velocity, V_{max} at a distance away from the surface X_{BL} defined as the thickness of the boundary layer. At any distance farther away from the surface than

X_{BL} the linear velocity remains nearly equal to V_{max}, the free stream velocity. The value of X_{BL} increases along the membrane.

Flow of a two-phase liquid near the surface of the porous membrane can be estimated in terms of boundary-layer theory if simplifying approximations are made:

(i) Chloroform and water are assumed to have the same viscosity, $\eta_{Av} = 7.1 \times 10^{-3}$ poise and the same density $\rho_{Av} = 1.24$ g/mL.

(ii) The interfacial viscosity η_s between chloroform and aqueous phases is assumed to be negligible, considering the wide membrane surface involved (140).

(iii) It is assumed that the flow through the boundary-layer is laminar, rather than turbulent, based on the measured length-Reynolds number. It is assumed that the laminar boundary-layer theory which was developed for thin flat plates can be applied to the flat membrane surface stretched across the end of a circular cylinder as shown in Fig 6.6.

(iv) Dispersed phase droplets are more or less rigid spheres and have been found to have an average diameter of 0.02 cm (116). It is assumed that the droplet dispersion in the laminar boundary-layer has a regular, layered structure as illustrated in Fig 6.7.A (138) and that the profile of linear velocities across the boundary layer is stepped, with each step being 0.02 cm high and having a linear velocity equal to that predicted from boundary-layer theory for a single-phase liquid at the location of the center of the drop (132). This is illustrated in Fig 6.7.B.

(v) The "worst case" or longest residence time will be calculated. This is the time required to transverse the full diameter of the membrane, 1.3 cm.

(vi) Another "worst case" assumption is that only droplets in the layer closest to the porous membrane coalesce with the wetting-layer during the time available.

Assumptions (i) and (ii) together are not likely to introduce an uncertainty greater than one-fold in the calculated residence time. The magnitude and direction of the uncertainty introduced in assumptions (iii) and (iv) are difficult to estimate but

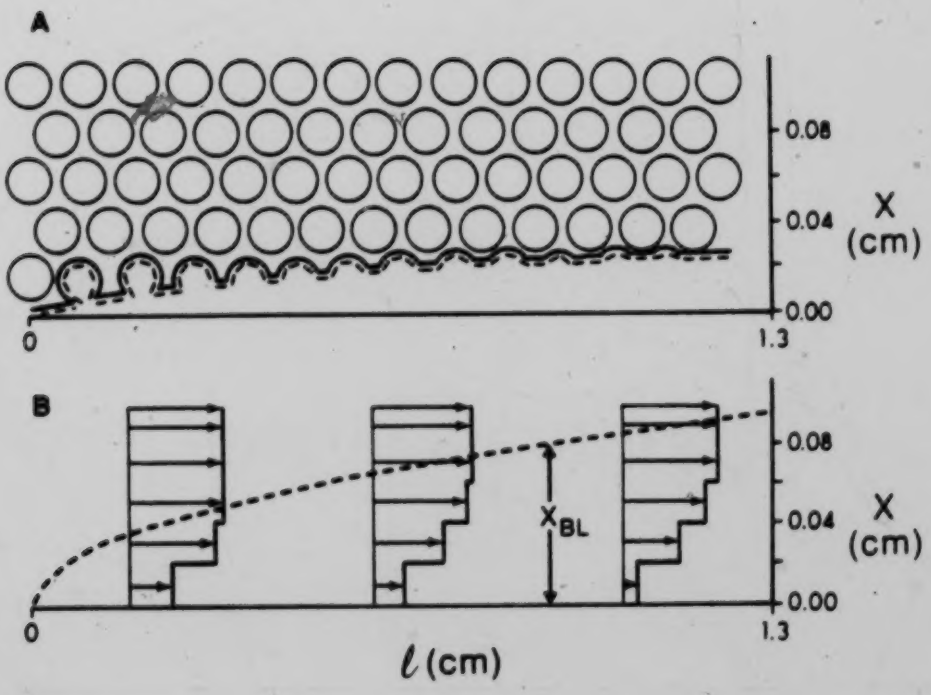

Fig 6.7: Flow of a two-phase liquid near the surface of a porous membrane. (A) Structure of two-phase flow showing droplet swarm of dispersed (wetting) phase, wetting layer, interface and Nernst diffusion layer in the wetting layer (dashed line). (B) Velocity profiles at various points in the boundary layer. Dashed line is at X_{BL}. Lengths of horizontal vectors are proportional to velocity at distance X. Membrane is located at X = 0.

may be as high as five-fold. The magnitude of uncertainty introduced in assumptions (v) and (vi) could also be several-fold but these errors will be in the direction which makes the calculated residence time larger than the true one. Consequently, while residence time calculated using this model may be longer than the true value, it is not likely to be shorter than the true value by more than two- or three-fold. Invoking the above assumptions, the thickness of the boundary-layer X_{BL} can be calculated by the expression:

$$X_{BL} = 5\left(\frac{\eta_{Av} \cdot l}{\rho_{Av} \cdot V_{max}}\right)^{0.5} \qquad \text{.....6.10}$$

for which V_{max}, the free-stream velocity, comes from equation 6.1. The boundary-layer thickness increases in direct proportion to the square root of distance along the membrane, *l*. The linear velocity V_X (cm/s) at any distance X cm from the surface can be obtained from tabulated values of $5(V_X/V_{max})$ as a function of X/X_{BL} (132).

The residence time of a patch of solute on the liquid-liquid interface is related to the velocity $V_{X,int}$ with which the interface is moving. $V_{X,int}$ is the linear velocity at distance (X,int) into the boundary-layer, at which the interface lies. The velocity of a patch of solute which appears on the interface as a result of droplet coalescence is equal to the velocity of the interface, because there is no slip between them (132). Based on assumptions (iv) and (vi) above, the velocity of the interface is taken as the velocity at a distance 0.01 cm away from the membrane. Near the leading edge of the membrane where the boundary-layer is thin this velocity is high, while near the downstream edge it is low, as seen from the velocity distribution plots in Fig 6.7.B. The average velocity along the diameter of the membrane at X,int = 0.01 cm can be obtained by numerical integration of the tabulated velocity distribution (132). This yields $V_{X,int} = 0.30$ V_{max}. In the present case $V_{max} = 45$ cm/s, as discussed above, so that $V_{X,int} = 13$ cm/s

and the residence time required to travel 1.3 cm is 0.1 s. (An analogous treatment assuming a turbulent (143) rather than a laminar boundary-layer yields $V_{x,int}$ = 0.77 V_{max} and a residence time = 0.04 s). Thus, the maximum time available for desorption/diffusion away from the patch of solute at the interface is about 0.1 s.

6.4.3 **Model of the Interface**

According to the Whitman two-film model of the interfacial region (139,144-146) there exist, immediately adjacent to either side of the interface, equilibrium layers in which the solutions are always at equilibrium with the interfacially adsorbed film of solute (Fig 6.8). The thickness of the equilibrium layers is about 10^{-7} cm (144). The activation energy for desorption from the interface into the equilibrium layers is considered to be negligible (140). This is a reasonable assumption for small molecules (141) and, in any event, is another "worst case" assumption since an activation barrier would decrease the desorption rate. Beyond the equilibrium layers two stagnant layers of solution exists, the Nernst diffusion layers, one on either side of the interface and extending into the solutions for a distance, δX, usually several tens of micrometers. Farther away from the interface than the distances δX are the bulk solutions which are considered to be so rapidly mixed that each bulk solution is entirely homogeneous at any time. Both the dispersed phase bulk solution and the continuous phase bulk solution experience this rapid convective mixing (144,147,148). In the dispersed phase rapid convection within the droplets is caused by the high rates of break-up of larger droplets into smaller ones and coalescence of smaller droplets to form larger ones. The layer of wetting liquid on the porous membrane experiences this same kind of convection due to coalescence of droplets with it. Just as they are present at the interface around a droplet of dispersed phase, so equilibrium layers, stagnant Nernst diffusion layers and bulk solutions are present also on both sides of the interface that exists between wetting liquid and overlying non-wetting liquid at the membrane.

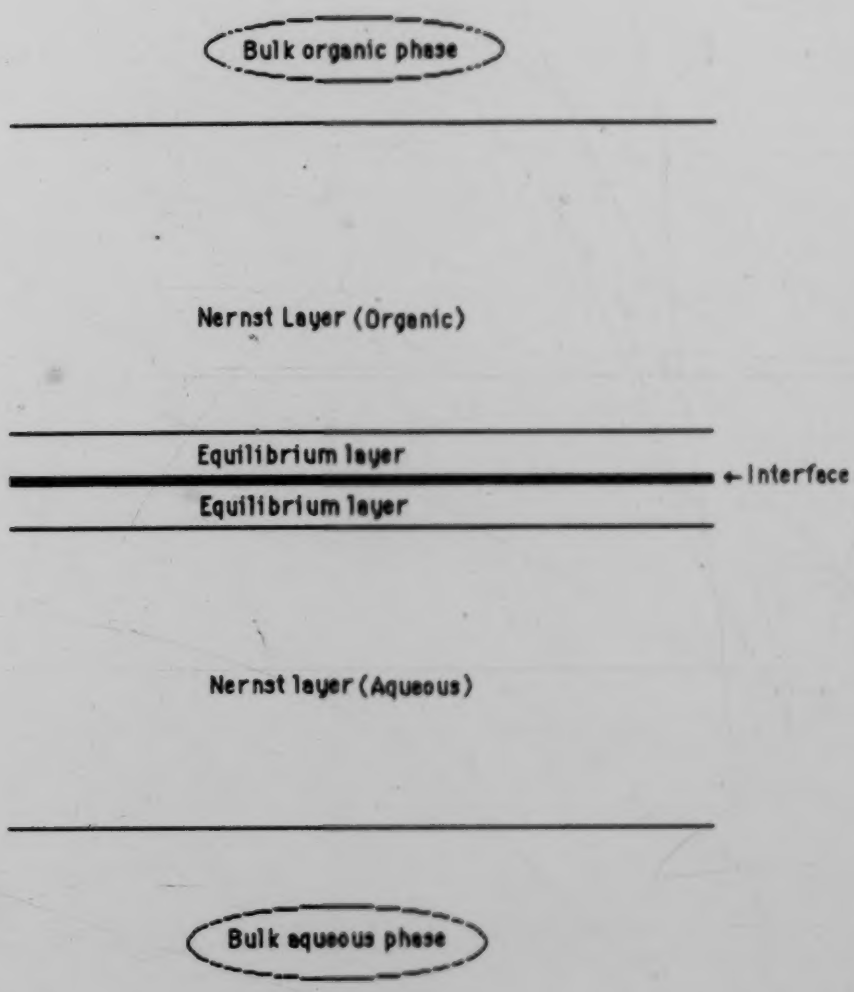

Fig 6.8: Whitman two film model of the interface.

6.4.4 Diffusion layer thickness

The value of the Nernst diffusion layer thickness δX is determined by hydrodynamic factors but its magnitude is difficult to calculate for the interface between wetting and non-wetting liquids at the membrane. A value will be estimated from what has been found in droplets of dispersed phase in a rapidly stirred chloroform-aqueous mixture and this value will be assumed to be the same for both the chloroform and aqueous sides of the interface. Based on the rate of extraction of o-nitroaniline, the Nernst layer thickness in the droplet dispersion is 0.003 cm (119). This value is maintained by frequent coalescence and re-dispersion of droplets in the rapidly stirred mixture. There is no reason to think that δX would become any smaller when a droplet coalesce with the layer of wetting phase at the surface of the membrane. In fact, in the less turbulent conditions in the boundary-layer some thickening of the Nernst films might be expected. Thus, a "worst case" (i.e. thinnest) value of δX will be taken as 0.003 cm. In Fig 6.7.A the Nernst layer in the wetting phase is shown by dashed lines adjacent to the interface. A similar layer, not shown, exists also on the non-wetting phase side of the interface.

6.4.5 Desorption/Diffusion

Transfer of desorbed solute from the Nernst layers to the bulk solutions via diffusion across the Nernst layers is the rate-determining processes. Desorption from the interface into the equilibrium layers is a pre-equilibration step which decreases the rate of diffusion in the same sense that a pre-equilibration step decreases the rate of a homogeneous chemical reaction. Calculation of the desorption/diffusion rate requires the mathematical solution of Fick's second law (149) which can be simplified by making some approximations.

(a) The diffusion coefficients of solute in the two phases are assumed to have the same value. The uncertainty introduced by this approximation is smaller than the uncertainties involved in hydrodynamic calculations.

(b) Diffusion away from the two very thin equilibrium layers is assumed to occur into infinitely thick Nernst layers (149). This corresponds to an irreversible process that does not approach an equilibrium distribution of solute between interface and solutions. However, the uncertainty introduced by this assumption is also small compared to hydrodynamic factors provided that diffusion occurs for such a short time that no more than a few percent of the desorbed solute reaches the end of the Nernst layer which is located at a distance δX.

With these approximations the problem is reduced to that of the one-dimensional diffusion of solute away from a very thin plane-source (equilibrium layers) into a homogeneous medium, but complicated by the fact that the disappearance of solute from the equilibrium layer as a result of diffusion is accompanied by desorption from the interface so that the total moles of solute diffusing increases with time. Since there is no analytical solution to Fick's second law for this case, the problem must be solved numerically by a finite-difference method (149). The algorithm for solving this problem was conceived by Tian Xiumin who wrote the compiled-BASIC program presented in the appendix and executed the calculations on an IBM-XT microcomputer (151). In the algorithm the total time t (either 0.01, 0.05, 0.1 or 0.5 s) is divided into n time steps ($\delta X = t/n$), where $n = 5000$ and the total distance being considered (either 0.001, 0.002 or 0.003 cm) is divided into 120 distance steps. For the first time step ($n = 0$) the concentration of solute in solution at a distance x and time t, $B_o(x,t)$ in moles/cm^3 is calculated from the analytical solution of Fick's second law for diffusion away from a very thin plane (149).

$$B_o(x,t) = \frac{C_o}{2\sqrt{\pi D' t}} \exp\left(\frac{-x^2}{4D' t}\right) \quad \text{..... 6.11}$$

in which C_o is the initial two dimensional concentration of solute in the equilibrium layer (the equilibrium layer is taken to be 5×10^4 cm^2 in area and 10^{-7} cm thick); t is the total time during which diffusion is assumed to have occurred (i.e. between 0.01 and 0.5 s); and D' is the diffusion coefficient, taken as 5×10^{-6} cm^2/s which is a typical value for small molecules in solution. For each of the subsequent n time steps, which are δt apart, a correction is made by the fact that diffusion of solute out of the equilibrium layer adjacent to the interface will cause desorption of solute from the interface into the equilibrium layer which, in turn, will increase the amount of solute diffusing away from the equilibrium layer. The amount of solute desorbed during each time step can be calculated from the experimentally measured distribution ratio of solute between the interface and the bulk solution ($K_{I/O} = 6 \times 10^{-4}$ cm for methylene blue). Thus, for each time step (0, 1, 2 . . . . n-1) a value of concentration ($B_o(x,t)$, $B_1(x,t)$ . . . . $B_{n-1}(x,t)$. The sum of all these B values over n steps gives B(x,t).

Results of these calculations for a total of 1.9×10^{-7} moles initially adsorbed (i.e. the highest concentration in Table 6.3), and for a total time of 0.1 s are presented as curve A in Fig 6.9. Curve B, included for comparison, was calculated for the hypothetical situation in which the same total number of moles are assumed to have all been present at time t = 0 in the equilibrium layers (no adsorption at the interface). For this hypothetical situation equation 6.10, which describes a Gaussian curve, is the analytical solution of Fick's second law (with $C_o = 1.9 \times 10^{-7}$ moles/5×10^4 cm^2). The areas under each curve are proportional to the number of moles in solution. The area of curve A is 47% of curve B indicating that only about half of the initially adsorbed solute has desorbed in 0.1 s. Of interest for present purposes is the fraction of the total moles which has diffused a given distance into the Nernst layer. This information is presented

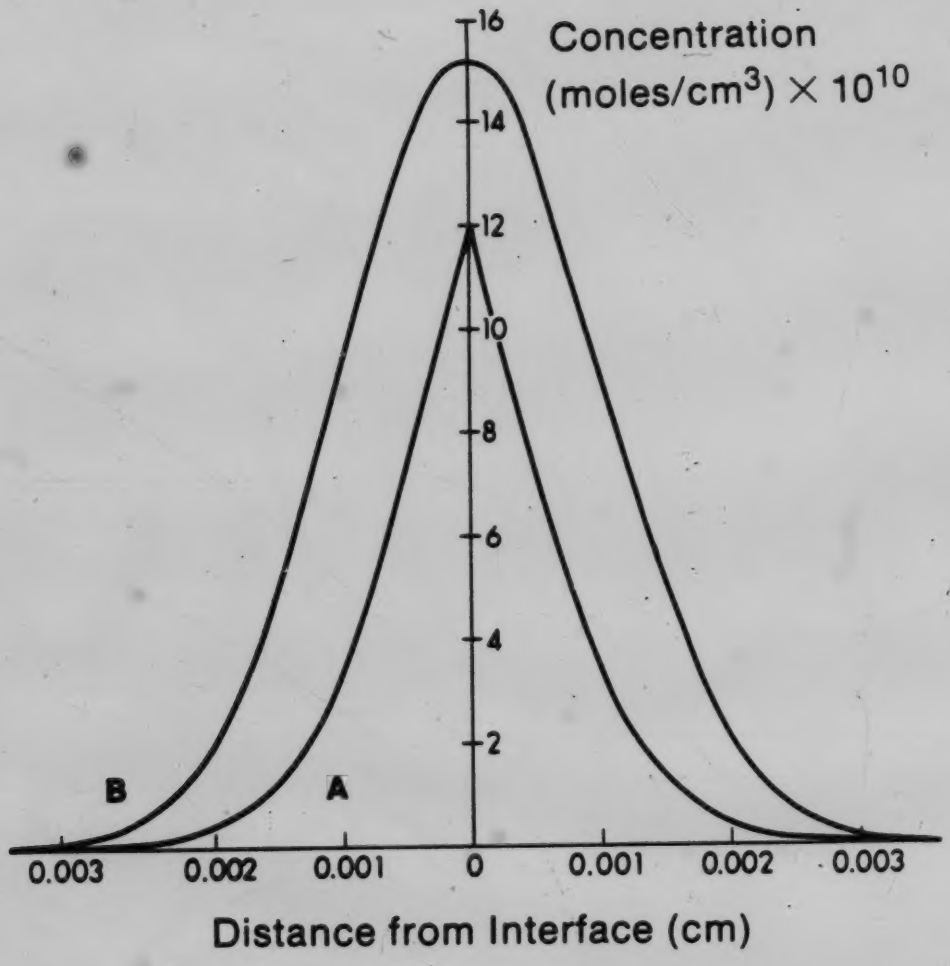

Fig 6.9: Solute concentration vs distance from the liquid-liquid interface at t = 0.1 s. Curve A includes the effect of desorption from the interface. Curve B shows the hypothetical behavior if interfacial adsorption were present. The interface is located at 0 cm.

in Table 6.4 for desorption/diffusion, not only for t = 0.1 s but also for t = 0.01, 0.05 and 0.5 s.

Any solute which diffuses 0.003 cm or more away from the interface toward the membrane will have entered the bulk-solution which passes through the porous membrane, and will have raised its solute concentration above the equilibrium value which exists in the stirred liquid-liquid dispersion. Solute which has not diffused as far as 0.003 cm during the residence time will be swept away from the membrane. From the values in Table 6.4 it is seen that, with a residence time of t = 0.1 s, the fraction of interfacially-adsorbed solute reaching the bulk liquid is negligible (<0.1%).

6.5 Conclusion

Taken together with the experimental findings reported in the Results section, these theoretical considerations constitute strong evidence that solute adsorbed at the interface does not enter the bulk liquid phases during membrane-induced phase separation in rapidly stirred systems. This justifies the use of porous membrane phase separators in studies of interfacial adsorption (116) and it makes possible quantitative interpretation of adsorption phenomena observed in analytical applications of solvent extraction (107).

There is another consequence of the slow desorption/diffusion behavior described here. In some phase separating devices used in solvent extraction the residence time is about 1 s. Examples are the various types of phase separators used in solvent extraction/flow injection analysis (see summary in reference 108). When surface active solutes are involved then the mere fact that coalescence of phases in the phase separator may be complete does not necessarily mean that the desorption/diffusion process has reached equilibrium. Bulk phase concentrations under these circumstances may be lower than expected.

Table 6.4: Percentages of the total amount of solute initially adsorbed at the interface which have desorbed and which have diffused to or beyond a given distance in a given time.

Distance (cm)	Time (s)			
	0.01 s	0.05 s	0.1 s	0.5 s
0.001	<0.1	1	8	27
0.002	<0.1	<0.1	0.3	12
0.003	<0.1	<0.1	<0.1	5
% Desorbed	34	44	47	53

Freiser (152) misinterpreted a published report of this work (153). Briefly, he incorrectly interprets our claim: specifically, he incorrectly assumes that we are applying the model to the total liquid-liquid interface in the beaker, rather than just to the local non-equilibrium situation associated with the membrane phase separator. Freiser misconceptions were identified and the model proposed in this present work vindicated in a rebuttal to his criticisms (154). Subsequently, Chamupathi and Freiser (155) published an article "Fate of Interfacial Adsorbates in Solvent Extraction Systems" which showed the same conclusions as this work. In their experiments (155), the organic phase was continuously removed out of the cell via a similar filter probe. They observed an increase in absorbance of the organic phase as the volume of organic phase inside the stirred mixture decreases which clearly shows, as we have, that solute adsorbed at the liquid-liquid interface does not leave the beaker in the solution filtered through the porous membrane phase separator.

REFERENCES

1. E. Steinnes in "Trace Element Speciation in Surface Waters and its Ecological Importance", G. G. Leppard (ed.), Plenum Press, NY (1983).
2. G. G. Leppard (ed.), "Trace Element Speciation in Surface Waters and its Ecological Importance", G. G. Leppard (ed.), Plenum Press, NY (1983).
3. J.R. Kramer and H.E. Allen (Eds.), "Metal Speciation: Theory, Analysis and Applications", Lewis publishers, Chelsea, Michigan (1988).
4. R.B. Braman in "Analytical Aspects of Environmental Chemistry", D.F.S. Natusch and P.K. Hopke (eds.), John Wiley and Sons, Toronto (1983).
5. T.M. Florence and G.E. Batley, CRC Crit. Rev. Anal. Chem., 9, 219-296, (1980).
6. A. Mizuike, Pure Appl. Chem., 59, 555-564 (1987).
7. T.M. Florence and G.E. Batley, Talanta, 24, 151-158 (1977).
8. T.M. Florence, Talanta, 29, 345-364 (1982).
9. T.A. Neubecker and H.E. Allen, Water Res., 17, 1-14 (1983).
10. G.E. Batley in "Trace Element Speciation in Surface Waters and its Ecological Importance", G. G. Leppard (ed.), Plenum Press, NY (1983).
11. R. Peterson, Environ. Sci. Technol., 16, 443-447 (1982).
12. R.D. Guy and A.R. Kean, Water Res., 14, 891-899 (1980).
13. R.L. Chaney in "Trace Element Speciation in Surface Waters and its Ecological Importance", G. G. Leppard (ed.), Plenum Press, NY (1983).
14. R.B. Martin, Metal Ions in Biological Systems, 20, 21-65 (1986).
15. D. Velso, R.W. Guynn, M. Oskarsson and R.L. Veech, J. Biol. Chem., 248, 4811-4819 (1973).
16. J.K. Aikawa, "The Relationship of Magnesium to Disease in Domestic Animals and in Humans", Charles C. Thomas Publisher, Springfield City, Illinois (1971).
17. J.K. Aikawa, "Magnesium: Its Biological Significance", CRC Press, Florida (1981).

18. B.E.C. Nordin, "Calcium, Phosphate and Magnesium Metabolism: Clinical Physiology and Diagnostic Procedures", Longman Group Ltd., Edinburgh (1976).

19. M.J. Halspern and J. Durlach (eds), "Magnesium Deficiency - Physiopathology and Treatment Implications", Karger, NY (1985).

20. W.E.C. Wacker, "Magnesium and Man", Harvard University Press, Cambridge, Massachusetts (1980).

21. L.L. Ingraham and D. Green, Science, 128, 310-312 (1958).

22. M. Walser, Anal. Chem., 32, 711-719 (1960).

23. A. Scarpa, Biochem., 13, 2789-2794 (1984).

24. E. Casillas, D.J. Harry and M. Kenny, Anal. Biochem., 116, 319-324 (1981).

25. E.P. Diamadis and B.R. Hoffman, Clin. Chem., 30, 1262 (1984).

26. R.P. Buck, J.C. Thompsen and O.R. Melroy in "Ion Selective Electrodes in Analytical Chemistry", H. Freiser (ed), Vol 2, Plenum Press, NY (1980).

27. M.V. Rouilly, M. Baldertscher, E. Pretsch, G. Suter and W. Simon, Anal. Chem., 60, 2013-2016 (1988).

28. F. Behm, D. Ammann, W. Simon, K. Brunfeldt and J. Halstrom, Helv. Chim. Acta., 68, 110-118 (1985).

29. M. Otto and J.D.R. Thomas, Anal. Chem., 57, 2647-2651 (1985).

30. F.W.Haeton, Clin. Chem. Acta., 15, 139-144 (1967).

31. W. Achilles and F.A. Cumme, Fresenius Z. Anal. Chem., 308, 112-116 (1981).

32. J.A. Swelleh, D. Lucyk, B. Kratochvil and F.F.Cantwell, Anal. Chem., 59, 586-592 (1987).

33. M. Spiech, B. Bousquet and G. Nicolas, Clin. Chem., 27, 246-248 (1981).

34. R.D. Guy and C.L. Chakrabarti, Proc. Int. Conf. Heavy Met. Environ. (Sym. Proc.), T. Hutchinson (ed.), Univ. of Toronto, 1, 275-294 (1975).

35. J.C. Wu and J.W. Robinson, Spectros. Lett., 19, 61-72 (1986).

36. F. Rousselet, B. Cherruau and M.H. Granier in "Magnesium Deficiency - Physiopathology and Treatment Implications", Karger, NY (1985).

37. J. Treit, J.S. Nielsen, B. Kratochvil, and F.F. Cantwell, Anal. Chem., 55, 1650-1653 (1983).

38. P.Y.T. Chow and F.F. Cantwell, Anal. Chem., 60, 1569-1573 (1988).

39. V. Mutacumura, M.Sc. Thesis, University of Alberta, Edmonton, Alberta (1988).

40. A. Hewavitharana, personal communication, Department of Chemistry, University of Alberta (1989).

41. K.F. Sugawara, H.H. Wetell and G.D. Schucker, Anal. Chem., 46, 489-492 (1974).

42. J.M. Hill, J. Chromatogr., 76, 455-458 (1973).

43. R.E. Sturgeon, S.S. Berman, S.N. Willie and J.A.H. Desauiniers, Anal. Chem., 53, 2337-2340 (1981).

44. R.E. Sturgeon. S.S. Berman and S.N. Willie, Talanta, 29, 167-171 (1982).

45. A. Warshswsky and R. Kalir, J. Appl. Poly. Sci., 24, 1125-1137 (1979).

46. J.M.J. Frechet and M.J. Farall in "Chemistry and Properties of Crosslinked Polymers", S.S. Labana (ed.), 59-81 (1976).

47. M.A. Kraus and A. Patchornik, J. Poly. Sci. : Macrom. Rev., 15, 55-106 (1980).

48. G.V. Myasoedova and S.B. Savvin, CRC Crit. Rev. Anal. Chem., 17, 1-63 (1987).

49. G.V. Myasoedova and S.B. Savvin, J. Anal. Chem. of USSR, 37, 383-399 (1982).

50. S.K. Sahni and J. Reedijk, Coord. Chem. Rev., 59, 1-139 (1984).

51. J.R. Parish and R. Stevenson, Anal. Chem. Acta., 70, 189-198 (1974).

52. F. Vernon, Chem. Ind., 15, 634-637 (1977).

53. F. Vernon and H. Eccles, Anal. Chim. Acta., 63, 403-414 (1973).

54. R.C. Degeiso, L.G. Donaruma and E.A. Tomic, J. Appl. Poly. Sci., 9, 411-419 (1965).

55. L.P. Pennington and M.B. Williams, Ind. Eng. Chem., 51, 759-762 (1959).

56. J.R. Parrish, Chem. Ind., 386-387 (1955).

57. S. N. Willie, R.E. Sturgeon and S.S. Berman, Anal. Chim. Acta., 149, 59-66 (1983).

58. J.R. Parrish, Anal. Chem., 54, 1890-1892 (1982).

59. A. Warshawsky, R. Kalir, and A. Patchornik, J. Org. Chem., 43, 3151-3157 (1978).

60. F.F.Cantwell, Anal. Chem., 48, 1854-1859 (1976).

61. J.H. Burckhalter and R.I. Leib, J.Org. Chem., 26, 4078-4083 (1961).

62. M. Kolobeilski, J. Heterocy. Chem., 3, 275 -277 (1966).

63. A. Corsini, W.J. Louch and M. Thompson, Talanta, 21, 252-255 (1974).

64. W.M. Landing, C. Haraldsson and N. Paxeus, Anal. Chem., 58, 3031-3035 (1986).

65. F. Vernon and K.M. Nyo, Anal. Chim. Acta., 93, 203-210 (1977).

66. B.A. Ulkelov, Ye. Ye. Yergozhin, B.A. Mukhitdinov and S.R. Rafikov, Poly. Chem. USSR, 532-540 (1978).

67. P.J. Hoek and J. Reedijk, J. Inorg. Nucl. Chem., 41, 401-404 (1979).

68. P.Y.T. Chow, Ph.D. Thesis, University of Alberta, Edmonton, Alberta, Canada (1988).

69. J.R. Jezorek, C. Fulcher, M.A. Crowell, R. Bayliss, B. Greenwood and J. Lyon, Anal. Chim. Acta., 131, 223-231 (1981).

70. D.K. Ryan and J.H. Weber, Talanta, 32, 859-863 (1985).

71. O. Szabadka and J. Inczedy, J. Chromatogr., 201, 59-66 (1980).

72. O. Szabadka, Talanta, 29, 177-181 (1982).

73. O. Szabadka, Talanta, 29, 183-187 (1982).

74. J.A. Marinsky in "Ion Exchange: A Series of Advances", J.A. Marinsky (ed.), Vol.1, Chapter 9, Marcel Dekker, New York (1966).

75. J.A. Marinsky, A. Wolf and K. Bunzyl, Talanta, 27, 461-468 (1980).

76. J.A. Marinsky, J. Phy. Chem., 89, 5294-5302 (1985).67. F. Vernon and K.M. Nyo, J. Inorg. Nucl. Chem., 40, 887-891 (1978).

77. J.A. Swelleh, Ph.D. Thesis, University of Alberta, Edmonton, Alberta, Canada (1988).

78. F.F. Cantwell, J.S. Neilsen and S.E. Hrudey, Anal. Chem., 54, 1498-1503 (1982).

79. N.E. Good, G.D. Winget, W. Winter, T.N. Conolly, S. Izawa and R.M.M. Singh, Biochem., 5, 467-477 (1966).

80. M.W. Brown and J. Ruzicka, Analyst, 109, 1091-1094 (1984).

81. J.A. Buono, R.W. Karin and J.L. Fasching, Anal. Chim. Acta. 80, 327-334 (1975).

82. Corning Works Technical Bulletin

83. F. Malamas, M.Bengtssos, and G. Johansson, Anal. Chim. Acta., 160, 1-10 (1984).

84. A.K. Kolstad, P.Y.T. Chow and F.F. Cantwell, Anal. Chem., 60, 1565-1569 (1988).

85. S. Puon and F.F. Cantwell, Anal. Chem., 49, 1256-1260 (1977).

86. A.E. Martell and R.M. Smith, Critical Stability Constants, Vols. 1- 5, Plenum Press, N.Y. (1974).

87. Documenta Geigy Scientific Tables, K. Diem and C. Lentner, eds., 7 th Ed., Geigy Pharmaceuticals, Quebec (1970).

88. W.E. Harris and H.A. Laitinen, "Chemical Analysis", 2 nd Ed., McGraw - Hill, Toronto (1975).

89. A. Ringbom, "Complexation in Analytical Chemistry", Interscience, New York (1963).

90. W.E. Harris and B. Kratochvil, "An Introduction to Chemical Analysis," Saundes College Publishing, Philadelphia (1981).

91. J. Kragten, Atlas of Metal-Ligand Equilibria in Aqueous solutions, John Wiley and Sons, Toronto (1978).

92. C.W. Davies, "Ion Association," Butterworth and Co., Toronto (1962).

93. D.D. Perrin and I.G. Sayce, Talanta, 14, 833-842 (1967).

94. D.A. Skoog and D.M. West, Foundamentals of Analytical Chemistry, 3rd Ed., Holt, Rinehart and Winston, Toronto (1976).

95. J. Bjerrum, G. Schwarzenbach and L.G. Sillen, "Stability Constants - Part 1: Organic Ligands," IUPAC Publication No. 6, London (1957).

96. "Stability Constants of Metal-ion complexes - Supplement No. 1," Special Publication No. 25, Chemical Society, London (1971).

97. D.D. Perrin, "Stability Constants of Metal-ion complexes, Part B, Organic Ligands," IUPAC Chemical Data Series No. 22, Pergamon Press, Toronto (1979).

98. J.S. Nielsen, Ph.D. Thesis, Univ. of Alberta, Alberta (1982).

99. S. Afrashtehfar and F.F. Cantwell, Anal. Chem., 54, 2422-2427 (1982).

100. F. Helfferich, " Ion Exchange," Mc Graw - Hill Co., Toronto (1962).

101. CRC Handbook of Chemistry and Physics, CRC Press, Fl (1982).

102. Rohm and Haas Technical Bulletin on XAD-2, Philadelphia.

103. R.A. Hux and F.F. Cantwell, Anal. Chem., 56, 1258-1263 (1984).

104. H.J. Liu, Ph.D. Thesis, Univ. of Alberta, Canada (1988).

104a. R.A.A. Muzarelli and R. Rouhetti in "Trace Metal Removal from Aqueous Solutions", R. Thompson (ed.), Whitstable Litho Ltd., U.K. (1986).

105. G.V. Jordan, Trans. Amer. Soc. Mech. Eng., 393-400 (1955).

106. T.E. Belk, Chem. Eng. Prog. 61, 72-76 (1965).

107. H.Y. Mohammed and F.F. Cantwell, Anal. Chem., 52, 553-557 (1980).

108. L. Fossey and F.F. Cantwell, Anal. Chem., 57, 1693-1697 (1985).

109. J.A. Sweileh and F.F. Cantwell, Anal. Chem., 57, 420-424 (1895).

110. C.A. Lucy and F.F. Cantwell, Anal. Chem., 58, 2727-31 (1986).

111. L. Fossey and F.F. Cantwell, Anal. Chem., 54, 1693-1697 (1982).

112. L. Fossey and F.F. Cantwell, Anal. Chem., 55, 1882-1885 (1983).

113. M. Carmichael and F.F. Cantwell, Can. J. Chem., 60, 1286-1290 (1982).

114. M. Carmichael and F.F. Cantwell, Anal. Chem., 54, 697-702 (1982).

115. H. Watari and H. Freiser, J. Am. Chem. Soc., 105, 191-194 (1983).

116. E. Aprahamian, H.Freiser and F.F. Cantwell, Langmuir, 1, 79-82 (1985).

117. L. Fossey and F.F. Cantwell, Anal. Chem., 57, 922-926 (1985).

118. H. Watarai, L. Cunningham and H. Freiser, Anal. Chem., 54, 2390-2392 (1982).

119. F.F. Cantwell and H. Freiser, Anal. Chem., 60, 226-230 (1988).

120. L. Amankwa and F.F. Cantwell, Anal. Chem., 61, 1036-40 (1989).

121. L. Amankwa and F.F. Cantwell, Anal. Chem., In press, (1989).

122. C.A. Lucy and F.F. Cantwell, Anal. Chem., 61, 101-7 (1989).

123. B. Kratochvil, J. Nolan and F.F. Cantwell, Can. J. Chem., 59, 2539-2542 (1981).

124. H. Watari, J. Phys. Chem., 89, 384-387 (1985).

125. M.L. Dietz and H. Freiser, Langmuir, 3, 467-470 (1987).

126. F.F. Cantwell and H.Y. Mohammed, Anal. Chem., 51, 218-223 (1979).

127. D.C. Abbot, Analyst (London), 87, 286-293 (1962).

128. P. Muckerjee and A.J. Ghosh, J. Am. Chem. Soc., 92, 6403-6407 (1970).

129. B.C. Sakiadis, Section 5 in "Perry's Chemical Engineer's Handbook; 6th Ed.; D.W. Green and J.O. Maloney, eds., McGraw-Hill: Toronto (1984).

130. A.W. Adamson, "Physical Chemistry of Surfaces", Interscience: N.Y., 1960. Chapter 9.

131. L. Prandtl, "Essentials of Fluid Dynamics", Hafner, N.Y., 1952. Chapter 2.

132. H. Schlichting, "Boundary-Layer Theory", 6th Ed., McGraw-Hill: Toronto, 1968. Chapters 2, 7.

133. S. Motomizu and K. Toei, Anal. Chim. Acta, 120, 267-277 (1980).

134. S.J. Valenty, J. Coll. Interface Sci., 68, 486-491 (1979).

135. J.T. Davies and E.K. Rideal, "Interfacial Phenomena", Academic Press: N.Y., 1961. Chapters 1, 5, 8.

136. D. Shaw, "Introduction to Colloid and Surface Chemistry", 3rd Ed., Butterworths: Toronto, 1980. Chapter 4.

137. A.W. Adamson, "Physical Chemistry of Surfaces", Interscience: N.Y. (1960). Chapter 3.

137a. Zitex membranes, Techincal Bulletin, Chemplast Inc., Wayne, NJ (1971).

138. G.V. Jefferies and G.A. Davies, in "Recent Advances in Liquid-Liquid Extraction", C. Hanson, ed., Pergamon: Toronto, 1971. Chapter 14.

139. J.C. Lee and T.D. Hodgon, Chem. Eng. Sci., 23, 1375-1397 (1968).

140. D.J. Crisp, Trans. Faraday Soc., 42, 619-635 (1946).

141. J.T. Davies, Trans. Faraday Soc., 48, 1050-1061 (1952).

142. L. Prandtl, "Essentials of Fluid Dynamics", Hafner: N.Y., 1952. Chapter 3.

143. H. Schlichting, "Boundary-Layer Theory", 6th ed., McGraw-Hill: Toronto, 1968. Chapter 21.

144. J.T. Davies and E.K. Rideal, "Interfacial Phenomena", Academic Press: N.Y., 1961. Chapters 4, 7.

145. O. Levenspiel, "Chemical Reaction Engineering", 2nd ed., Wiley: N.Y. 1972. Chapters 11,13.

146. P.R. Danesi and R. Chiarizia, "The Kinetics of Metal Solvent Extraction", in 'Critical Reviews in Analytical Chemistry', Chemical Rubber Co.: Akron, OH, 1980.

147. P.M. Heertjes and L.H. DeNie in "Recent Advances in Liquid-Liquid Extraction", C. Hanson, ed., Pergamon: Toronto, 1971. Chapter 10.

148. M. Linton and K.L. Sutherland, Proc. 2nd Intl. Cong. on Surface Activity, 1, 494-502 (1957).

149. J. Crank, "The Mathematics of Diffusion", 2nd ed., Oxford: London, 1975. Chapters 2, 3, 4, 8.

151. T. Xiu-min, Dept. of Chemistry, University of Alberta (1986).

152. H. Freiser, Anal. Chem., 60, 180-181 (1988).

153. G. Persaud, T. Xiu-min and F.F. Cantwell, Anal. Chem., 59, 2-7 (1987).

154. F.F. Cantwell, Anal. Chem., 60, 181-182 (1988).

155. V.G. Chamupathi and H. Freiser, Langmuir, 4, 49-51 (1988).

Appendix

Program by T. Xiu-min (151) to calculate the concentration of desorbed solute as a function of distance from the interface.

计称用的程序.

```
10 REM INTERFACE--EQUILIBRIUM LAYER DIFFUSION
20 REM TIAN XIUMIN--F.F.CANTWELL MODEL
30 INPUT "ENTER DIFFUSION TIME T=";T
40 INPUT "ENTER NUMBER OF TIME STEPS N=";N
50 LET Q=N+1
60 DIM M(Q),C(Q),U(Q)
70 LET A1=3.8E-12:D=.000005:K=6000:K1=6001
80 LET M(1)=A1*K/K1:C(1)=A1/K1:U(1)=A1/K1
90 LET F=3.14159:T1=T/N
100 FOR I=2 TO Q
110 FOR J=1 TO (I-1)
120 LET C(I)=U(J)*.0000001/(2*SQR(T1*F*D*(I-J)))+C(I)
130 NEXT J
140 LET U(J)=(M(J-1)-K*C(I))/K1
150 LET M(J)=M(J-1)-U(J-1):T2=T1*(I-1)
160 PRINT "DIFFUSION TIME=",(T-T2),"INC CON OF EQUIL.LAYER="
170 PRINT USING "#.######^^^^",U(I)
180 NEXT I
182 PRINT"M(N)=";:PRINT USING "#.######^^^^",M(N)
183 LPRINT"M(N)=";:LPRINT USING"#.######^^^^",M(N)
190 LPRINT "T=";T,"NUMBER OF STEPS=",N
200 FOR R=1 TO 120
210 LET X1=.003/120:X=(R-1)*X1:B1=0:B=0
220 FOR J=1 TO N
230 LET B1=U(J)*EXP(-X^2/(4*D*(T-(J-1)*T1)))/(2*SQR(F*D*(T-(J-1)*T1)))
235 IF B1<1D-20 THEN 260
240 LET B=B+B1
250 NEXT J
260 PRINT "NUMBER OF DISTANCE STEPS=",(R-1),"X=", PRINT USING "#.######^^^^",X,
270 LPRINT "NUMBER OF DISTANCE STEPS =",(R-1),"X=", LPRINT USING "#.######^^^^",X, LPRINT" ",
280 PRINT "B(T,X)=";:PRINT USING "#.######^^^^",B
290 LPRINT "B(T,X)=";:LPRINT USING "#.######^^^^",B
300 PRINT
310 LPRINT
320 IF B<1D-20 THEN 340
330 NEXT R
340 PRINT "END"
350 LPRINT "END"
360 END
```